NASA TECHNICAL NOTE

NASA TN D-2551

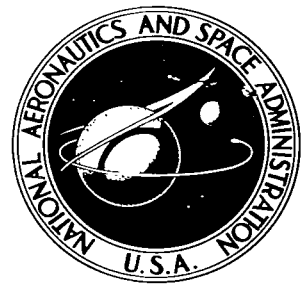

NASA TN D-2551

EFFECTS OF CANOPY SHAPE ON LOW-SPEED AERODYNAMIC CHARACTERISTICS OF A 55° SWEPT PARAWING WITH LARGE-DIAMETER LEADING EDGES

by Delwin R. Croom, Rodger L. Naeseth, and William C. Sleeman, Jr.

Langley Research Center
Langley Station, Hampton, Va.

NATIONAL AERONAUTICS AND SPACE ADMINISTRATION • WASHINGTON, D. C. • DECEMBER 1964

EFFECTS OF CANOPY SHAPE ON LOW-SPEED AERODYNAMIC CHARACTERISTICS OF A 55° SWEPT PARAWING WITH LARGE-DIAMETER LEADING EDGES

By Delwin R. Croom, Rodger L. Naeseth, and William C. Sleeman, Jr.

Langley Research Center
Langley Station, Hampton, Va.

NATIONAL AERONAUTICS AND SPACE ADMINISTRATION

For sale by the Office of Technical Services, Department of Commerce, Washington, D.C. 20230 -- Price $3.00

EFFECTS OF CANOPY SHAPE ON LOW-SPEED AERODYNAMIC CHARACTERISTICS OF A 55° SWEPT PARAWING WITH LARGE-DIAMETER LEADING EDGES

By Delwin R. Croom, Rodger L. Naeseth,
and William C. Sleeman, Jr.
Langley Research Center

SUMMARY

A low-speed wind-tunnel investigation was conducted to study effects of wing-canopy shape on the aerodynamic characteristics and spreader-bar load of a 55° swept parawing having large-diameter leading edges and keel. The canopy-flat-pattern sweep angles investigated on the 55° swept wing were 42.5°, 45°, 47.5°, 50°, and 52.5°. Several other modifications to the canopy shape were also studied, such as removal of single, double, and compound gores from the rear part of each canopy lobe. A study of the effects of wing-leading-edge sweep angle was made between sweep angles of 50° and 60° and effects of leading-edge diameter were obtained at the basic 55° sweep angle. Effects of keel web height were determined for a constant trailing-edge length and also for trailing-edge lengths that varied with web height.

The test results indicated that the maximum lift-drag ratios for the 55° swept wing varied from approximately 3.0 to 4.8 as the flat-pattern sweep angle increased from 42.5° to 52.5°. The spreader-bar compression load increased with flat-pattern sweep and the tension load that was encountered at high angles of attack for the low canopy-flat-pattern sweep was not present for the high canopy-flat-pattern sweep. Shortening the trailing-edge boltrope a small amount from the slack condition provided increases in lift at a given angle of attack, increases in maximum lift-drag ratio, and increases in spreader-bar compression for the high flat-pattern sweep angles. The amount of boltrope shortening required for the highest maximum lift-drag ratio appeared to be less at the high flat-pattern sweep angles than the amount required for the low flat-pattern sweep angles. A limited study of the effects of leading-edge sweep and flat-pattern sweep indicated that several combinations of those two variables can provide about the same value of maximum lift-drag ratio and that wings having the highest leading-edge sweep provided the least compressive axial load in the spreader bar.

INTRODUCTION

A number of research investigations have been conducted by the National Aeronautics and Space Administration to determine the aerodynamic characteristics

of parawings. Results of a general parawing study in which wing sweep and canopy-flat-pattern sweep were the primary variables are presented in reference 1, and aerodynamic characteristics of high-performance parawings are presented in reference 2. Longitudinal and lateral stability and control characteristics of parawings having conical and cylindrical canopy shapes are summarized in reference 3. Most of the currently available parawing information has been obtained on wings having relatively small cross-section leading edges and keel and these results therefore are not directly applicable to inflated-tube configurations which would have fairly large-diameter leading edges and keel. Some limited data on effects of leading-edge diameter are, however, presented in reference 1, and aerodynamic characteristics and cable tension for a parawing and spacecraft configuration having large-diameter leading edges are presented in reference 4.

Effects of canopy shape investigated in the research reported in reference 1 were for parawings having small leading edges and conical canopies. The present investigation was undertaken to study effects of different conical-shaped canopies on a parawing having large-diameter leading edges and keel and to study twisted and cambered canopies whose surfaces were not conical. The conical-shaped canopies investigated on the present 55° swept parawing were defined by canopy-flat-pattern sweep angles which varied from 42.5° to 52.5°. A number of nonconical canopy shapes were also studied in which the primary modification was an increase in camber.

In addition to the canopy-shape investigations, several other basic variables were studied briefly. The basic model had a leading-edge diameter of 7-percent keel length; effects of reducing this leading-edge size to 5.1 and 3.5 percent were also obtained. Effects of small incremental changes in sweep angle from the basic 55° sweep were also obtained for a range of sweepback from 50° to 60°.

The present low-speed investigation was conducted in the Langley high-speed 7- by 10-foot tunnel at test dynamic pressures of 10, 15, and 20 pounds per square foot. The test angle-of-attack range for many of the configurations varied from approximately 19° to 43°. However, inasmuch as the test angle-of-attack range varied greatly with the canopy shape, angles of attack as low as 7° were obtained on some configurations and as high as 54° were obtained on others. The investigation was primarily concerned with the determination of longitudinal aerodynamic characteristics and axial load in the spreader bar for the 0° sideslip condition. Static lateral stability derivatives were, however, obtained for some selected configurations from tests of the model over the angle-of-attack range at fixed sideslip angles of ±5°.

SYMBOLS

The data presented in this report are referred to the axis system shown in figure 1. The moment reference was located 50 percent of the keel length aft of the wing apex and on the center line of the keel as shown in figure 2. Static lateral stability derivatives are presented with respect to the stability axis system shown in figure 1 rather than with the commonly used body axes. Selection

of the stability axes was made because in a typical parawing application, the center of gravity lies an appreciable distance below the wing and the axis of least inertia may be oriented more nearly perpendicular to the flight path rather than nearly along the flight path as in conventional aircraft. It was therefore believed that stability-axis data would be more directly indicative of expected lateral stability characteristics than a body-axis presentation. Coefficients and symbols used in presentation of the data are as follows:

b span of wing taken between the leading-edge center lines at the tip at $\Lambda = 55^{\circ}$, 3.7556 ft

$b_o/2$ semispan dimension of canopy flat pattern (see fig. 3), in.

C_A axial-force coefficient, $\frac{\text{Axial force}}{qS}$

C_D drag coefficient, $\frac{\text{Drag}}{qS}$

C_L lift coefficient, $\frac{\text{Lift}}{qS}$

C_l rolling-moment coefficient, $\frac{\text{Rolling moment}}{qSb}$

C_m pitching-moment coefficient, $\frac{\text{Pitching moment}}{qSl_k}$

C_N normal-force coefficient, $\frac{\text{Normal force}}{qS}$

C_n yawing-moment coefficient, $\frac{\text{Yawing moment}}{qSb}$

C_Y side-force coefficient, $\frac{\text{Side force}}{qS}$

C_{SB} spreader-bar axial load coefficient (positive when spreader bar is in compression), $\frac{\text{Spreader-bar axial load}}{qS}$

C_{L_α} wing lift-curve slope, per degree

C_{l_β} effective dihedral parameter, $\frac{\Delta C_l}{\Delta \beta}$

C_{n_β} directional stability parameter, $\frac{\Delta C_n}{\Delta \beta}$

C_{Y_β} side-force parameter, $\frac{\Delta C_Y}{\Delta \beta}$

h theoretical lobe height of canopy based on assumption of conical-shaped lobes (see fig. 3), in.

L/D lift-drag ratio

l lobe width of canopy from keel vertical center line at trailing edge to leading-edge horizontal center line at tip (see fig. 3), in.

l_k length of wing keel from apex at intersection of leading-edge center lines to rear of the constant-diameter section of keel, 3.2738 ft

l_{le} leading-edge length of canopy flat pattern (see fig. 3), in.

l_{te} trailing-edge length of canopy flat pattern (see fig. 3), in.

q free-stream dynamic pressure, lb/sq ft

S wing reference area (taken as area between leading-edge center lines for projected area of $\Lambda = 55^\circ$ wing), 6.1476 sq ft

S_o canopy-flat-pattern area based on l_{le} and l_{te} dimensions (see fig. 3), sq ft

x_{cp} longitudinal position of center of pressure, expressed in terms of the keel length, $0.50 - \frac{C_m}{C_N}$

α angle of attack of wing keel, deg

$\alpha_{L=0}$ angle of attack of wing keel for zero lift, deg

β angle of sideslip of wing, deg

Λ leading-edge sweepback angle of wing, deg

Λ_o leading-edge sweepback angle of canopy flat pattern, deg

$(\Lambda_o)_E$ sweep of a line from apex to wing tip of flat pattern of canopy after gores have been removed and edges joined (fig. 4) or for various keel web configurations (fig. 6)

Subscript:

max maximum

MODEL DESCRIPTION

The general arrangement of the frame of the basic model which had 55° sweepback is shown in figure 2. The diameter of the leading edges and keel was 7 percent of the keel length and the diameter of the spreader bar was 3.5 percent of the keel length. The model shown in figure 2 was constructed to allow measurement of the axial load in the spreader bar and consequently the leading edges were attached to the keel and spreader bar through bearings such that no moment restraint in the plane of the leading edges and keel was encountered at the attachment points. In order to expedite the investigation three different wing frames were used. The original wing (model 1) used in the tests was identical in overall dimensions to that shown in figure 2. The construction, however, was of welded steel tube throughout; consequently, spreader-bar loads were not obtained on this model. The fixed-sweep wing shown by heavy lines in figure 2 (model 2) was constructed during tests of model 1 and some of the tests were rerun with model 2 in order to obtain spreader-bar loads data. Leading edges having diameters of 7, 5.1, and 3.5 percent keel lengths were fitted to model 2. For all models, however, the keel diameter was 7 percent of keel length. Model 3 which was identical to model 2 with the exception of the details of the spreader-bar attachment at the leading edge was constructed to allow data to be obtained at fixed sweep angles other than the basic 55° sweep. The highest and lowest sweep angles tested on model 3 are indicated by dashed lines at the left leading edge in figure 2. The apex portion of the leading edge of model 3 was relieved at the front and rear edges to allow changes to be made in the sweep angle.

Sketches of the basic canopy-flat-pattern configurations investigated are shown in figure 3 and modifications to the basic flat pattern are shown in figure 4. A sketch of the airfoil sections of the three-dimensional template used in construction of the $\Lambda = 55°$ cambered canopy is given in figure 5. Details of the keel-web configurations investigated are given in figure 6 and sketches of the covers attached to the bottom side of the wing apex region for some tests are presented in figure 7. The leading-edge fairing and the simulated keel catenary curtain (which is a means for distributing cable loads to the canopy) investigated on the model are also shown in figure 7.

The fabric for all the wing canopies investigated was 4.4 ounce per square yard stabilized synthetic textile fiber sailcloth having essentially zero porosity. The fabric weave for all the basic flat patterns was oriented with the warp parallel to the trailing edge. A hem was sewn in the trailing edge of each canopy and a 1/32-inch-diameter stranded steel cable boltrope was inserted inside the hem and attached to the leading edges and keel as shown in figure 3.

The use of a boltrope in the trailing edge of the wing canopy has been found to be useful in many cases to prevent excessive trailing-edge flapping at low angles of attack, particularly for canopies having fairly deep lobes. The

percent boltrope is defined as the amount that the boltrope is shortened from the flat-pattern trailing-edge length divided by the flat-pattern trailing-edge length. Calculated trailing-edge lengths and canopy areas for each flat-pattern sweep investigated are shown in figure 3. In addition to tests with the boltrope shortened, tests were also made with the boltrope slack (boltrope not attached at leading edge) and zero percent boltrope (boltrope attached but not shortened).

The basic $\Lambda_o = 45^\circ$ canopy was modified for some tests by removing fabric from the trailing edge as shown by the gored canopies of figure 4 and by modified keel attachments as shown in figure 6. These modified canopies were designated by values of $(\Lambda_o)_E$ which are the flat-pattern leading-edge sweep angles of equivalent canopy flat patterns having the same trailing-edge length as the modified canopies.

One test was made in which the $\Lambda_o = 45^\circ$ canopy attachment varied along a helix from the inside of the leading edge at the apex to the outside of the leading edge at the tip.

TESTS AND CORRECTIONS

The present investigation was conducted in the Langley high-speed 7- by 10-foot tunnel. Test dynamic pressures of 15 and 20 pounds per square foot were used for the determination of longitudinal characteristics. The tests conducted at $q = 20$ lb/sq ft were made in order to obtain increased accuracy of data; however, the maximum test angle of attack was usually limited by balance loads. Longitudinal characteristics presented in this report were obtained at a test dynamic pressure of 15 lb/sq ft and lateral stability derivatives were obtained at 10 lb/sq ft inasmuch as these test conditions were required in order to allow data to be obtained over the desired angle-of-attack range.

The test angle-of-attack range for many of the wing configurations extended from approximately 19° to 45°. Inasmuch as the operational range varied greatly with canopy shape, angles of attack as low as 7° were obtained on some configurations and as high as 54° were obtained on others. The sting support system was limited in angle-of-attack range to 24°. Test results for a wing, which were obtained over an angle-of-attack range in excess of 24° above the lowest test angle, were obtained from separate runs with different sting coupling angles. Lateral stability derivatives were obtained from tests through the angle-of-attack range at fixed sideslip angles of $\pm 5^\circ$.

Forces and moments acting on the complete wing were measured by means of a six-component strain-gage balance which was located in the wing keel and attached to the sting support. The spreader-bar axial load was measured with a three-component strain-gage balance which was located in, and rigidly attached to, the spreader bar at one end and was attached to the left leading edge through a rod-end bearing. The leading-edge attachments were designed only for measurement of axial load in the spreader bar; consequently, the other outputs from the spreader-bar balance were used only for computation of balance interaction on the measured spreader-bar axial load.

The usual jet-boundary corrections to angle of attack and drag coefficient and the blockage corrections to dynamic pressure as determined from references 5 and 6 were applied to the data. The angles of attack and sideslip have been corrected for deflection of the main balance and sting resulting from aerodynamic load. Balance chamber pressures were measured inside the wing keel, near the balance, and were found to have a negligibly small effect on measured drag coefficients. No corrections have been made for sting-support interference tares inasmuch as such tares are believed to be negligibly small for the present model.

PRESENTATION OF RESULTS

The longitudinal characteristics were obtained at a dynamic pressure of 15 pounds per square foot and the lateral stability derivatives were obtained at a dynamic pressure of 10 pounds per square foot unless otherwise indicated. The figures presenting the results are as follows:

	Figure
Effect of test dynamic pressure:	
$\Lambda_o = 45^\circ$	8
$\Lambda_o = 52.5^\circ$	9
Comparison of aerodynamic characteristics for the three wings tested	10
Effect of boltrope length for basic flat-pattern sweeps:	
$\Lambda_o = 42.5^\circ$	11
$\Lambda_o = 45^\circ$	12
$\Lambda_o = 47.5^\circ$	13
$\Lambda_o = 50^\circ$	14
$\Lambda_o = 52.5^\circ$	15 to 17
Aerodynamic characteristics with modified canopies:	
Scalloped trailing; $\Lambda_o = 45^\circ$; $\Lambda = 55^\circ$	18
Effect of canopy attachment; $\Lambda = 55^\circ$	19
Single gore removed from each canopy lobe:	
$\Lambda_o = 42.5^\circ$; $\Lambda = 55^\circ$	20
$\Lambda_o = 45^\circ$; $\Lambda = 55^\circ$	21
Two gores removed from each canopy lobe; $\Lambda_o = 45^\circ$; $\Lambda = 55^\circ$	22
Single compound gore removed from each canopy lobe $\Lambda_o = 45^\circ$ to $\Lambda_o = 52.5^\circ$ at trailing edge; $\Lambda = 55^\circ$	23
Cambered canopy from three-dimensional template; $\Lambda = 55^\circ$	24
Leading-edge fairing on $\Lambda_o = 45^\circ$ canopy; $\Lambda = 55^\circ$	25
Effect of keel web height:	
Trailing-edge length varied; $\Lambda = 55^\circ$	26 to 27
Trailing-edge length held constant $\left((\Lambda_o)_E = 52.5^\circ\right)$; $\Lambda = 55^\circ$	28 to 29
Effect of keel web fairing. $\Lambda = 55^\circ$; $(\Lambda_o)_E = 52.5^\circ$	30

The figures presenting data for each of the three models tested are summarized in the following table:

TABLE I.- TABULATION OF DATA FIGURES FOR THE THREE MODELS TESTED

Model	Figure
[a]1	8, 11, 14, 18, 20, [b]41, [b]42, 43, 44
2	15, 19
3	9, 16, 21 to 33, [c]34, 35, 36, 37, [d]38, [d]39, 40

[a]Spreader-bar loads presented with data for model 1 were obtained on model 2.
[b]Model 1 with spreader bar removed.
[c]Model 2 used for $\Lambda_o = 50^\circ$; $\Lambda = 55^\circ$ wing.
[d]Model 2 used for 7-percent diameter.

DISCUSSION

Characteristics Obtained in Basic Flat-Pattern Series

Effect of test dynamic pressure.- Lift, drag, and pitching-moment characteristics obtained at $q = 15$ and $q = 20$ are presented in figures 8 and 9 for the 55° swept model with flat-pattern sweep angles of 45° and 52.5°, respectively. These test results indicate that there was little effect of test dynamic pressure over the range investigated on the overall longitudinal aerodynamic characteristics. Most of the configurations studied were tested at both dynamic pressures; however, the data of $q = 15$ have been selected for presentation of the basic results, inasmuch as they were obtained over a larger angle-of-attack range. In some cases there was some difference in characteristics or there was enough scatter in the data obtained at $q = 15$ to make a comparison of lift slopes and $(L/D)_{max}$ difficult. In these instances data obtained at $q = 20$ have been used.

Comparison of data for the three basic models tested.- Longitudinal aerodynamic characteristics of the three models used in this investigation are presented in figure 10 and show good overall agreement when it is considered that three separate models were used. There is some difference in the level of the pitching-moment curves which indicates slightly less negative pitching moments for the variable-sweep wing (model 3). The stability throughout the angle-of-attack range, however, is in good agreement.

In the course of this investigation several check runs were made on the basic configuration ($\Lambda_o = 45^\circ$, $\Lambda = 55^\circ$) and these runs were found to be in very good agreement. These check data and the agreement of results among the three models of figure 10 indicate that the repeatability of data is very good when it is considered that the data were obtained on parawings having flexible cloth lifting surfaces. The good overall repeatability of the present test results is attributed primarily to the relatively high test dynamic pressures used in this investigation.

Effect of boltrope length.- Inasmuch as the effects of boltrope length were studied on most of the wing-canopy modifications investigated, some of the most important effects common to all the wing configurations are discussed briefly.

The largest effect of boltrope length was on the pitching-moment characteristics about the chosen moment reference. (For example, see figs. 11 to 16.) Decreasing the length of the trailing-edge boltrope caused a negative increment in pitching moment for almost all configurations and angles of attack. In some instances, a small amount of boltrope shortening from the 0-percent or slack condition had little effect at low angles where the canopy was not fully inflated (for example, see fig. 16), and this condition is discussed later in connection with the lift characteristics. The primary purpose for using a boltrope is to stabilize the trailing edge in order to prevent excessive flapping at low lift, inasmuch as excessive flapping leads to deterioration and tearing of the canopy at the trailing edge. The fairly large magnitude of the negative increments in pitching moment accompanying boltrope shortening are not considered desirable from the standpoint of longitudinal stability and trim. For a parawing

configuration to be trimmed at positive lift and have stability, the extrapolated pitching-moment intercept at zero lift must, of course, be positive and this condition may be achieved on a complete parawing application by lowering the center of gravity a considerable distance below the wing. (See ref. 3.) From the standpoint of vertical location of the center of gravity for stability and trim, therefore, the smallest amount of boltrope shortening consistent with its primary purpose is desirable. There are, however, other factors that can be of importance in regard to boltrope length, such as effects on lift-drag ratio and lift at a given angle of attack.

The data of figures 11 to 16 show in general that there was an increase in $(L/D)_{max}$ for a relatively small amount of boltrope shortening. With the greatest amount of shortening, however, maximum lift-drag ratios were decreased. Effects of boltrope length on lift-drag ratios were smallest on the wing canopies having the largest lobes (see figs. 11 and 12); and for flat-pattern sweep angles up to 50°, the highest lift-drag ratios in the canopy-flat-pattern series of tests were obtained with 4-percent boltrope. The $\Lambda_o = 52.5°$ wing (fig. 16), on the other hand, had the highest lift-drag ratios when the 2-percent boltrope condition was used. A detailed study to determine optimum boltrope settings was not made; however, some test results indicated that higher lift-drag ratios could be obtained with less than 4-percent shortening on the $\Lambda_o = 45°$, $\Lambda = 55°$ wing. For example, the maximum lift-drag ratio obtained in the web-height study (figs. 26 and 49) indicated that the zero web-height canopy $(\Lambda_o)_E = 45°$ had a maximum lift-drag ratio of 3.5 for the 2-percent boltrope setting used in comparison with the value of 3.3 obtained on the basic $\Lambda_o = 45°$, $\Lambda = 55°$ wing with 4-percent boltrope (fig. 12). Observation of the wing canopies during testing, however, and consideration of the pitching-moment increment accompanying changes in boltrope length indicated generally that the desirable amount of boltrope shortening decreased with an increase in canopy flat-pattern sweep for canopies having relatively shallow lobes.

Some fairly consistent trends are evident in effects of boltrope length on the lift characteristics shown in figures 11 to 16. An increase in lift coefficient at a given angle of attack generally accompanied shortening of the boltrope and the lift-curve slopes for the slack boltrope and 7-percent boltrope settings were approximately the same. (See figs. 11 to 14.) The lift-curve slope for the intermediate boltrope setting was, however, somewhat higher over most of the angle-of-attack range. In some cases there was a relatively small effect of boltrope at the low angles and small boltrope shortening. (See figs. 11, 12, and 16.) This difference in lift characteristics is believed to be associated with some canopy deformation which the intermediate boltrope setting was insufficient to eliminate entirely at low angles of attack. As the angle of attack increased, the effect of the intermediate boltrope setting appeared to increase and to cause the lift-curve slope to vary over the test angle-of-attack range.

Another important effect of boltrope length shown in figures 12 to 16 is the effect on the axial load in the spreader bar. The spreader-bar load coefficients presented in figure 12 for the $\Lambda_o = 45°$, $\Lambda = 55°$ wing indicate that the spreader bar was in compression for angles of attack below about 33° and was in tension at higher angles. There was a relatively small effect of boltrope length on the spreader-bar load for the wing canopies having fairly deep lobes

($\Lambda_o = 45.0^\circ$ and 47.5°, figs. 12 and 13). For flat-pattern sweep angles of $\Lambda_o = 50^\circ$ and greater, increasing the amount of boltrope shortening caused appreciable increases in the compression load in the spreader bar at low angles of attack and increased the angle of attack for reversal of spreader-bar load for the $\Lambda_o = 50^\circ$ wing. (See fig. 14.) A relatively large increment of compressive load was indicated for the $\Lambda_o = 52.5^\circ$ wing when the boltrope length was decreased from the slack or 0-percent condition to the 4-percent setting. Tension in the spreader bar was not obtained for this wing for any of the boltrope and angle-of-attack conditions investigated. Effects of boltrope shortening on spreader-bar loads were therefore found to be relatively small for canopies having deep lobes but were fairly large and unfavorable (compressive) for the flatter canopies.

The effects of flat-pattern sweep on the spreader-bar load are summarized in figure 46 as the variation of wing-lift coefficient for zero spreader-bar load with flat-pattern sweep. The curves for each boltrope condition can be considered to define the lift coefficient at which the spreader-bar load changes from compression to tension. Combinations of C_L and Λ_o falling above each line indicate that the spreader bar was in tension and combinations falling below each line indicate a compression load in the spreader bar. The results of figure 46 indicate that for the canopies having deep lobes, tension in the spreader bar would be expected to occur in the operational high-lift range whereas for the tighter canopies a compression load would be expected throughout the normal lift range.

The spreader-bar loads presented in this report are the loads resulting from the aerodynamic input of the canopy and leading edges. These loads would be expected to apply to a configuration in which the only attachment to the payload was through the keel. For a configuration in which the leading edges were also connected to the payload (by cables, for example), the component of cable tension directed axially along the spreader bar must, of course, be accounted for in determining the total spreader-bar load.

Effect of canopy-flat-pattern sweep.- The effects of canopy-flat-pattern sweep on the longitudinal aerodynamic characteristics of the model are summarized in figures 45 to 48. These summary figures, with the exception of the spreader-bar load characteristics (fig. 46) were obtained from data obtained at a test dynamic pressure of 20 pounds per square foot which is believed to provide somewhat better accuracy for purposes of analysis than the basic data obtained at a test dynamic pressure of 15 pounds per square foot.

The primary purpose of the present investigation was to determine the extent to which the maximum lift-drag ratios of the $\Lambda_o = 45^\circ$, $\Lambda = 55^\circ$ wing could be improved by modifications to the canopy flat pattern while retaining the basic 55° leading-edge sweep. The variation of maximum lift-drag ratios with flat-pattern sweep presented in figure 45 shows that $(L/D)_{max}$ increased from a value of about 3.0 for the $\Lambda_o = 42.5^\circ$ canopy to about 4.5 for the $\Lambda_o = 52.5^\circ$ canopy with 4-percent boltrope shortening. The effects of boltrope length discussed previously indicated that a 2-percent boltrope setting provided a higher maximum lift-drag ratio for the $\Lambda_o = 52.5^\circ$ canopy than was obtained with the 4-percent setting. The data of figure 16 show that a maximum

lift-drag ratio of about 4.8 was obtained with the $\Lambda_o = 52.5^\circ$ canopy at the 2-percent boltrope setting.

An analysis of the experimental drag characteristics obtained in this investigation has not been made because sufficient data for a meaningful analysis were not obtained. For example, determination of the drag at zero lift for a flexible lifting surface has inherent difficulties which may possibly be resolved more easily by a combination of both theory and special experimental results. Some general observations on the drag characteristics can be made, however, on the basis of presently available information. A comparison of the drag polars presented in figure 47 shows a progressive decrease in drag coefficient at a given lift as the flat-pattern sweep increased. This drag reduction is believed to have occurred primarily as a result of changes in the basic span loading due to twist and camber as the flat-pattern sweep increased. These changes in span loading are also indicated by the lift curves, which show that reducing the twist also reduced the angle of attack required for a given lift coefficient (fig. 33). A conical-shaped parawing with deep lobes has a large amount of aerodynamic twist across the span and the very high washout over the outboard portion of the wing can cause the wing to carry negative lift near the tip at lift coefficients near maximum lift-drag ratio. A discussion of the type of span loading encountered on conical-shaped parawings is given in reference 3, and a procedure for determining the twist and camber is presented in reference 2.

Decreasing the washout by increasing the canopy-flat-pattern sweep angle had a significant effect on the angle of attack for zero lift as indicated in figure 45. The zero-lift angle varied from about 10° to about -1° when the flat-pattern sweep increased from 42.5° to 52.5° for the 4-percent boltrope setting. The minimum angle of attack attained in the tests usually varied with flat-pattern sweep and was frequently determined by the severity of trailing-edge flutter as the canopy tended to unload near the tips. The occurrence of trailing-edge flutter and canopy luffing was, of course, less pronounced on the canopies having shallow lobes and in these cases, the canopy becomes depressed near the apex at low angles of attack. The true angle of attack for zero lift, therefore, was not determined in the tests and the values presented in figure 45 were obtained from an extrapolation of the linear portions of the lift curve by using the values of C_{L_α} also presented in figure 45.

Effects of flat-pattern sweep on pitching-moment characteristics of the model are presented in figure 48 for three boltrope conditions. Increasing the flat-pattern sweep with the boltrope slack generally produced positive increments of pitching moment and some overall decrease in instability; shortening the boltrope tended to minimize the changes with flat-pattern sweep in both pitching moment and stability, and for the 7-percent boltrope condition the effect of flat-pattern sweep on pitching moment was relatively small. This pitching-moment characteristic might be expected in that the increment of pitching moment associated with increasing flat-pattern sweep was opposite in sign and much smaller than the increment resulting from 7-percent boltrope shortening.

Modification to the Canopy Shape

An appreciable number of modifications were made to the basic canopy shape (fig. 4) in order to determine the extent to which the maximum lift-drag ratios of a given canopy could be improved. Inasmuch as several approaches were tried and the gains in L/D obtained were relatively small in comparison with the values obtained with the $\Lambda_o = 52.5^\circ$ wing with 2-percent boltrope, no detailed discussion of the results is made. Many of the modifications to the canopy shape were not related and therefore the maximum lift-drag ratios obtained are summarized in bar graph form in figure 50. The maximum lift-drag ratio shown for each basic wing is extended by a dotted line across the chart for ease in assessing the incremental effect of each modification.

The removal of some of the canopy fullness was found to be the most effective means of improving maximum lift-drag ratios as indicated by results obtained when either a single gore or two gores were removed from the aft part of the canopy. (See figs. 21, 22, and 50.) The gore removal modification effectively increased the camber of the canopy, decreased the twist variation across the span, and gave a trailing-edge length equal to that for a flat-pattern sweep of 50°. These gains obtained with gore removal suggested the possibility that further gains in L/D could be obtained by extending the modification in order to decrease the twist further and increase the camber. A compound-gore-removal modification was made to the canopy fabric such that the flat-pattern sweep varied across the span from 45° over the forward portion of the wing to 52.5° at the tip. Test results for this modification are presented in figure 23 for the zero boltrope shortening condition. The summary results of figure 50 show that an appreciable gain in L/D was obtained with Λ_o varying across the span when compared with the basic $\Lambda_o = 45^\circ$ wing. This modification, however, was not as effective in improving the maximum lift-drag ratio as the canopy having a 52.5° flat-pattern sweep along the entire leading edge.

Results showing the effect of varying the canopy attachment (fig. 19) were not included in figure 50 because this modification had no effect on maximum lift-drag ratio.

Effect of Keel Web Height

A study of the effects of a vertical web between the wing keel and canopy was made to investigate effects of web height on both lateral stability characteristics and maximum lift-drag ratios. In this study, two canopies having a flat-pattern sweep of 45° were used. The canopy lobes were pulled together at the center and stitched to give the various web heights. For the series of tests in which the trailing-edge length $(\Lambda_o)_E$ (fig. 6) varied with web height, the seams were removed progressively from the top. For the tests with $(\Lambda_o)_E = 52.5^\circ$, the seams were removed progressively from the bottom and the excess fabric wrapped around the keel. For these modifications, the trailing-edge length was measured from the top of the web along the trailing edge to the tip.

Maximum lift-drag ratios presented in figure 49 showed a progressive increase with increasing web height when the trailing-edge length varied. This increase in maximum lift-drag ratio occurred primarily because of the flat-pattern sweep rather than because of the web height. Results obtained with $(\Lambda_o)_E = 52.5^\circ$ (fig. 49) showed relatively little change in maximum lift-drag ratio with web height except near zero web height.

Lateral stability derivatives presented in figure 27 show only relatively small changes in C_{n_β} and C_{l_β} at a given angle of attack when the trailing-edge length varied with web height. With the trailing-edge length invariant and the web height increasing, C_{l_β} progressively increased (fig. 29) and the directional stability became lower.

Effect of Leading-Edge Sweep

A study of the effects of leading-edge sweep between 50° and 60° was made at three different canopy-flat-pattern sweep angles. The purpose of this study was to determine possible advantageous aerodynamic combinations of leading-edge and flat-pattern sweep angles. The basic results of this part of the investigation are presented in figures 33 to 35 and are summarized in figures 45 and 46. Maximum lift-drag ratios presented in figure 45 indicate that there are several combinations of flat-pattern sweep and leading-edge sweep that will provide the same value of $(L/D)_{max}$. For example, a value for $(L/D)_{max}$ of approximately 3.7 was achieved with the following sweep combinations: $\Lambda_o = 45^\circ$, $\Lambda = 50^\circ$; $\Lambda_o = 47.5^\circ$, $\Lambda = 55^\circ$; $\Lambda_o = 50^\circ$, $\Lambda = 57.5^\circ$; and $\Lambda_o = 52.5^\circ$, $\Lambda = 60^\circ$. If the value of $(L/D)_{max}$ provided by these sweep combinations was considered adequate for a particular application, the selection of a wing could be based on other factors; a better overall optimization of the wing design may therefore be allowed than would be obtained by using the best $(L/D)_{max}$ as the primary criterion. Attention is given therefore to some of the aerodynamic characteristics of the wing that should be considered in addition to the maximum lift-drag ratios.

The test results of figures 33 to 35 are based on a common reference area (projected wing area between leading-edge center lines on the 55° swept wing); however, for purposes of the present discussion it appears desirable to use the corresponding projected area for each wing leading-edge sweep angle being considered. The data presented in figures 51 and 52 are therefore based on the projected area between leading-edge center lines for each respective sweep angle tested. The results presented in figure 51 are plotted against a canopy-shape parameter inasmuch as the changes in aerodynamic characteristics with flat pattern and leading-edge sweep are believed to have resulted primarily from changes in the wing twist and camber. The canopy-shape parameter is defined as the ratio of the canopy lobe height h to the lobe width l, as computed for portions of right circular cones. The canopy lobe height is not a fundamental correlating parameter; however, its use may provide a better insight into the results than can be obtained from figure 45.

The variations of maximum lift-drag ratio and the spreader-bar axial load for two lifting conditions are summarized in figure 51. These results indicate that for the range of leading-edge sweep angles tested, a higher value of maximum lift-drag ratio could be obtained at a given lobe height with the greatest leading-edge sweep angles. There was generally little difference in spreader-bar axial load at the lift coefficient for $(L/D)_{max}$, and the spreader bar was in compression for all but the highest canopy-lobe-height parameter. At a lift coefficient of 1.5, however, most of the configurations had a tension load in the spreader bar and this tension load at a given lobe-height parameter was greater for the higher sweep angles. It would appear, therefore, from the standpoint of the influence of aerodynamic loads on structural requirements, that considerations could be given to the use of wing leading-edge sweep angles greater than the basic 55° sweep.

Some aerodynamic characteristics of the two wings having the lowest and highest leading-edge sweep angles and having about the same value of $(L/D)_{max}$ are presented in figure 52. These results are presented to indicate some of the aerodynamic factors that should be considered in addition to maximum lift-drag ratio. The lift curves for the two wings show that a higher angle of attack was required to provide a given lift coefficient for the highest sweep angle. However, the lift-curve slopes for the two wings were not markedly different. Although the maximum lift-drag ratios for the two wings were about the same, the value of L/D at high lift was somewhat lower than that for the more highly swept wing.

Pitching-moment characteristics for the 60° swept wing show an appreciable improvement over those of the 50° swept wing in that the stability was higher and the pitching-moment intercept at zero lift was less negative with the 60° swept wing. As previously mentioned, the spreader-bar load was significantly improved when the sweep angle was increased from 50° to 60°.

Effects of Leading-Edge Diameter

The effect of leading-edge diameter on maximum lift-drag ratio is presented in figure 49 and indicates the expected progressive increase in $(L/D)_{max}$ as the diameter decreased for the 45° flat-pattern sweep. Results obtained with the 50° flat-pattern sweep show a fairly large increase in $(L/D)_{max}$ in going from a 7-percent- to 5.1-percent-diameter leading edge and a small change in going from 5.1-percent to 3.5-percent diameter. The results obtained with the 50° flat-pattern sweep do not appear to represent the expected effects of leading-edge diameter. The basic data for these two wings presented in figures 36 and 38 do not indicate consistent or progressive effects of leading-edge diameter on lift and pitching-moment characteristics. The differences in measured lift coefficients at a given angle of attack and observation of the canopy during tests suggest that inaccuracies in installation of the canopies produced aerodynamic effects that tended to obscure the effects of leading-edge diameter.

Effects of Spreader Bar

The effects of boltrope length with the spreader bar removed are presented in figures 40 and 41 for flat-pattern sweep angles of 45° and 50°. Effects of the presence of the spreader bar for the 4-percent boltrope condition are presented in figure 42. Data for the two flat-pattern sweep angles were obtained because the effect of spreader bar on the canopy was expected to increase as the canopy lobe became flatter. The results of figure 42 show that the increment in maximum lift-drag ratio attributable to the spreader bar was about 0.50 with 50° flat-pattern sweep and was about 0.30 with the 45° flat-pattern sweep. Removal of the spreader bar from the welded tube model (model 1) caused a negative increment in pitching moment that was largest for the 50° flat-pattern sweep.

Effects of Apex Covers

Effects of sealed and vented covers attached to the bottom of the wing apex region are presented in figures 43 and 44, respectively. These covers were placed on the wing in order to determine whether gains in lift-drag ratio could be obtained by covering the juncture of the relatively large diameter tubes that intersected at the apex. The data of figures 43 and 44 show that no beneficial effect on maximum lift-drag ratios was obtained and in most cases the covers caused a decrease in $(L/D)_{max}$. Both the sealed and vented apex covers caused a reduction in lift at a given angle of attack.

The apex covers had a very beneficial effect on pitching moments in that a substantial positive increment in the pitching-moment intercept at zero lift and an increase of stability accompanied the addition of the covers. The significance of these pitching-moment effects lies in the fact that for a parawing configuration to have stable trim points, the pitching-moment intercept at zero lift must be positive. Most parawings have a negative pitching-moment intercept at zero lift for the wing alone and a positive value for a complete vehicle is achieved by locating the vehicle center of gravity an appreciable distance below the wing keel. The wing with apex cover B, on the other hand, could be trimmed with positive stability over the test angle-of-attack range with the center of gravity located at the center line of the keel.

The use of an apex cover on the bottom of the wing may provide an effective means for reducing the vertical displacement of the center of gravity required for stable trim for parawings having relatively large leading edge and keel tubes. In like manner, a sufficiently large cover may allow the use of a keel-loaded parawing vehicle without recourse to artificial longitudinal stabilization.

SUMMARY OF RESULTS

The results of a low-speed wind-tunnel investigation of the effects of canopy shape on the performance and spreader-bar load of a 55° swept parawing having large-diameter leading edges may be summarized as follows:

1. The maximum lift-drag ratios for the 55° swept wing varied from approximately 3.0 to 4.8 as the canopy flat-pattern sweep angle increased from 42.5° to 52.5° for the most favorable boltrope setting tested at each sweep angle.

2. Shortening the trailing-edge boltrope a small amount from the slack condition provided increases in lift at a given angle of attack, increases in maximum lift-drag ratio, and increases in spreader-bar compression for the high flat-pattern sweep angles. The amount of boltrope shortening required for the highest maximum lift-drag ratio appeared to be less at the high flat-pattern sweep angles than the amount required for the low flat-pattern sweep angles.

3. The axial load in the spreader bar was compressive at low lift for all wing configurations; however, at high lift a tension load occurred in the spreader bar for all wing configurations except those having relatively shallow canopy lobes.

4. A limited study of the effects of leading-edge sweep and flat-pattern sweep indicated that several combinations of those two variables can provide about the same value of maximum lift-drag ratio and that wings having the highest leading-edge sweep provided the most favorable axial load in the spreader bar. The more highly swept wings, however, had slightly lower values of lift-drag ratios at high lift coefficients even though the maximum lift-drag ratios were about the same as for the wings of lower sweep.

5. The use of a cover on the lower side of the wing apex generally caused a small reduction in maximum lift-drag ratio but also provided a significant beneficial effect on pitching moments by increasing the stability and providing a large positive increment in pitching-moment intercept at zero lift.

Langley Research Center,
National Aeronautics and Space Administration,
Langley Station, Hampton, Va., September 1, 1964.

REFERENCES

1. Naeseth, Rodger L.; and Gainer, Thomas G.: Low-Speed Investigation of the Effects of Wing Sweep on the Aerodynamic Characteristics of Parawings Having Equal-Length Leading Edges and Keel. NASA TN D-1957, 1963.

2. Polhamus, Edward C.; and Naeseth, Rodger L.: Experimental and Theoretical Studies of the Effects of Camber and Twist on the Aerodynamic Characteristics of Parawings Having Nominal Aspect Ratios of 3 and 6. NASA TN D-972, 1963.

3. Sleeman, William C., Jr.; and Johnson, Joseph L., Jr.: Parawing Aerodynamics. Astronautics and Aerospace Eng., vol. 1, no. 5, June 1963, pp. 49-55.

4. Sleeman, William C., Jr.: Low-Speed Investigation of Cable Tension and Aerodynamic Characteristics of a Parawing and Spacecraft Combination. NASA TN D-1937, 1963.

5. Gillis, Clarence L.; Polhamus, Edward C.; and Gray, Joseph L., Jr.: Charts for Determining Jet-Boundary Corrections for Complete Models in 7- by 10-Foot Closed Rectangular Wind Tunnels. NACA WR L-123, 1945. (Formerly NACA ARR-L5G31.)

6. Herriot, John G.: Blockage Corrections for Three-Dimensional-Flow Closed-Throat Wind Tunnels, With Consideration of the Effect of Compressibility. NACA Rep. 995, 1950. (Supersedes NACA RM A7B28.)

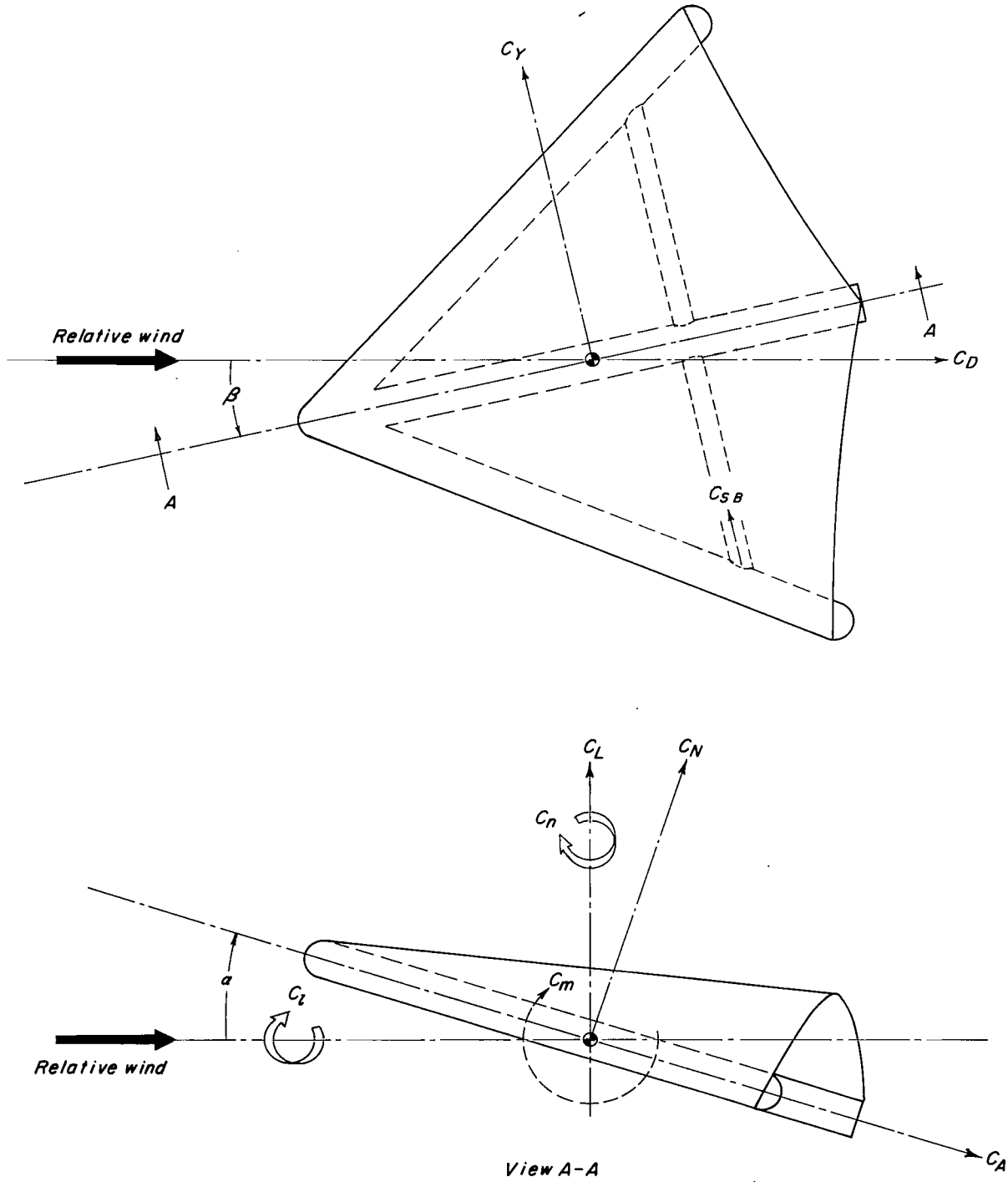

Figure 1.- System of axes and positive directions of forces and moments used in presentation of data.

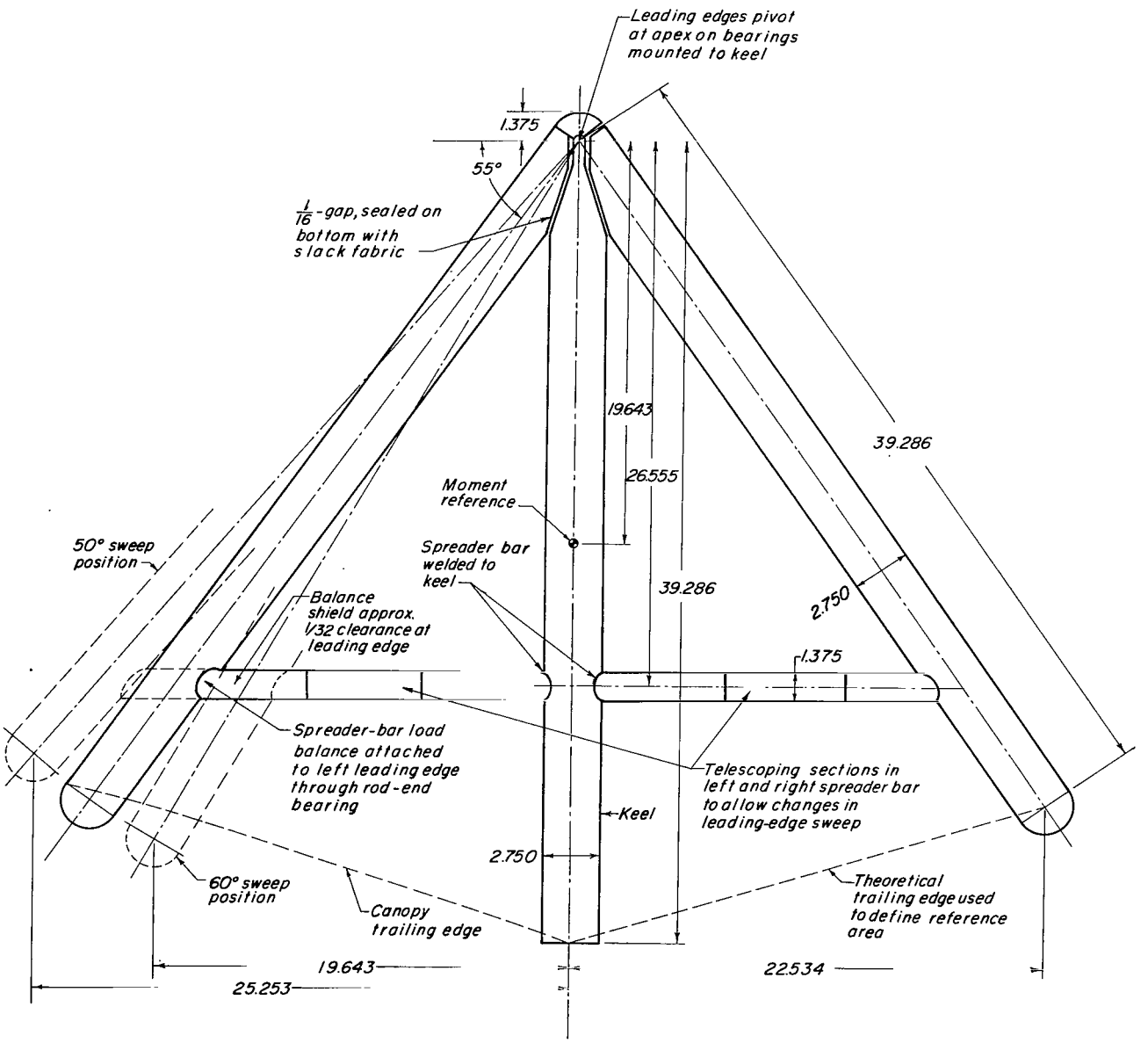

Figure 2.- Plan view of basic parawing frame. The lowest and highest sweep angles tested are indicated by dashed lines. All dimensions are in inches unless otherwise denoted.

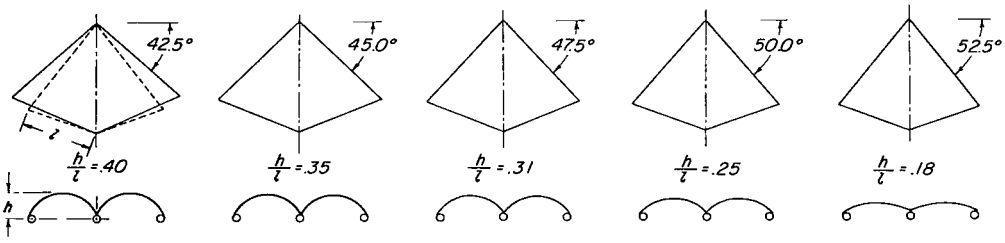

Canopy flat patterns and lobe-height parameter at trailing edge for the basic 55° leading-edge sweep.

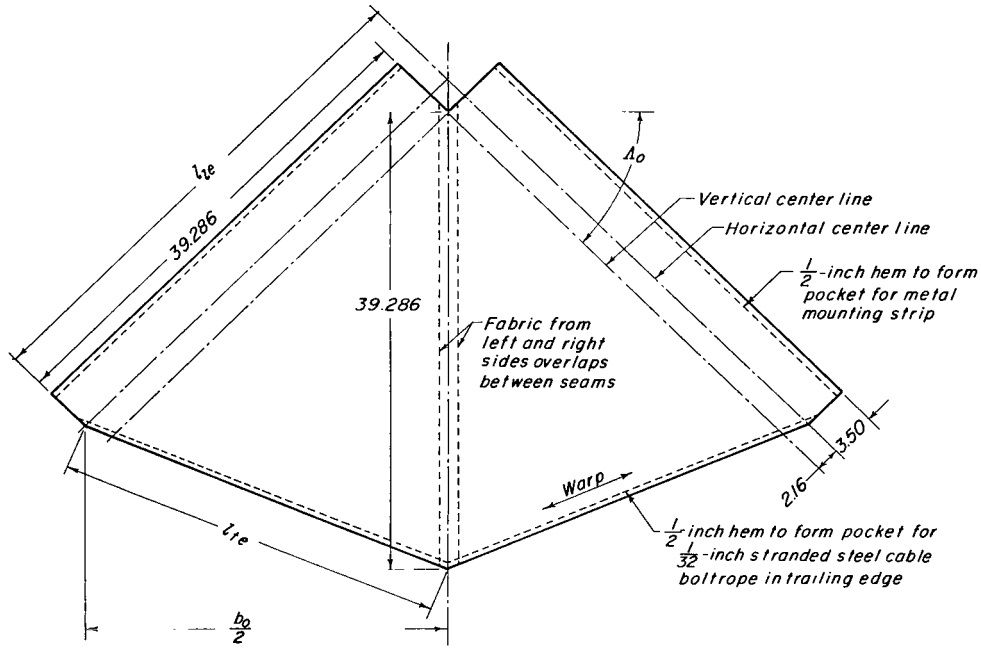

Construction details for canopy flat patterns

A_o, deg	S_o, sqft	l_{te}, in.	l_{te}, in.	$\frac{b_o}{2}$, in.
42.5	8.92	33.63	41.27	30.43
45.0	8.62	32.08	41.45	29.31
47.5	8.30	30.50	41.64	28.14
50.0	7.97	28.91	41.86	26.91
52.5	7.62	27.31	42.10	25.63

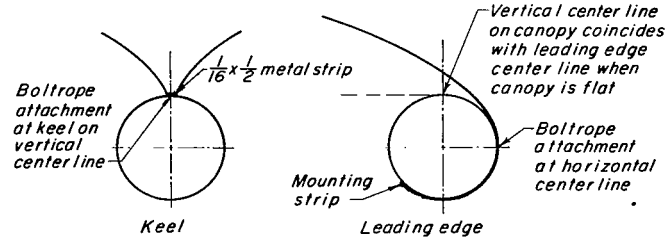

Enlarged views of canopy attachment at leading edge and keel.

Figure 3.- Geometric characteristics and construction details of the basic series of canopy flat patterns investigated. All dimensions are in inches unless otherwise denoted.

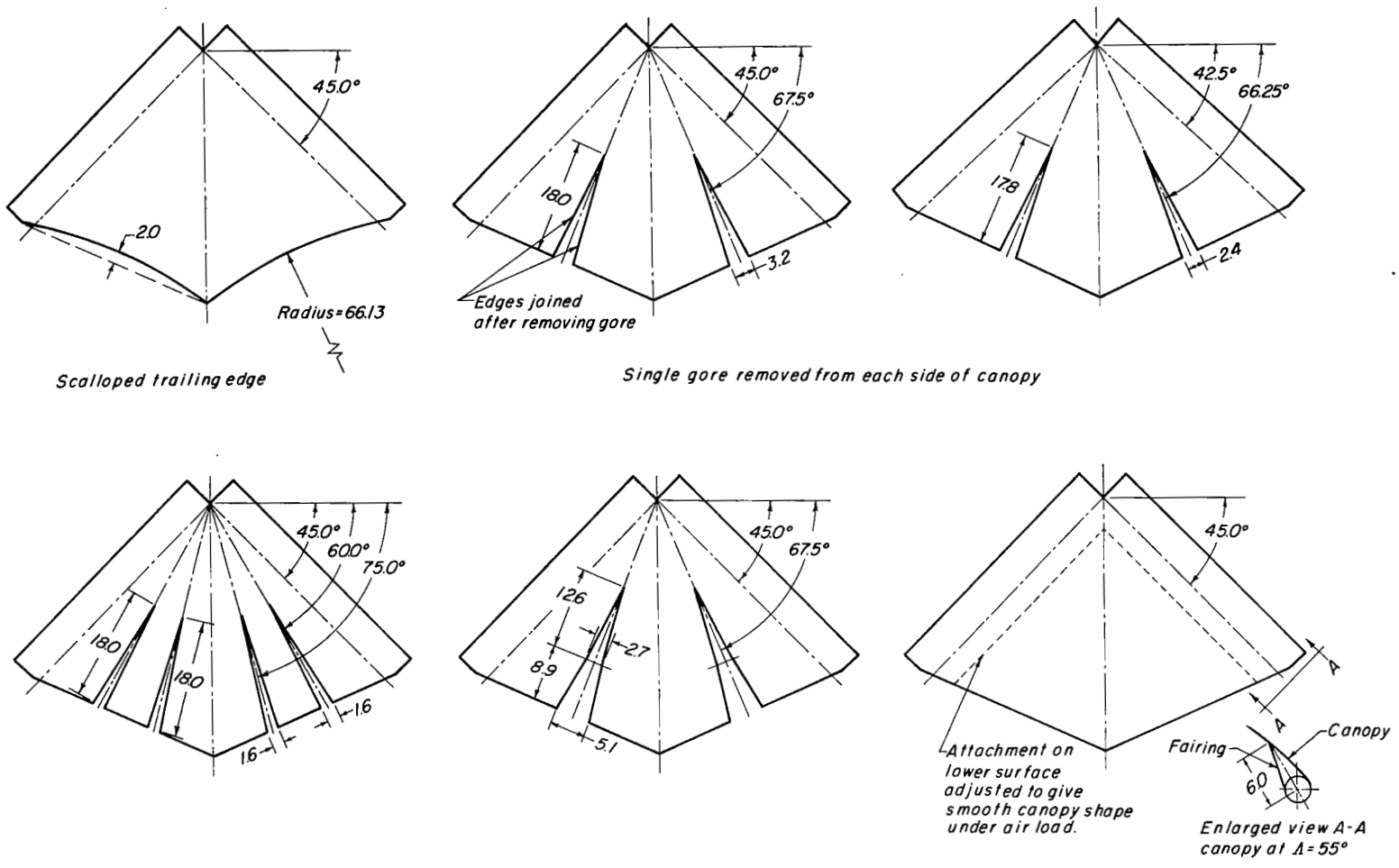

Figure 4.- Modifications to basic canopy flat patterns investigated. All dimensions are in inches unless otherwise denoted.

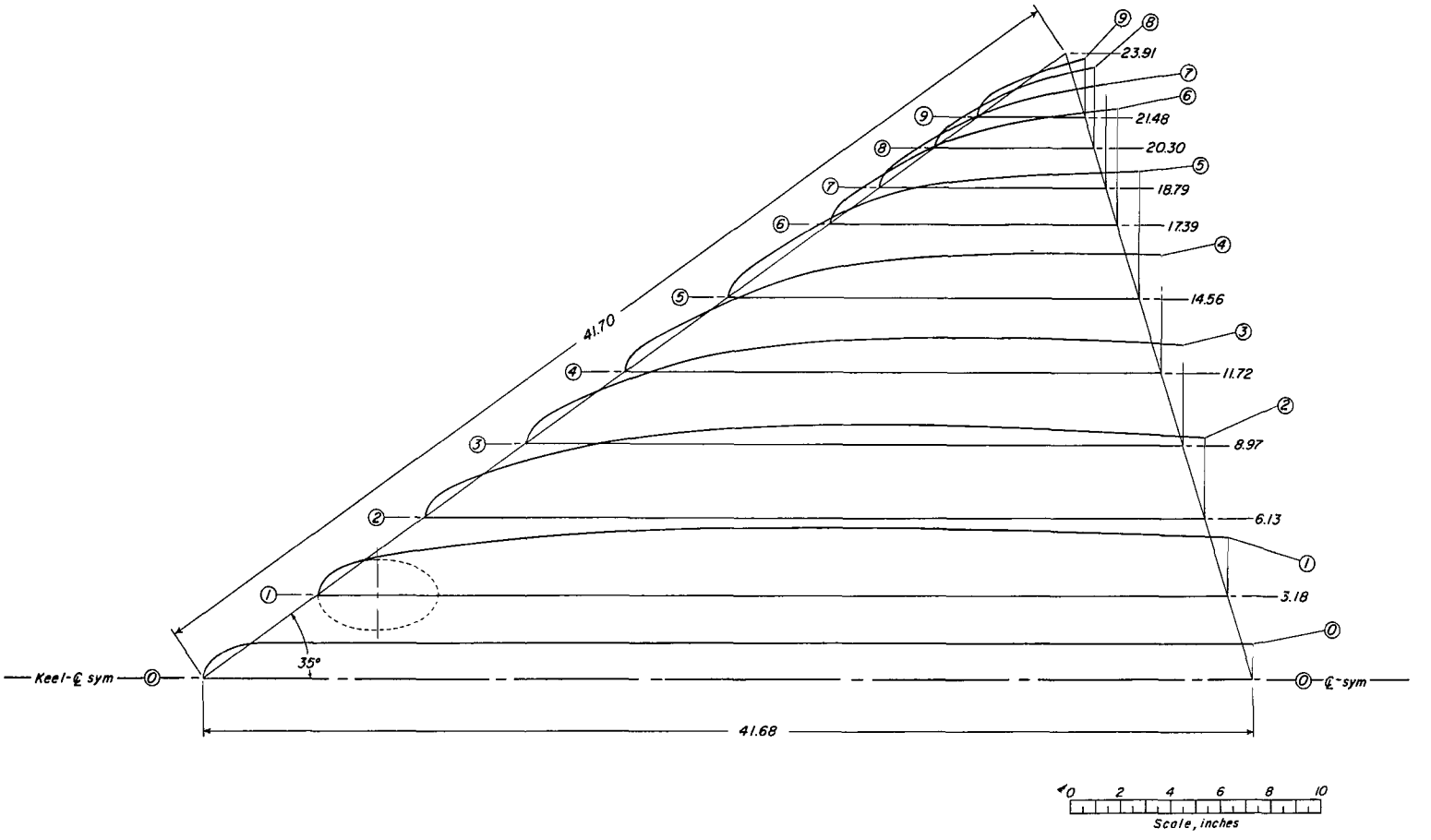

Figure 5.- Sketch of streamwise airfoil sections of the three-dimensional template used in construction of the 55° swept cambered canopy. All dimensions are in inches unless otherwise denoted.

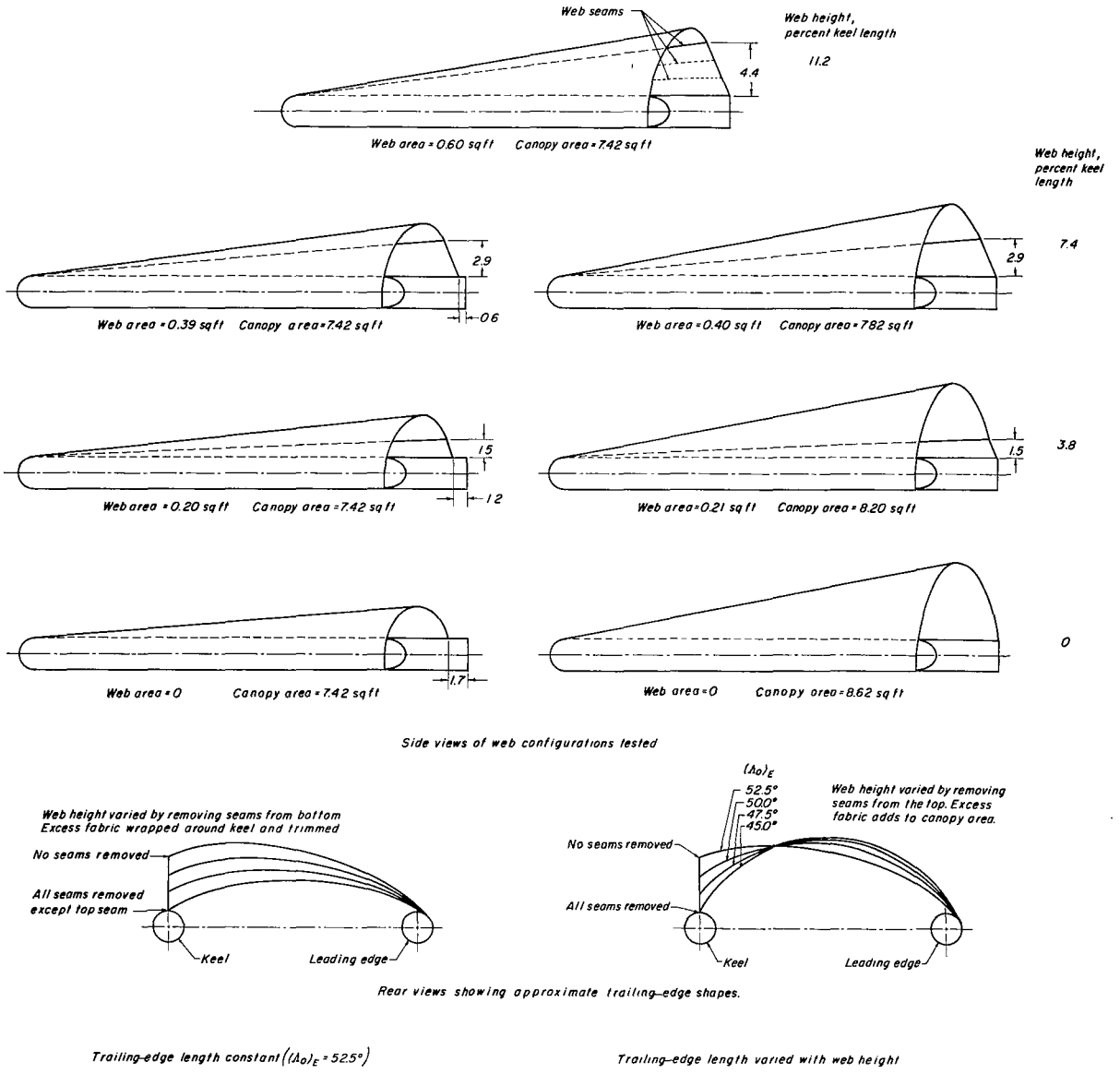

Figure 6.- Details of the keel web configurations tested on the 55° swept wing. Basic canopy flat-pattern sweep of 45° used. All dimensions are in inches unless otherwise denoted.

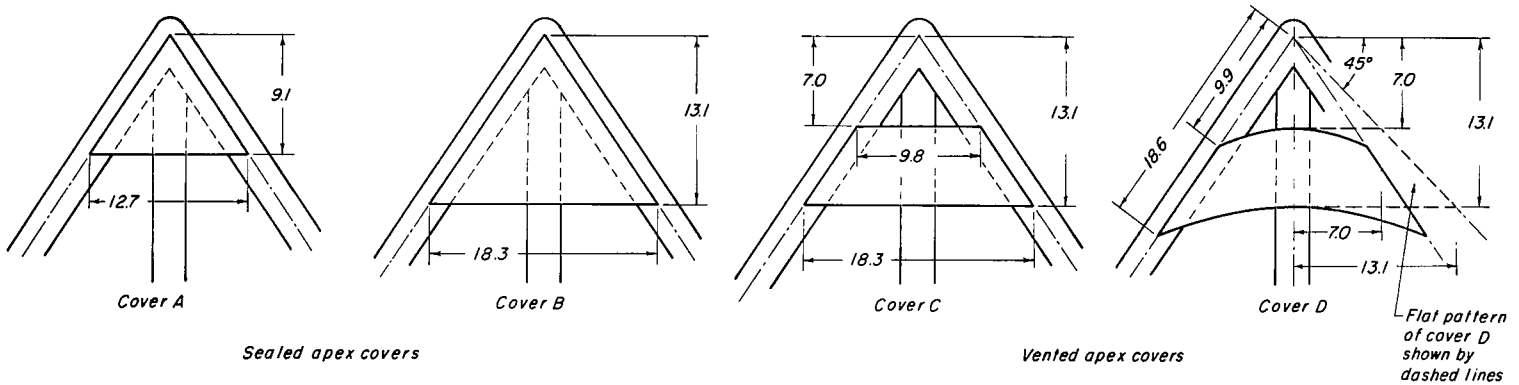

Apex covers on bottom side of the 55° swept wing.

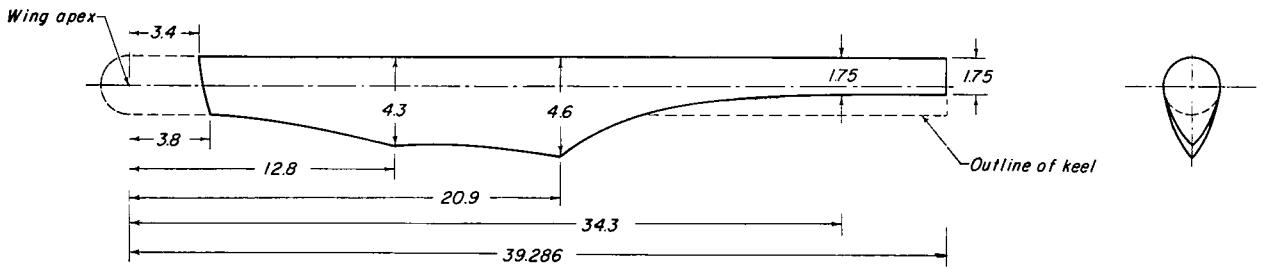

Simulated catenary curtain on keel.

Figure 7.- Details of apex covers and simulated keel catenary curtain investigated on the model. All dimensions are in inches unless otherwise denoted.

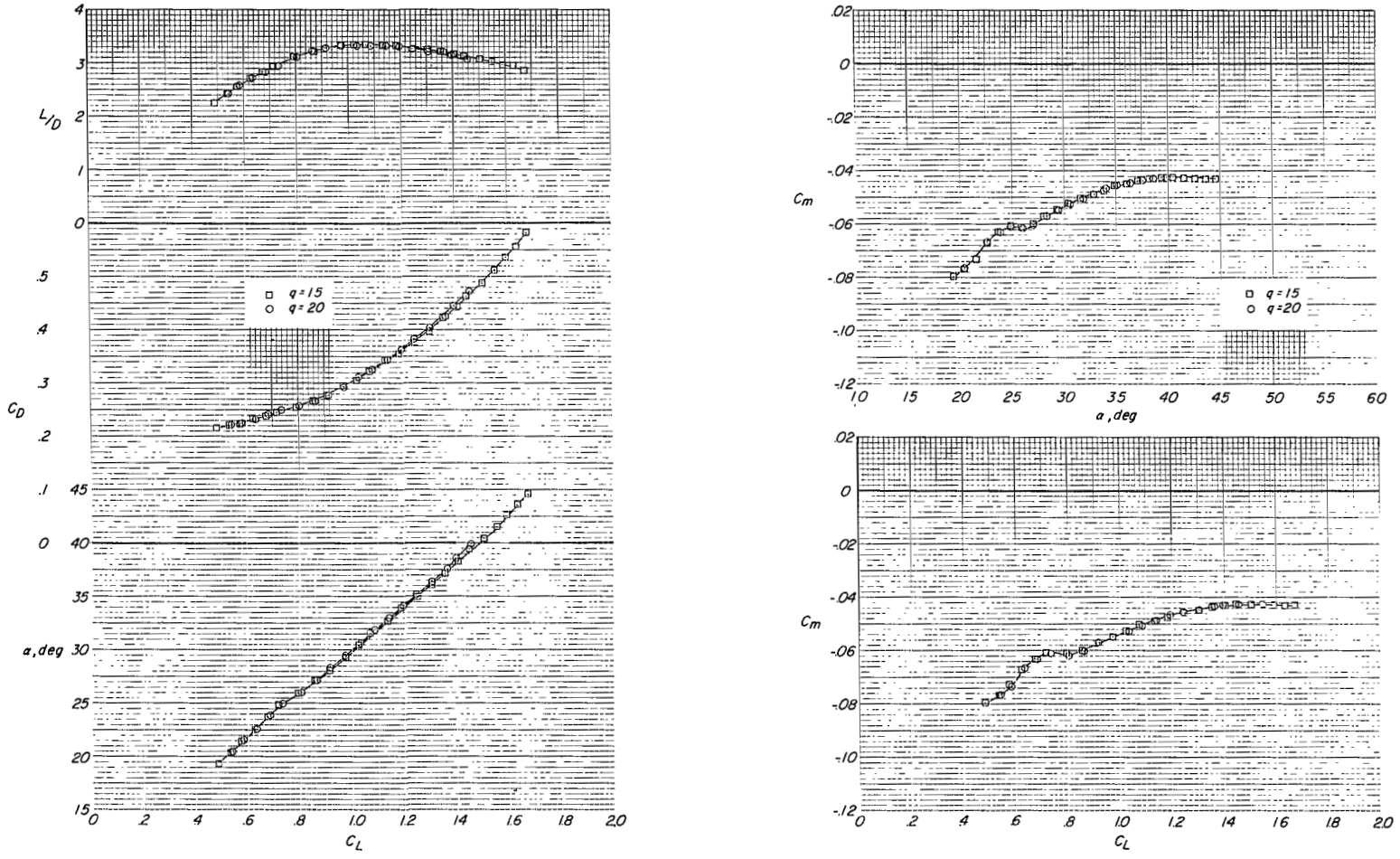

Figure 8.- Comparison of test results obtained at two values of test dynamic pressure. $\Lambda_o = 45°$; $\Lambda = 55°$; 4-percent boltrope.

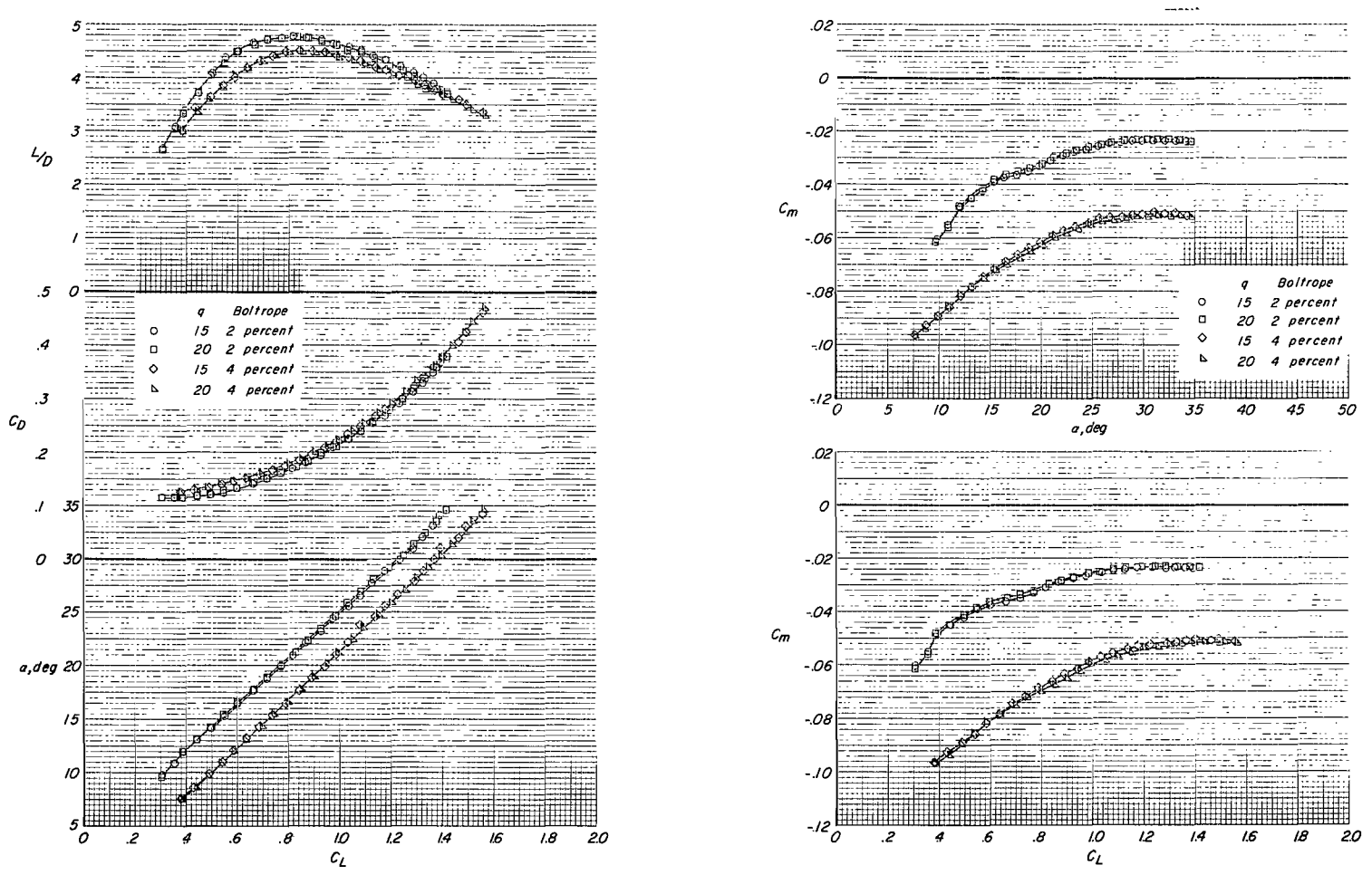

Figure 9.- Effects of test dynamic pressure and boltrope length on the aerodynamic characteristics of the $\Lambda_o = 52.5^\circ$, $\Lambda = 55^\circ$ wing.

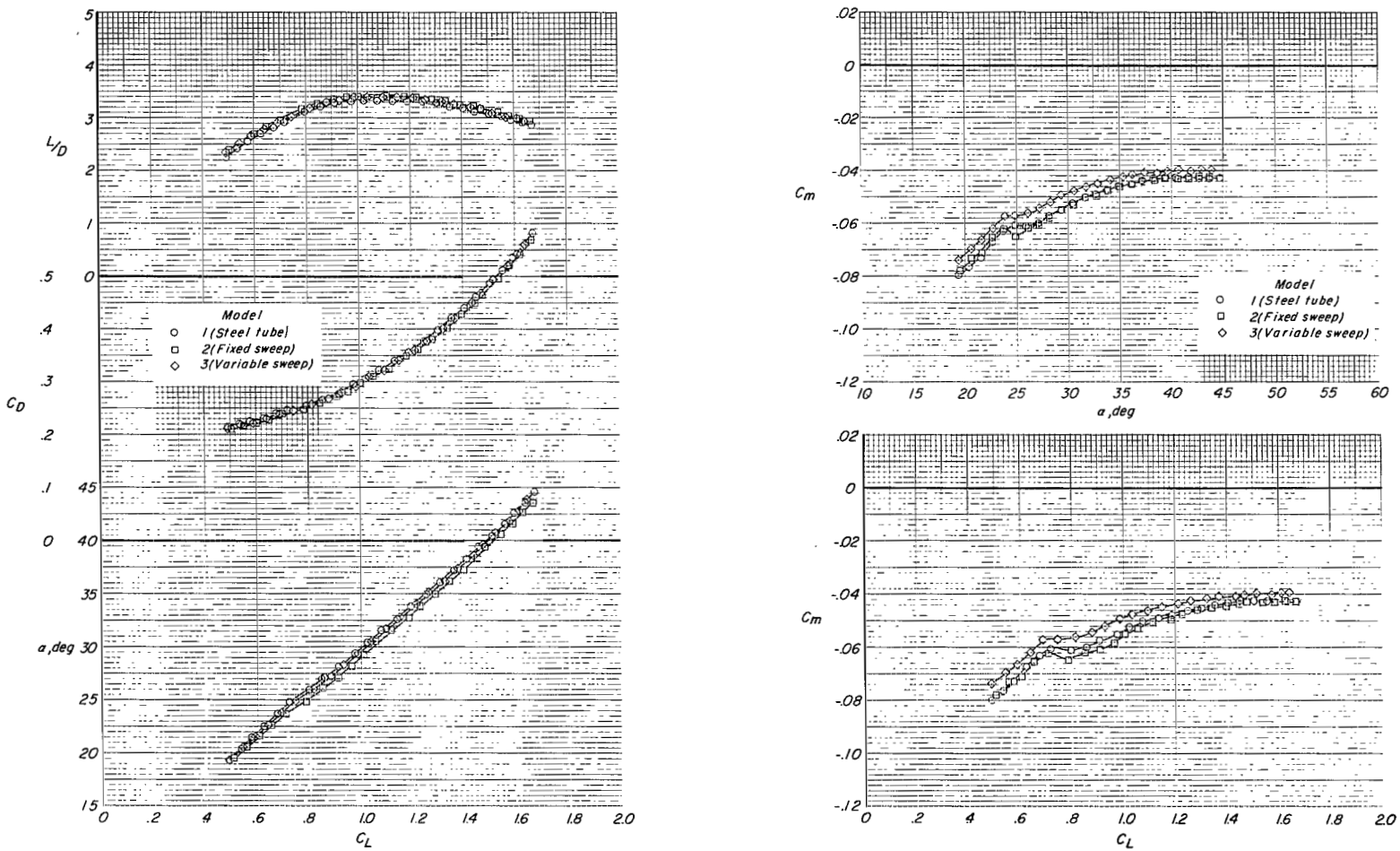

Figure 10.- Comparison of aerodynamic characteristics obtained on the three basic wings used in this investigation. Λ_o = 45°; Λ = 55°; 4-percent boltrope.

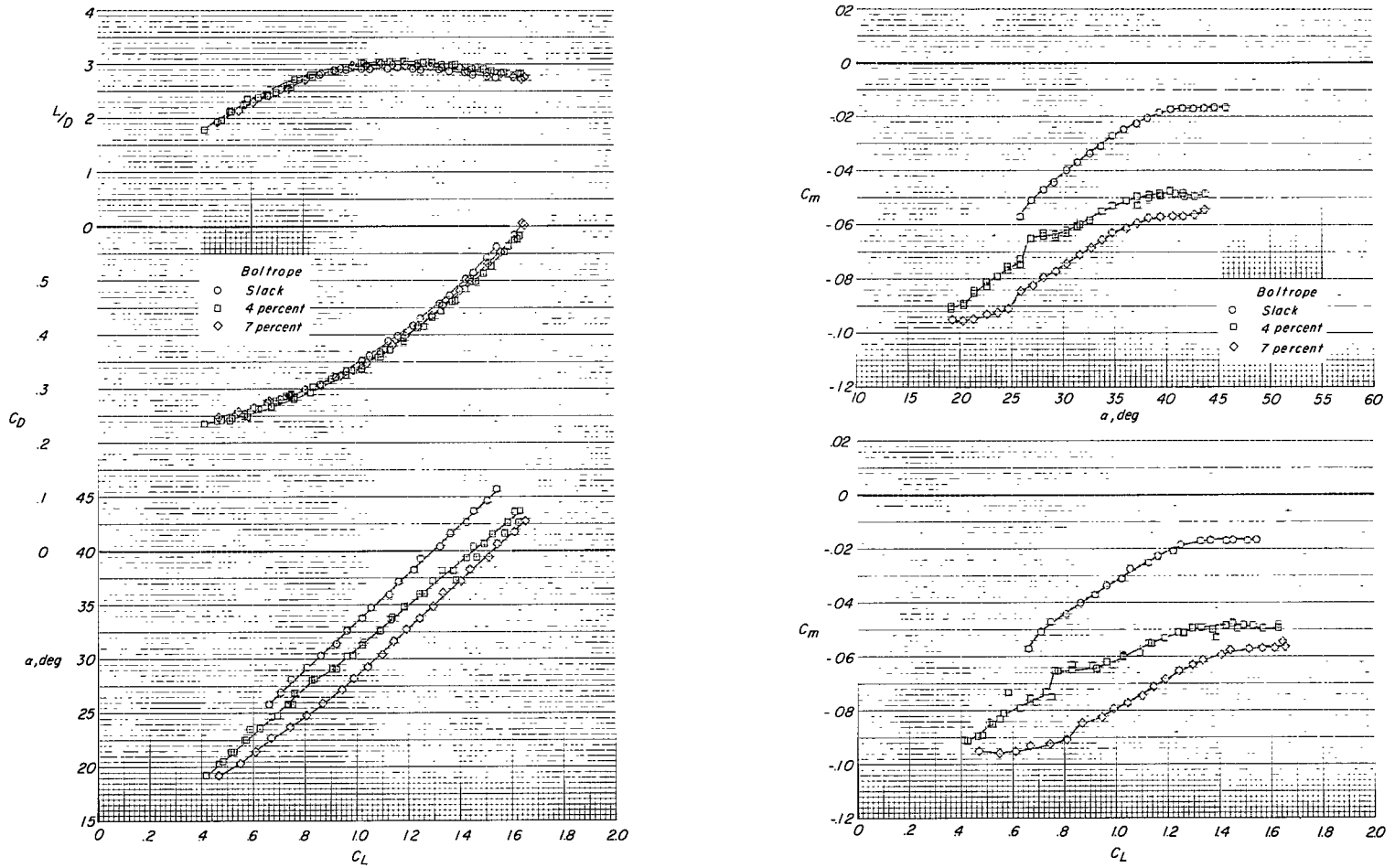

Figure 11.- Effect of boltrope length on the aerodynamic characteristics obtained on the $\Lambda_o = 42.5^o$, $\Lambda = 55^o$ wing.

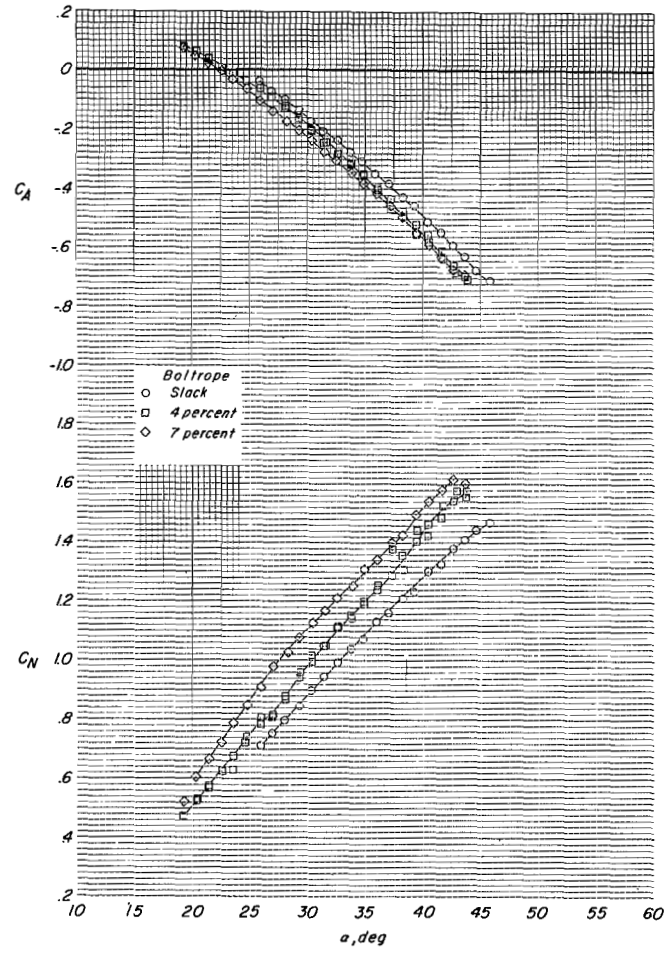

Figure 11.- Concluded.

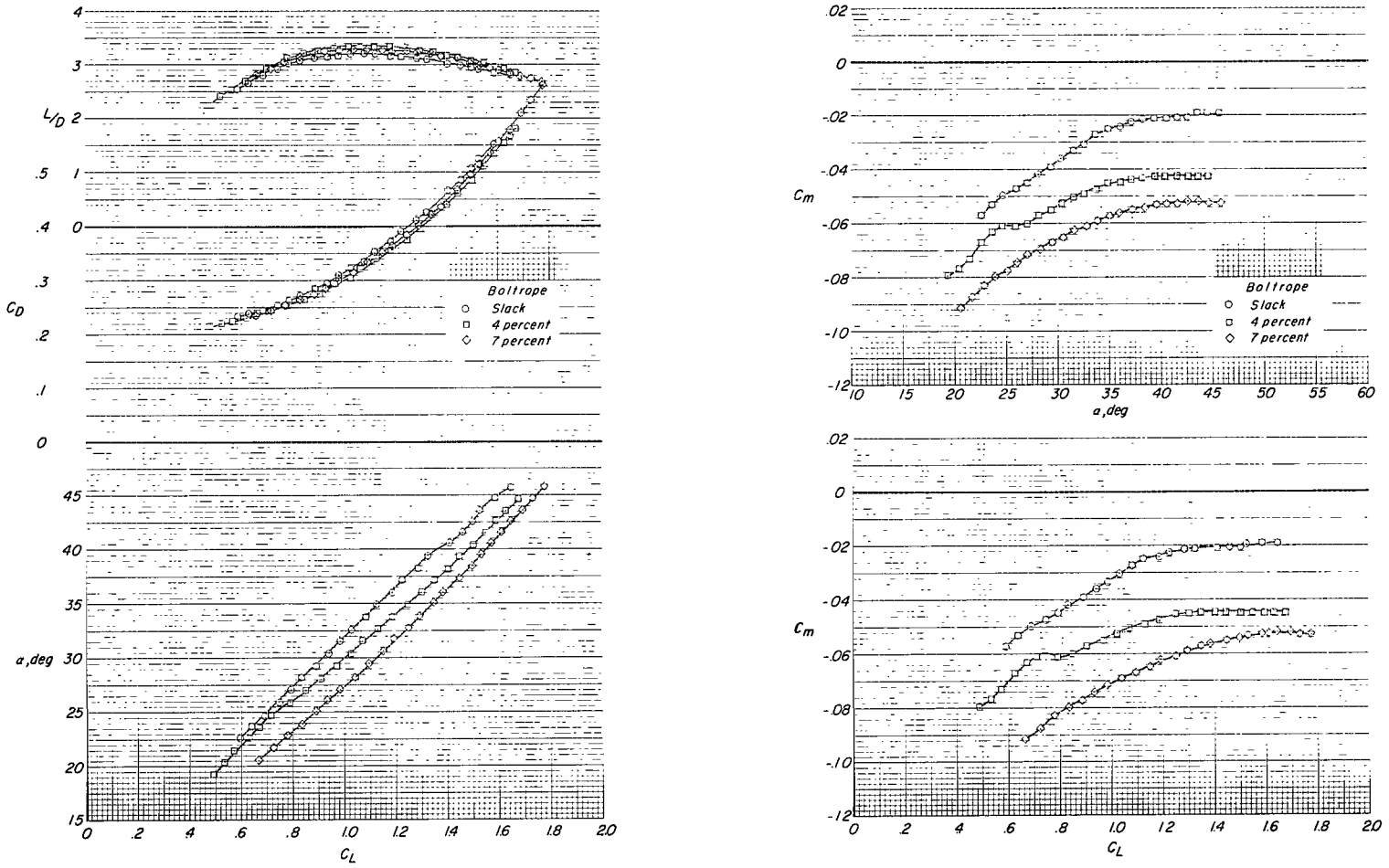

Figure 12.- Effect of boltrope length on the aerodynamic characteristics and spreader-bar load obtained on the $\Lambda_o = 45^o$, $\Lambda = 55^o$ wing.

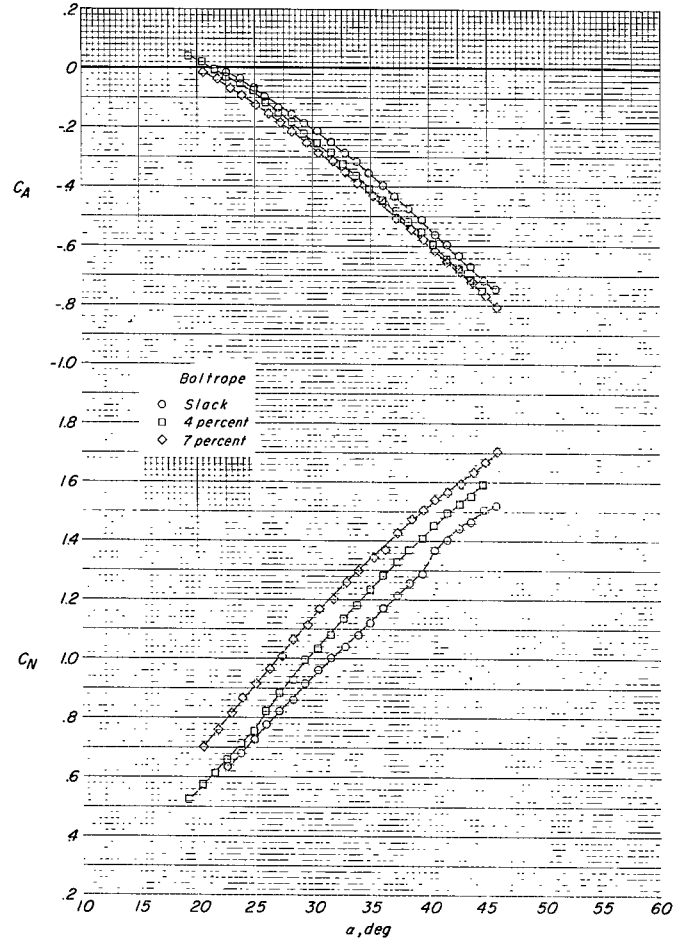

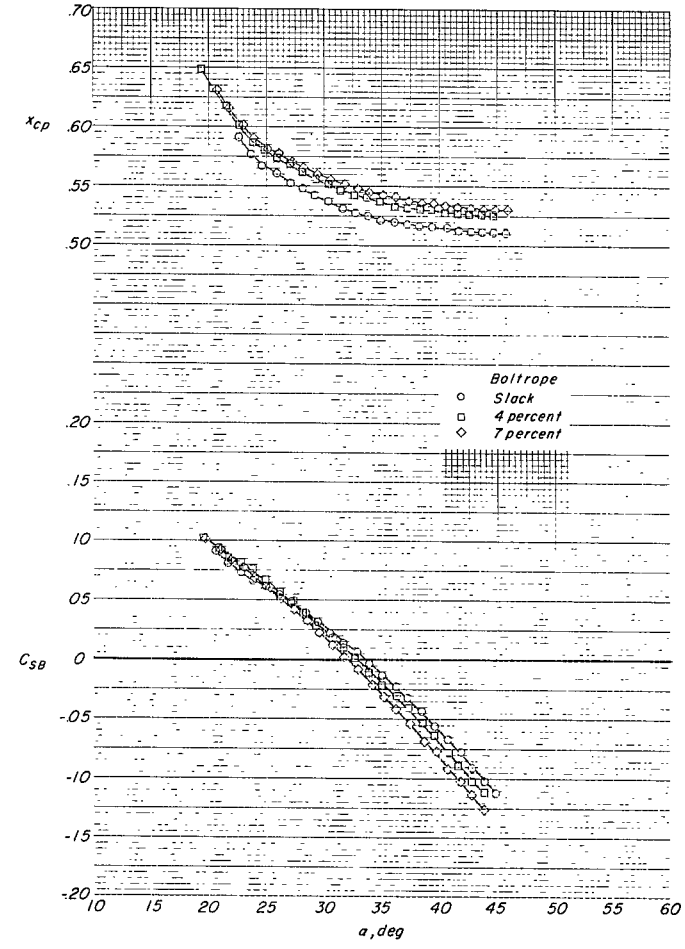

Figure 12.- Concluded.

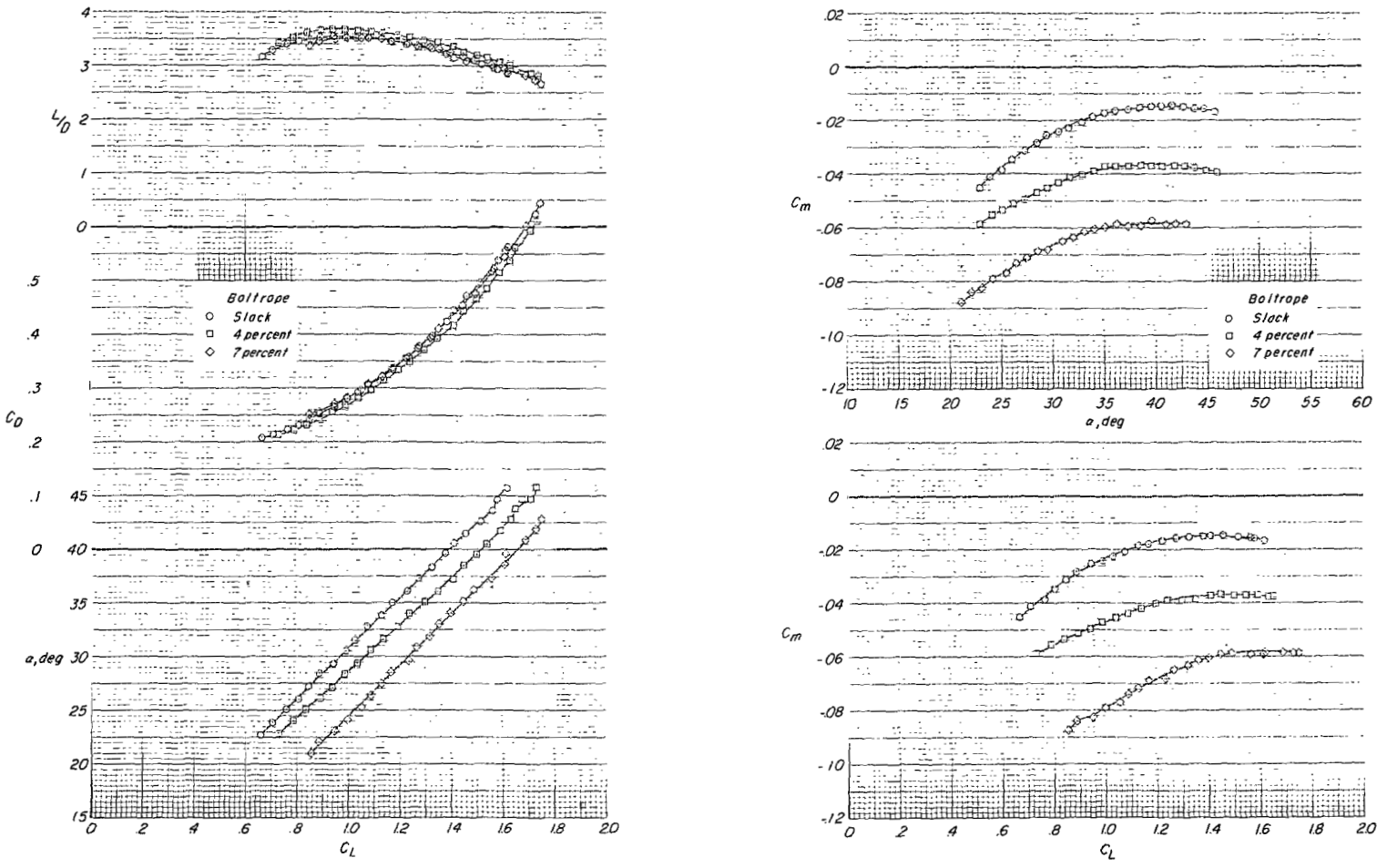

Figure 13.- Effect of boltrope length on the aerodynamic characteristics and spreader-bar load obtained on the $\Lambda_o = 47.5^o$, $\Lambda = 55^o$ wing.

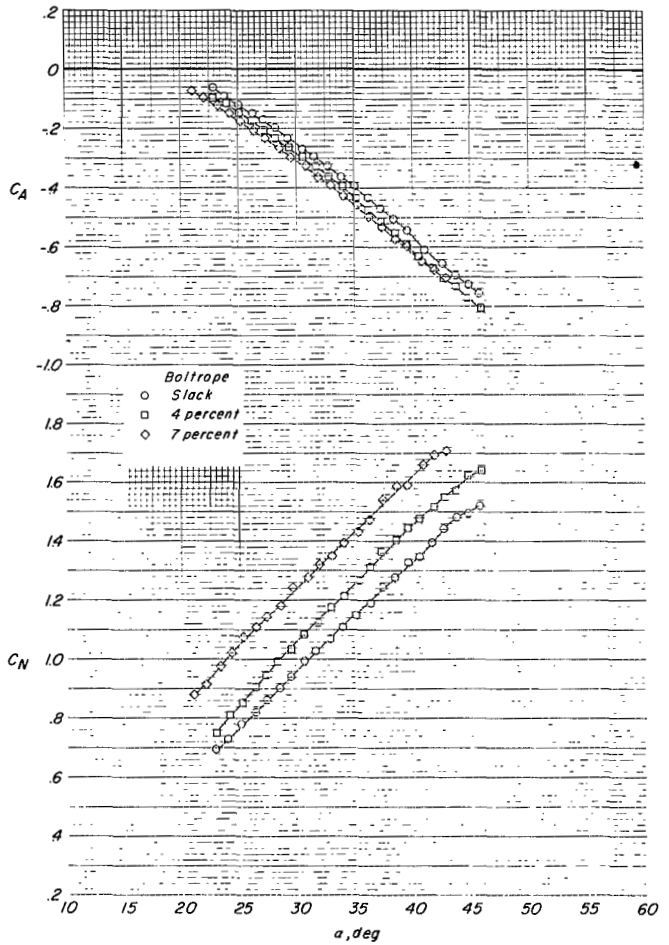

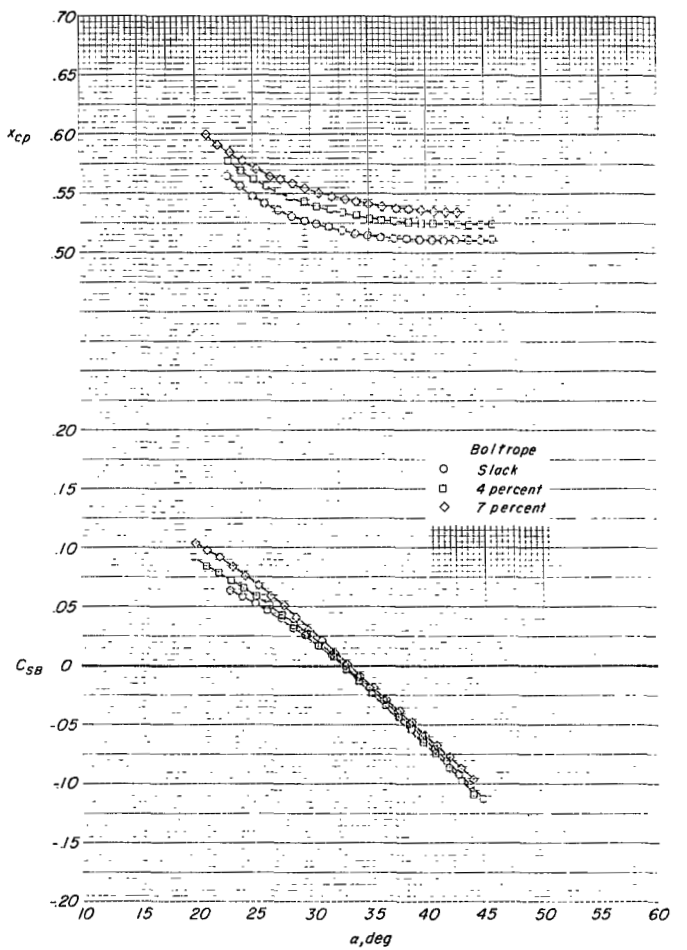

Figure 13.- Concluded.

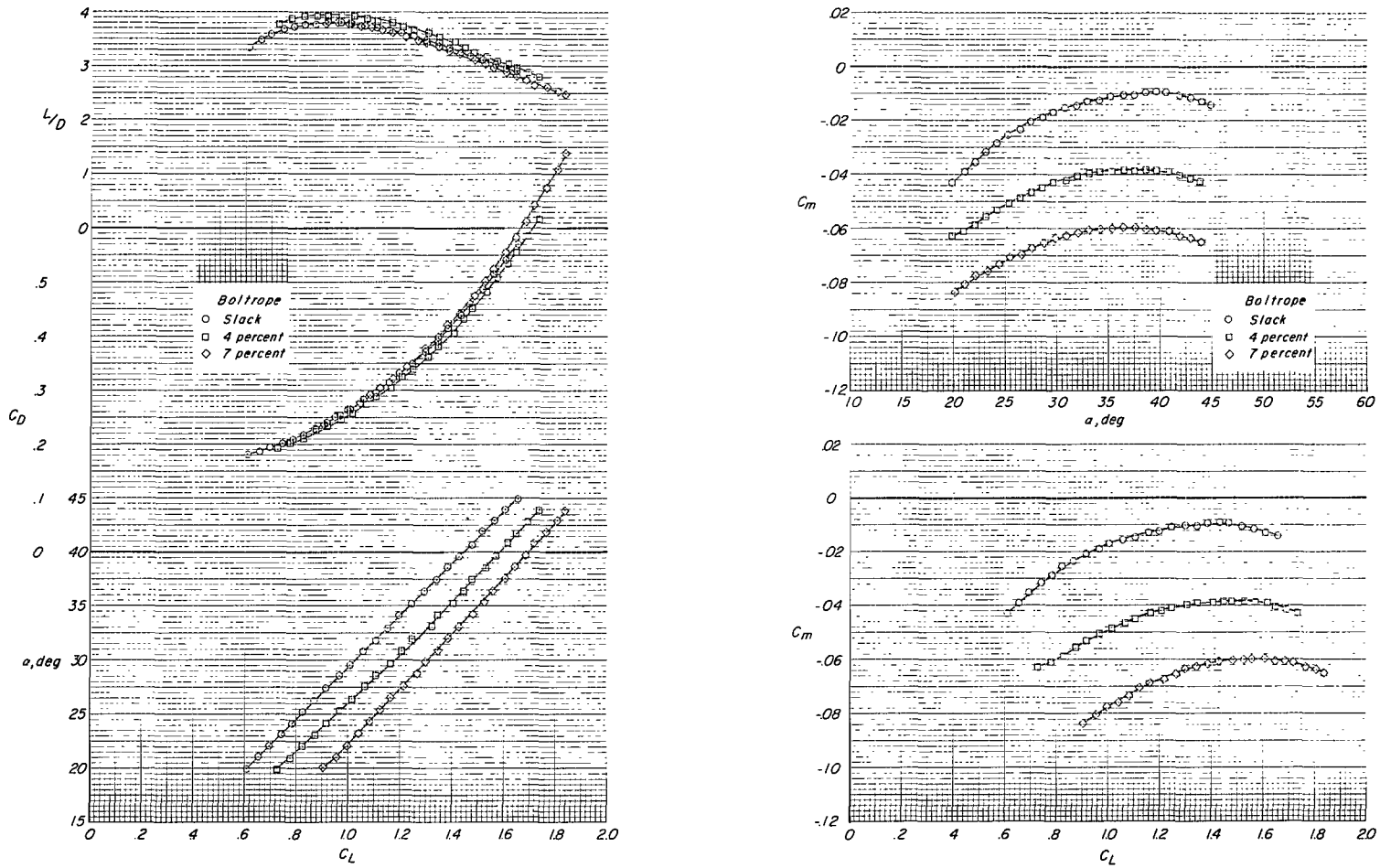

Figure 14.- Effect of boltrope length on the aerodynamic characteristics and spreader-bar load obtained on the $\Lambda_o = 50^\circ$, $\Lambda = 55^\circ$ wing.

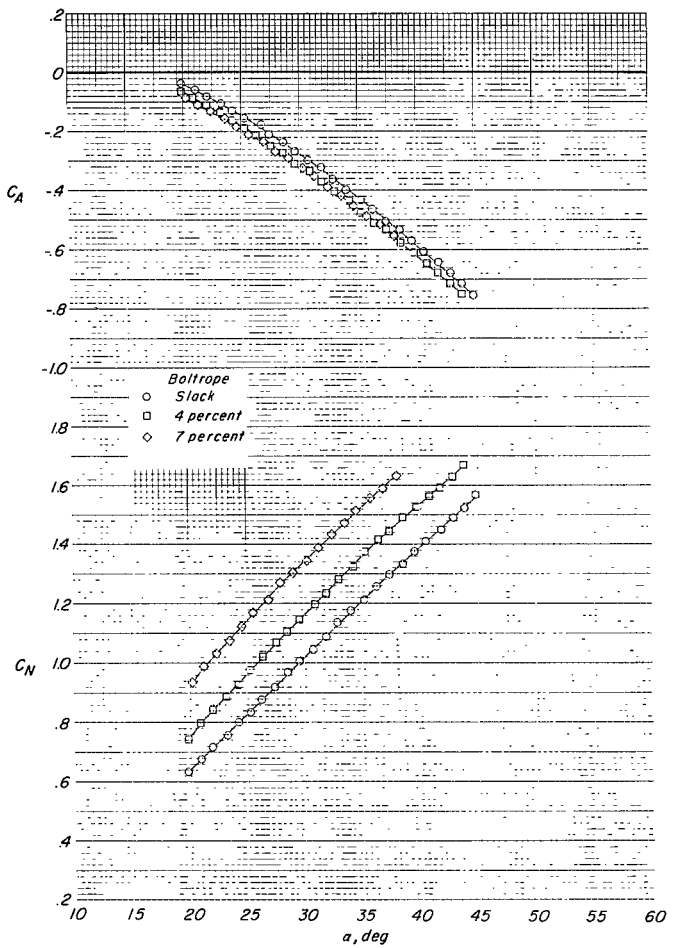

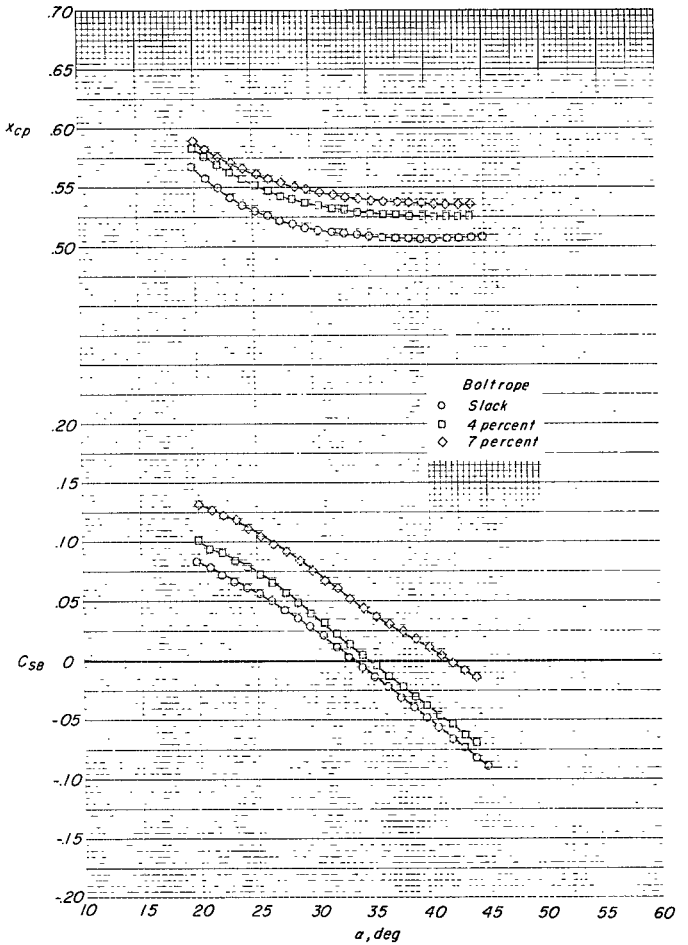

Figure 14.- Concluded.

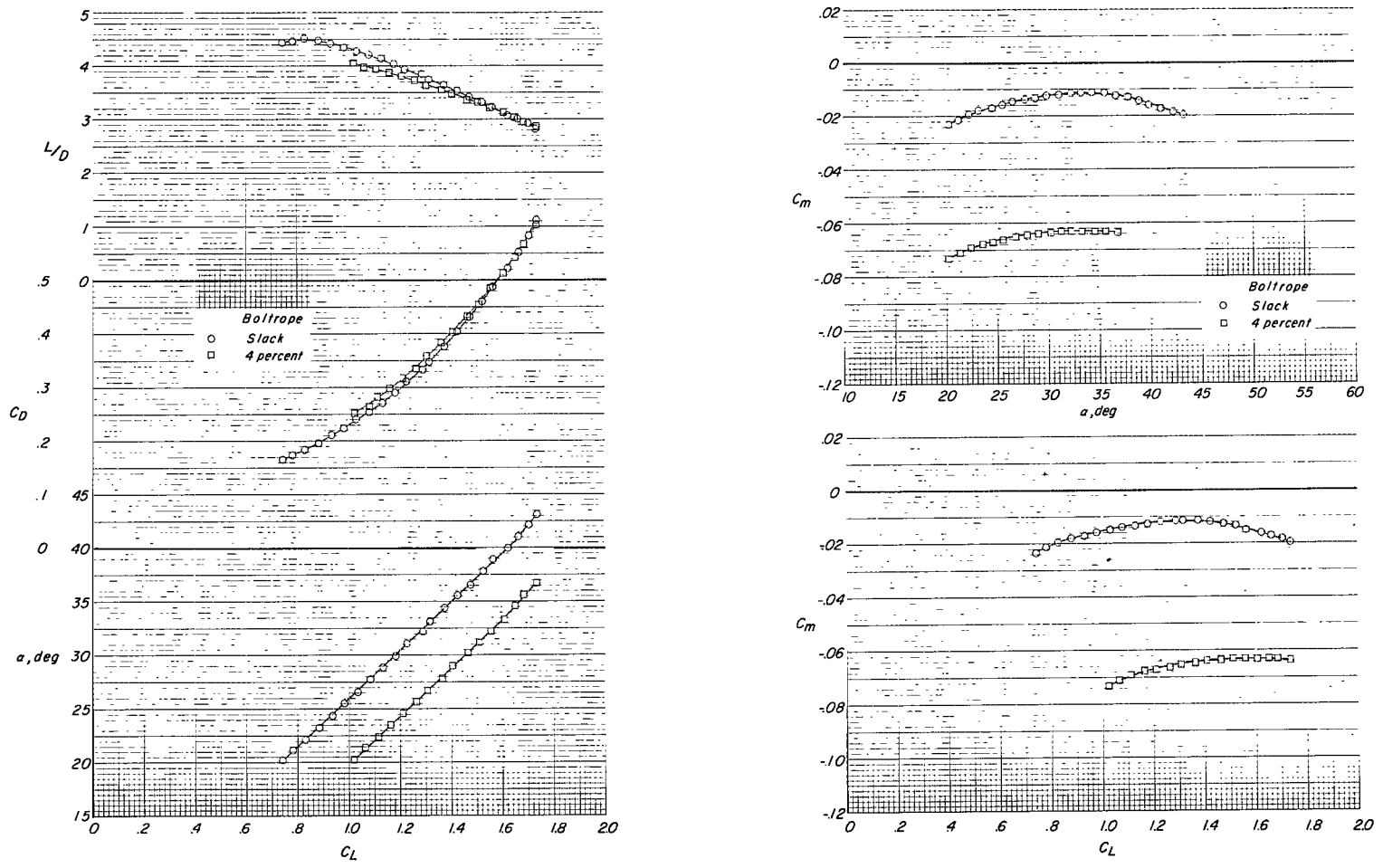

Figure 15.- Effect of two boltrope conditions on the aerodynamic characteristics and spreader-bar load of the $\Lambda_o = 52.5°$, $\Lambda = 55°$ wing.

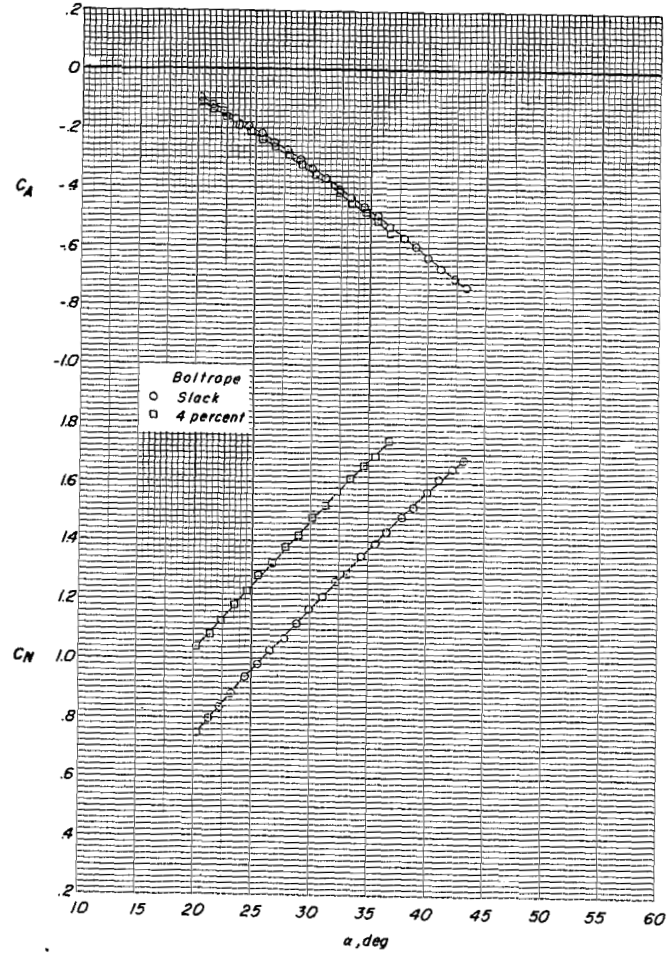

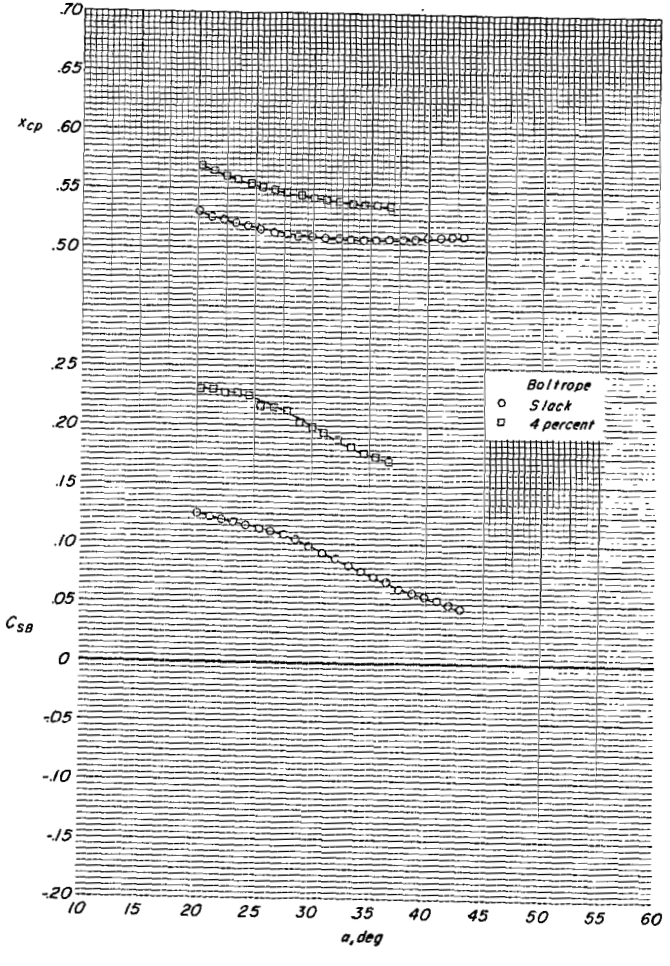

Figure 15.- Concluded.

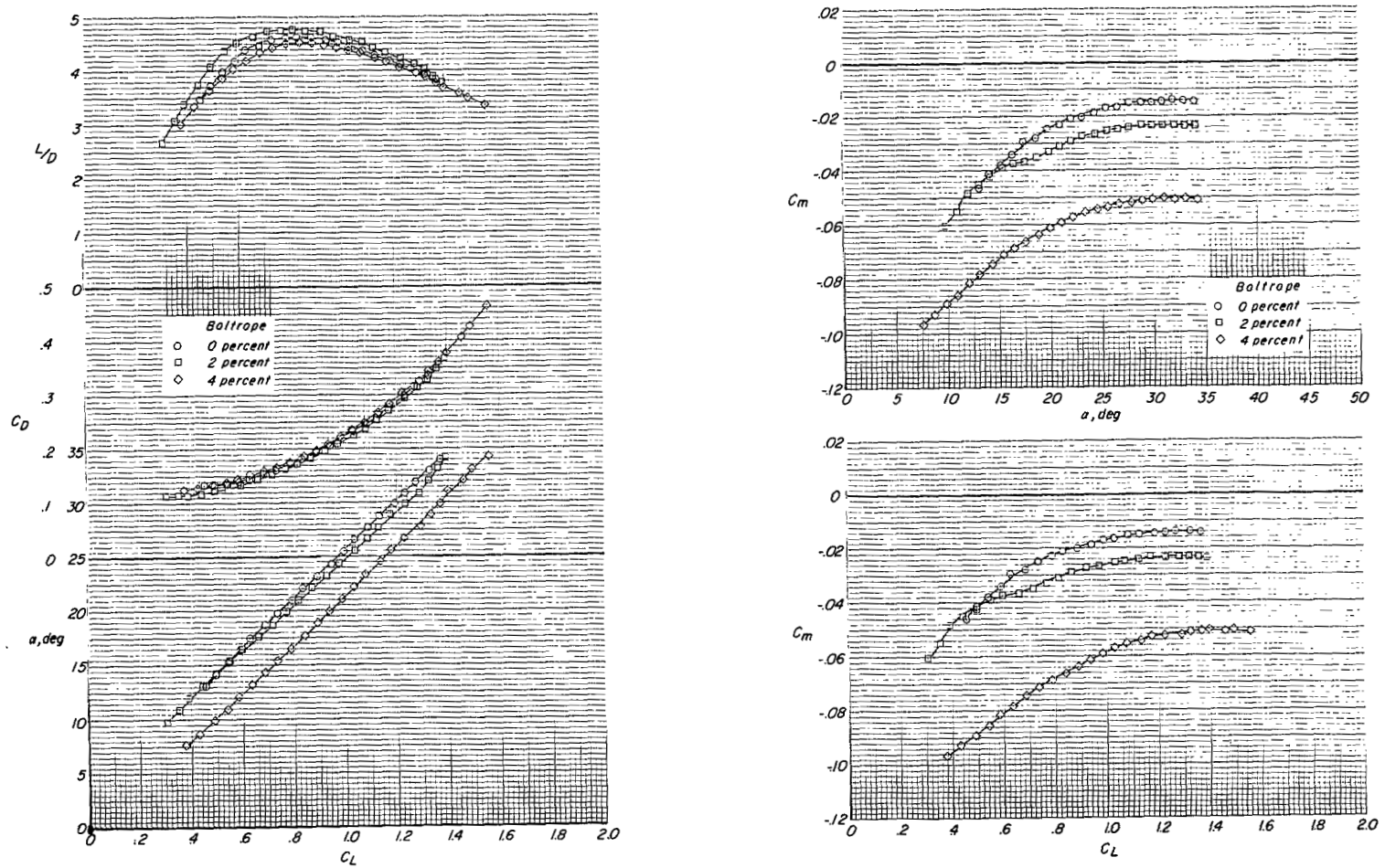

Figure 16.- Effect of boltrope length on the aerodynamic characteristics and spreader-bar load obtained on the $\Lambda_o = 52.5^o$, $\Lambda = 55^o$ wing.

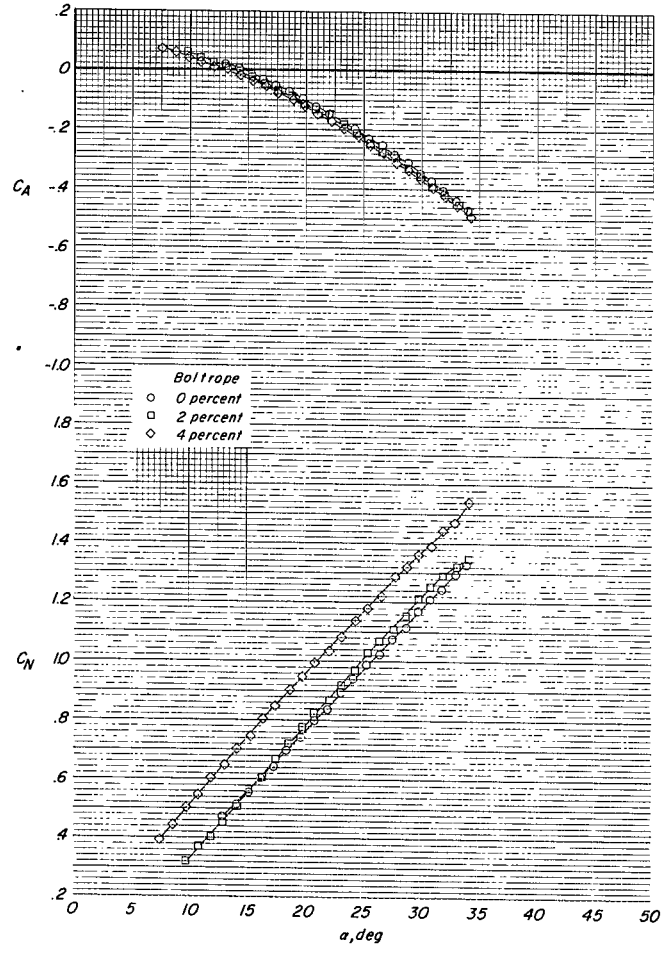

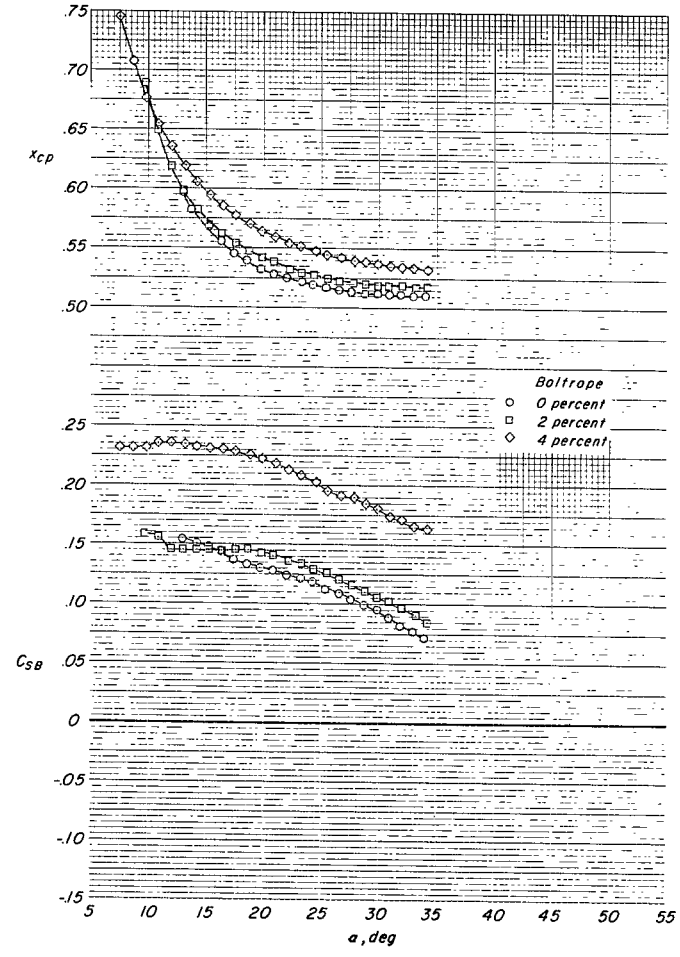

Figure 16.- Concluded.

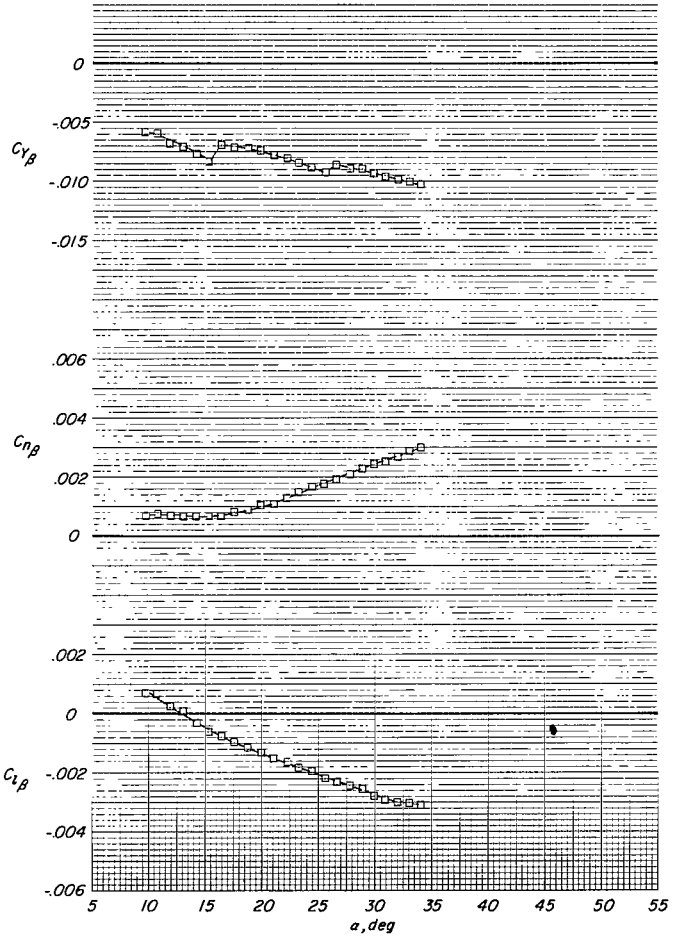

Figure 17.- Lateral stability derivatives of the $\Lambda_o = 52.5^o$, $\Lambda = 55^o$ wing with 2-percent boltrope.

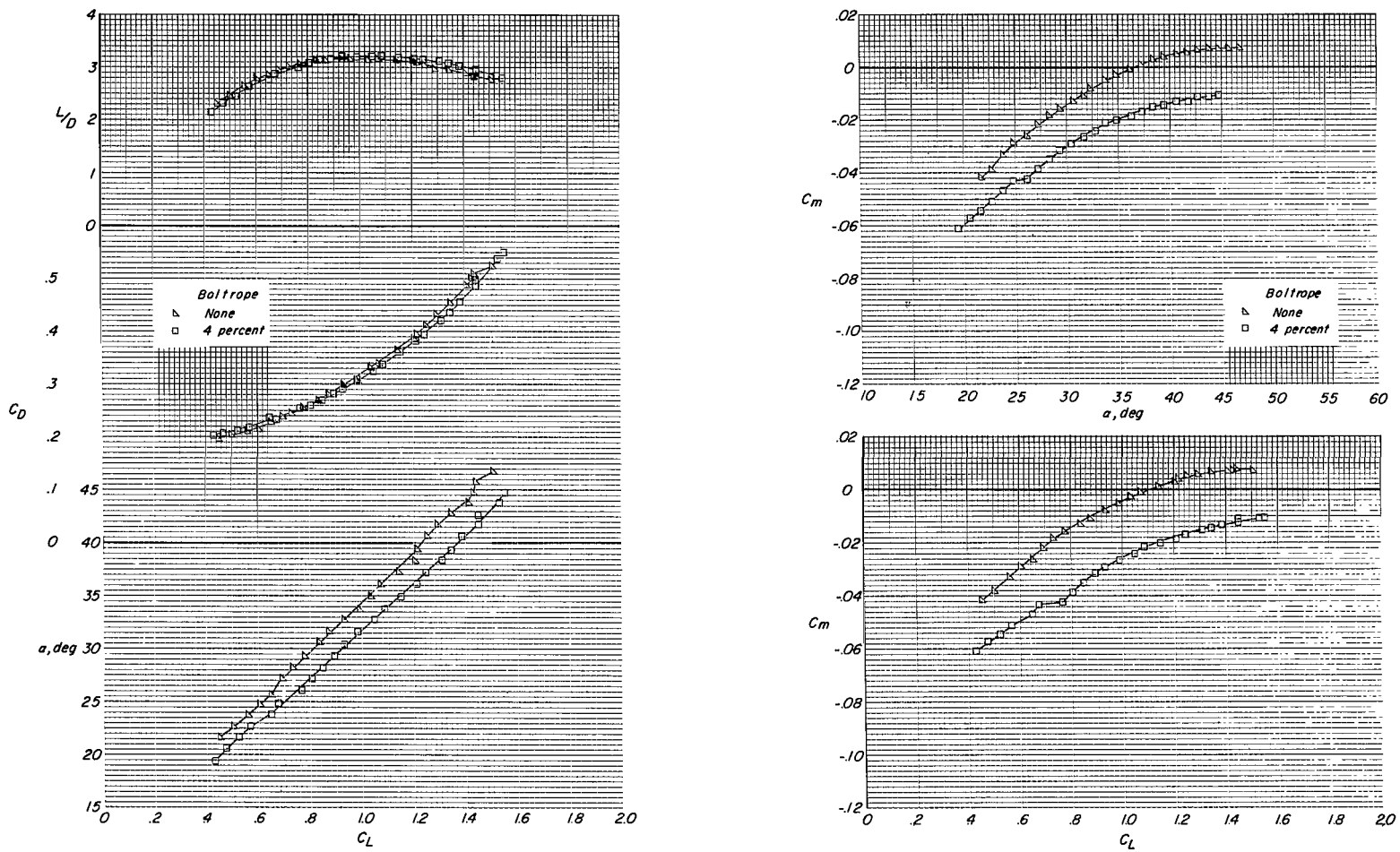

Figure 18.- Aerodynamic characteristics and spreader-bar load of the $\Lambda_o = 45^\circ$, $\Lambda = 55^\circ$ wing with the scalloped trailing edge for 4-percent boltrope and no boltrope in the trailing edge.

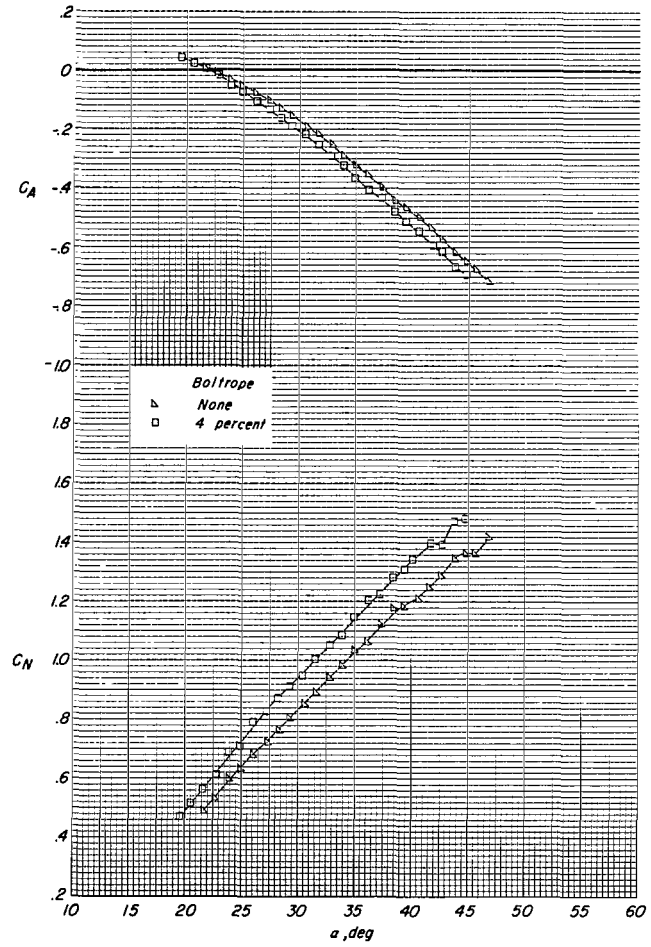

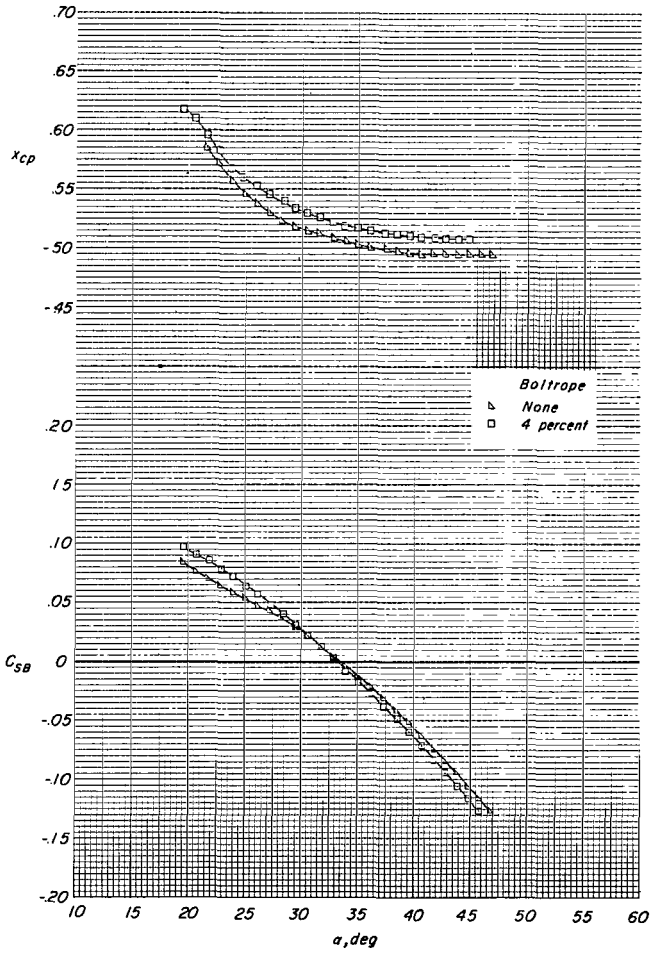

Figure 18.- Concluded.

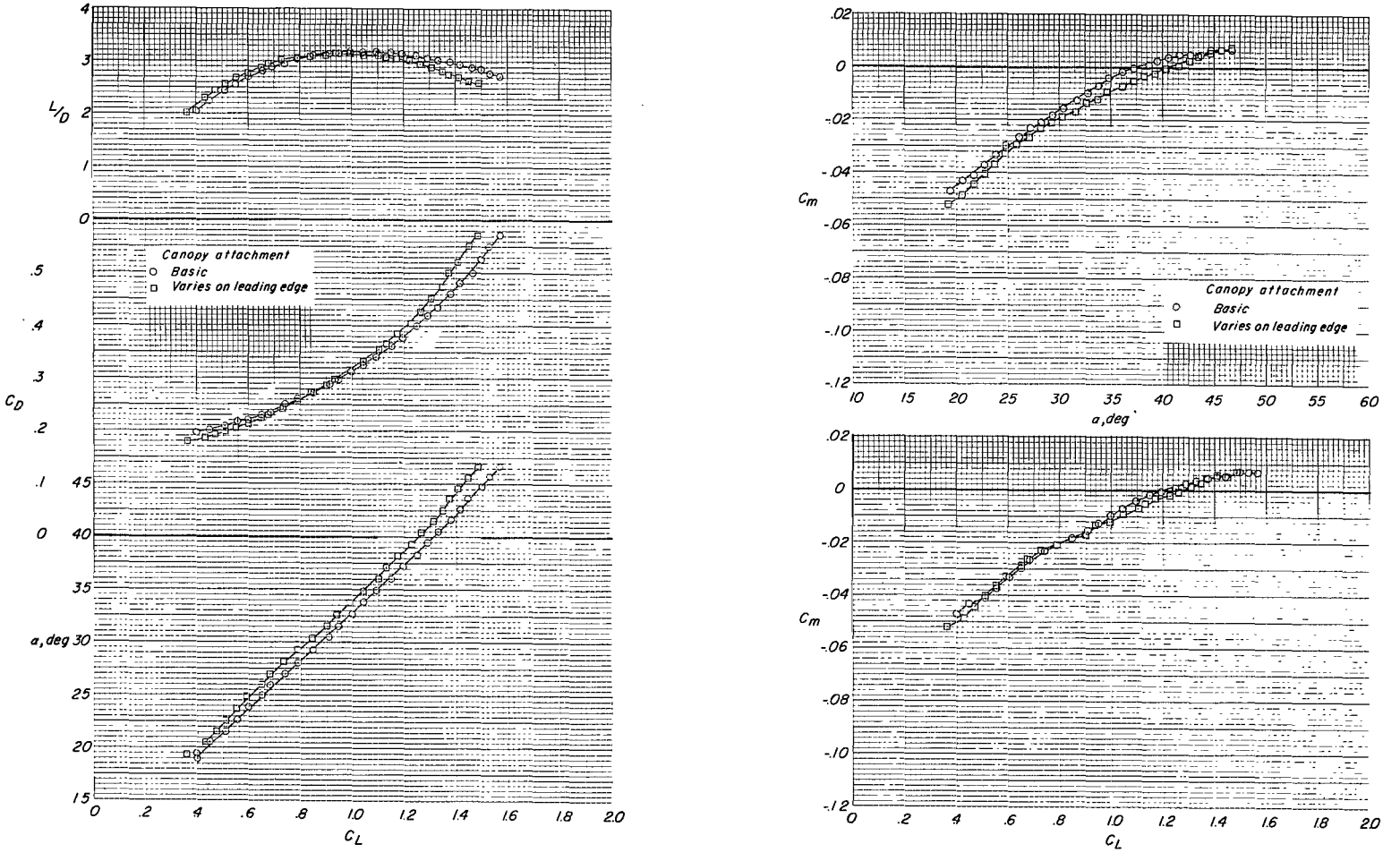

Figure 19.- Effect on aerodynamic characteristics of varying the canopy attachment location to the wing leading edge. $\Lambda_o = 45^\circ$, $\Lambda = 55^\circ$ wing with the scalloped trailing edge; no boltrope in the trailing edge.

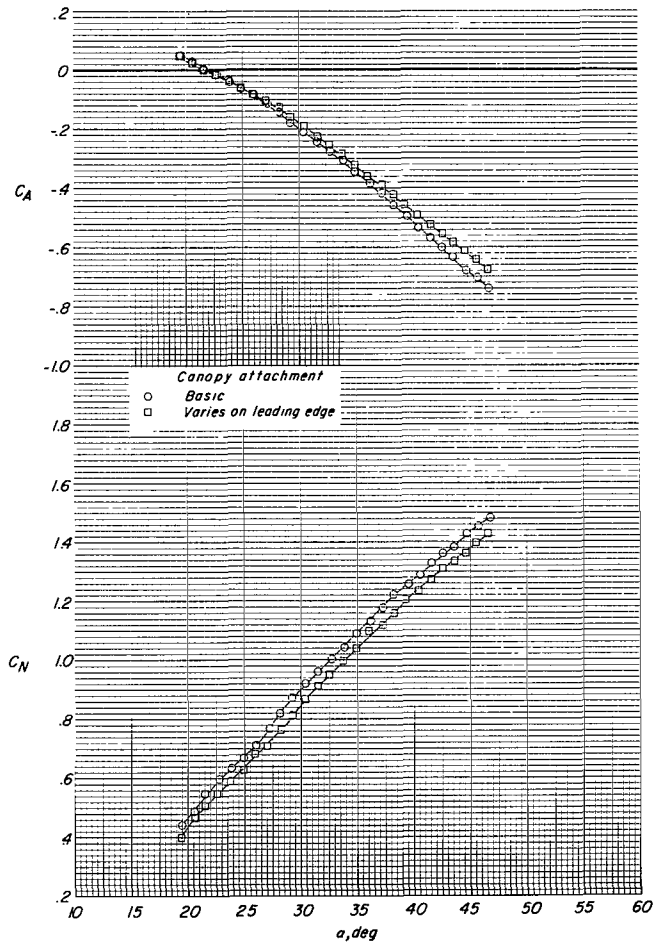

Figure 19.- Concluded.

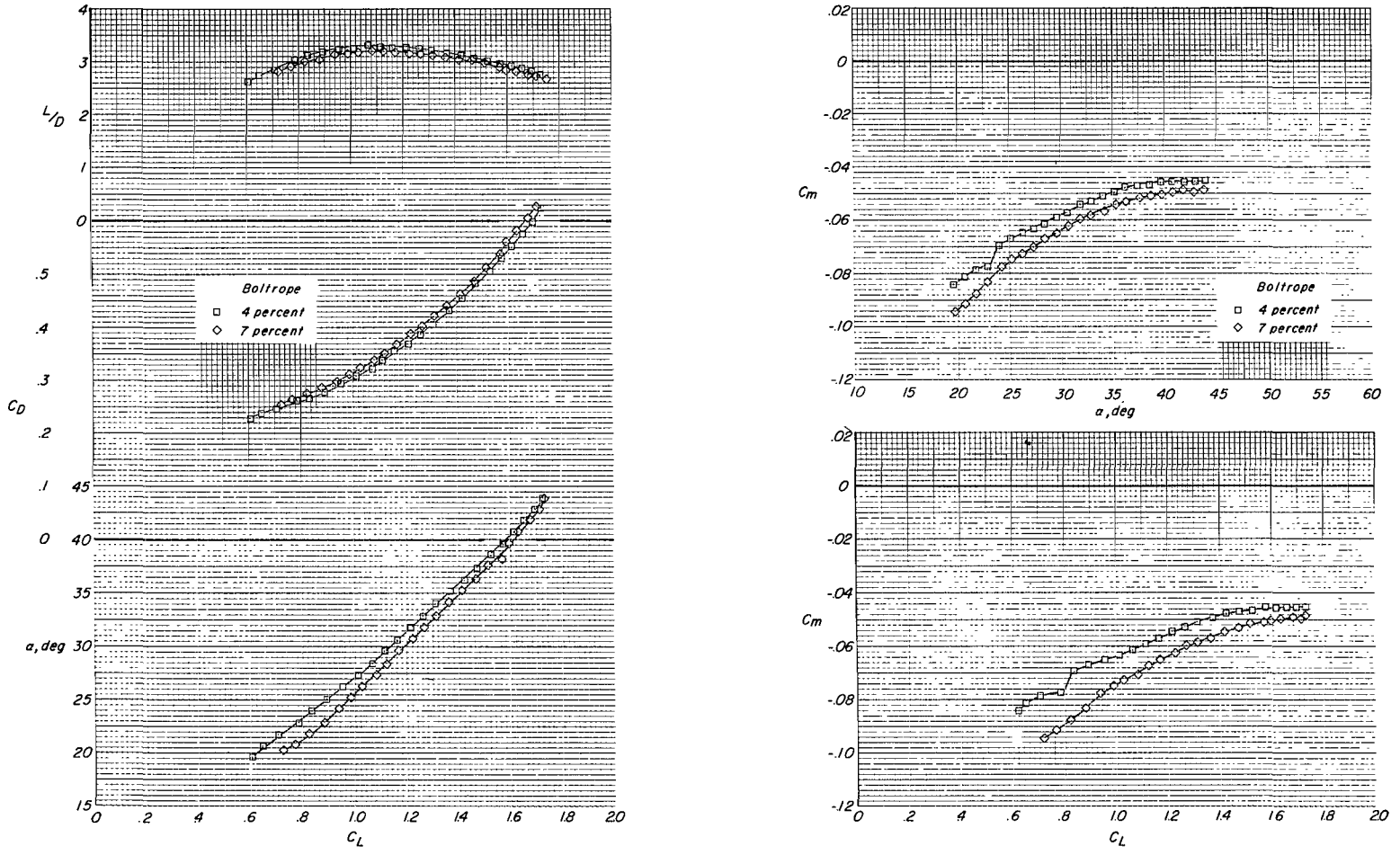

Figure 20.- Effect of boltrope length on the aerodynamic characteristics and spreader-bar load of the $\Lambda_o = 42.5^o$, $\Lambda = 55^o$ wing modified by removing a single gore from the rear part of each canopy lobe.

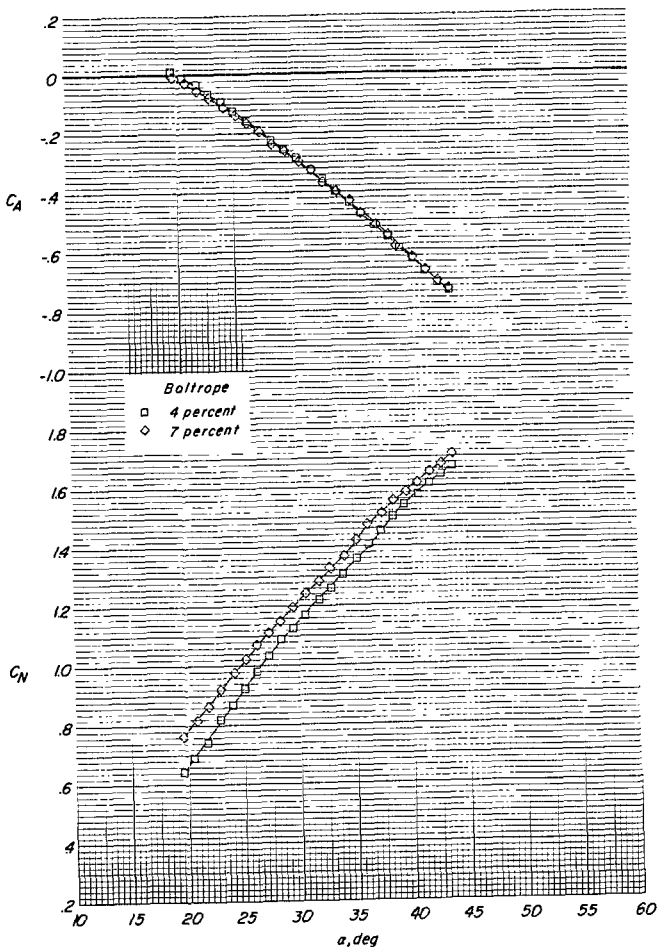

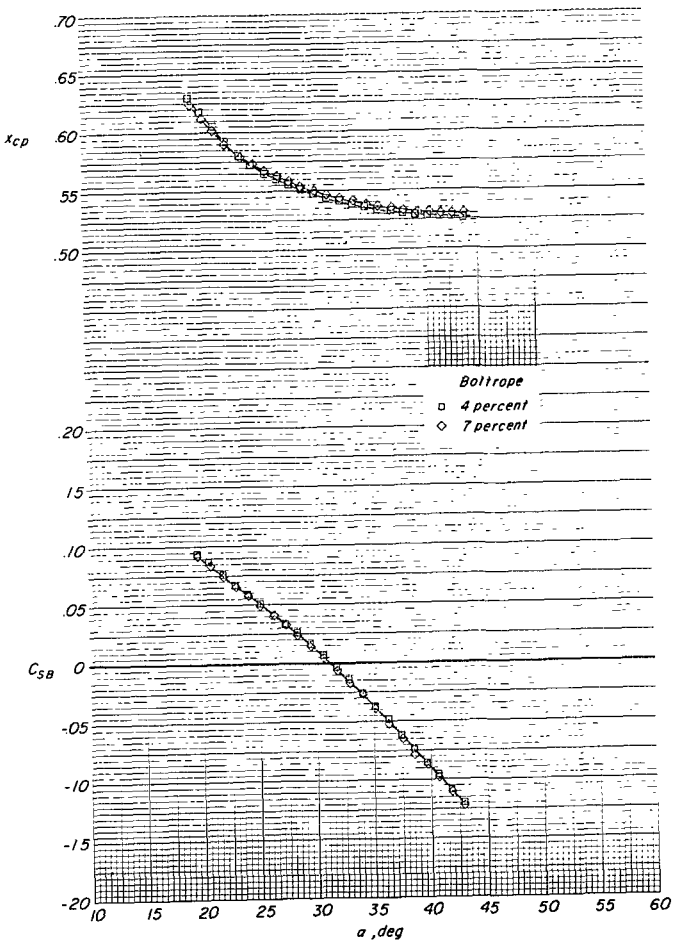

Figure 20.- Concluded.

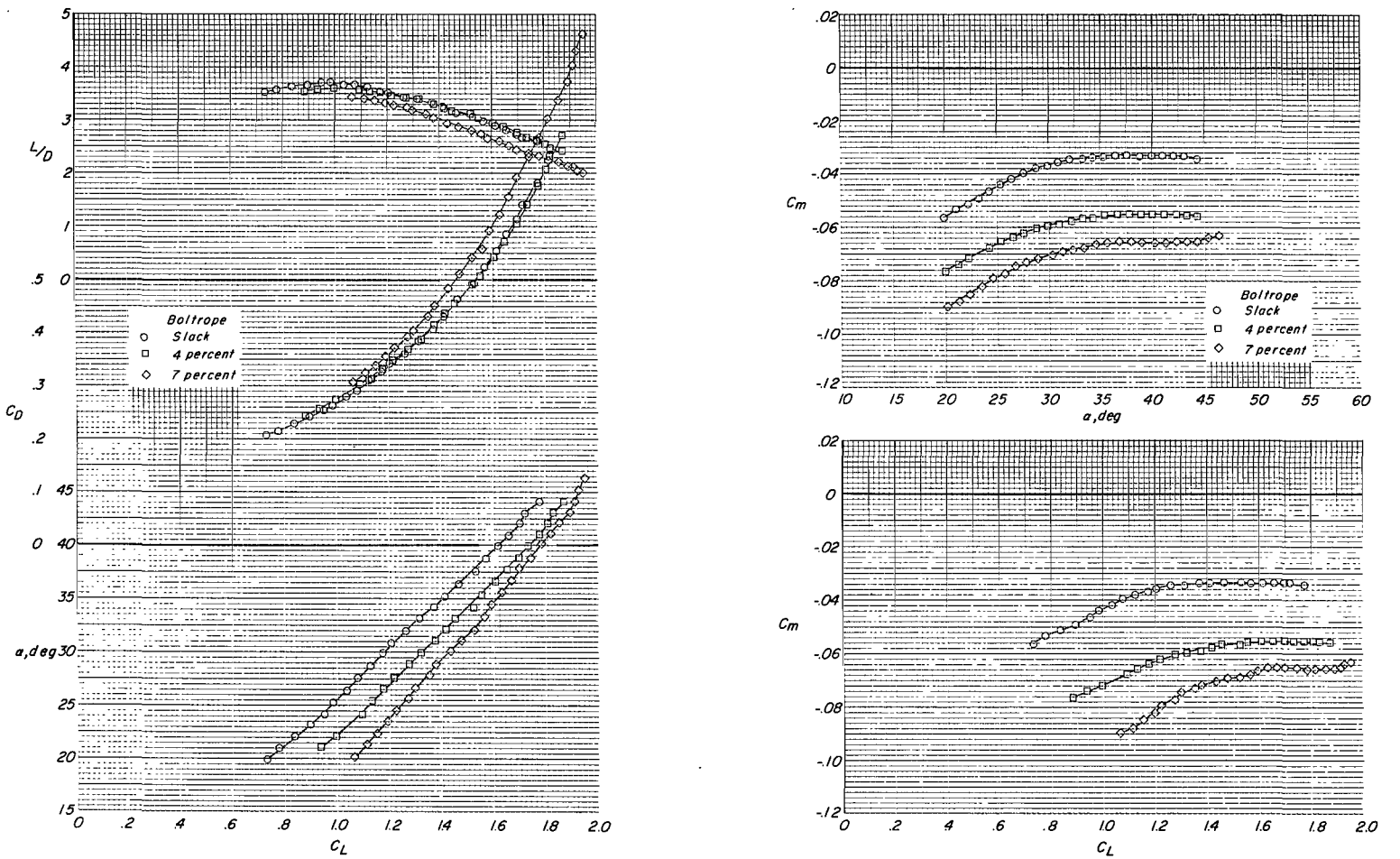

Figure 21.- Effect of boltrope length on the aerodynamic characteristics and spreader-bar load of the $\Lambda_o = 45^o$, $\Lambda = 55^o$ wing modified by removing a single gore from the rear part of each canopy lobe.

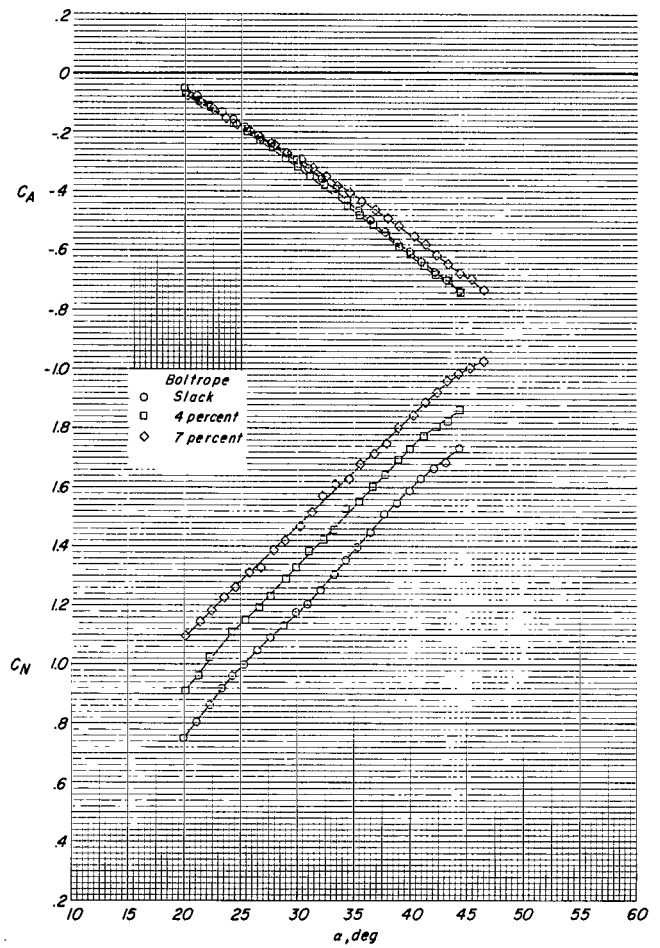

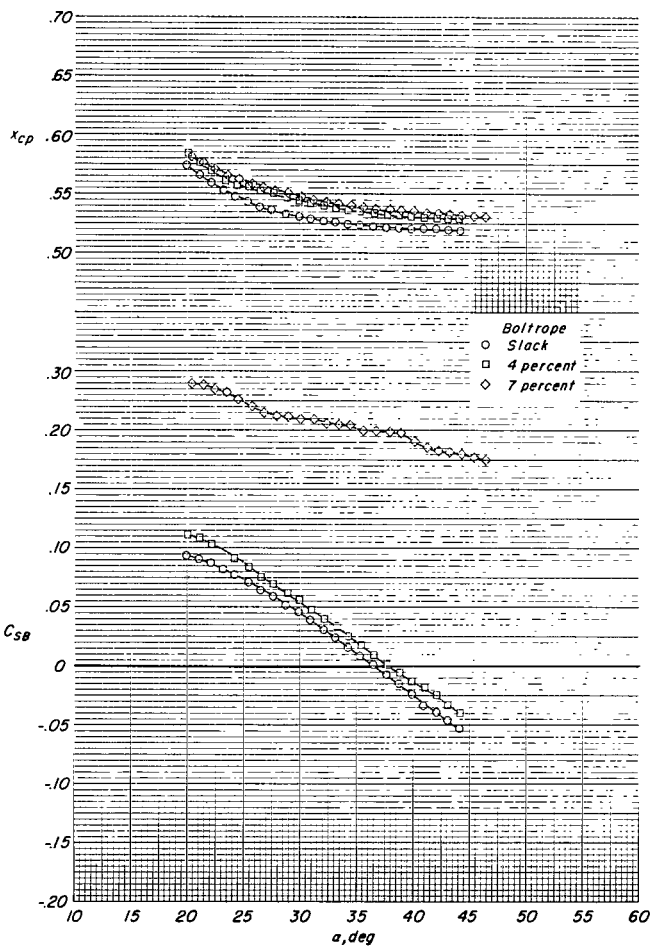

Figure 21.- Concluded.

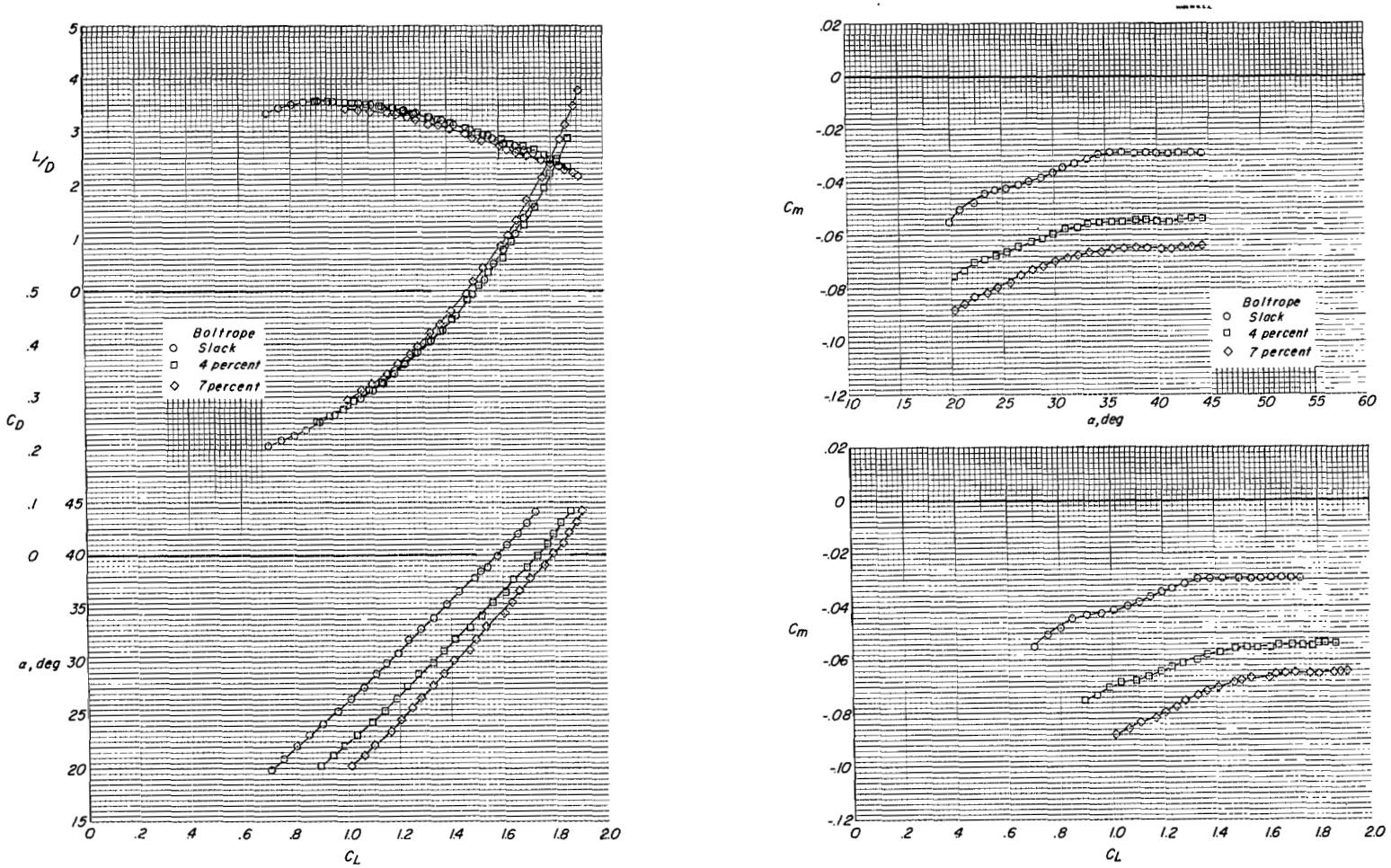

Figure 22.- Effect of boltrope length on the aerodynamic characteristics and spreader-bar load of the $\Lambda_o = 45^\circ$, $\Lambda = 55^\circ$ wing modified by removing two gores from the rear part of each canopy lobe.

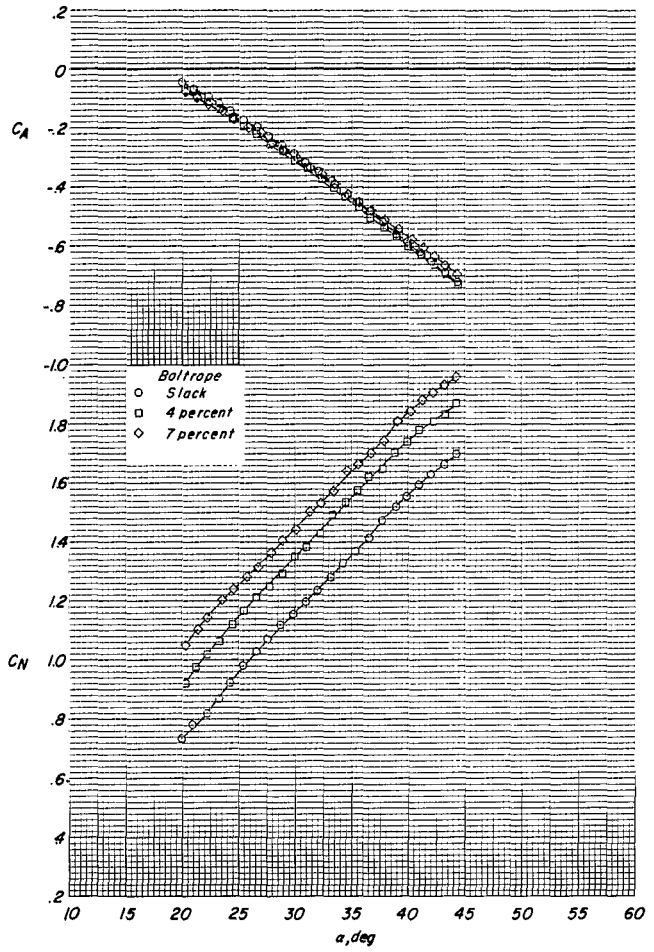

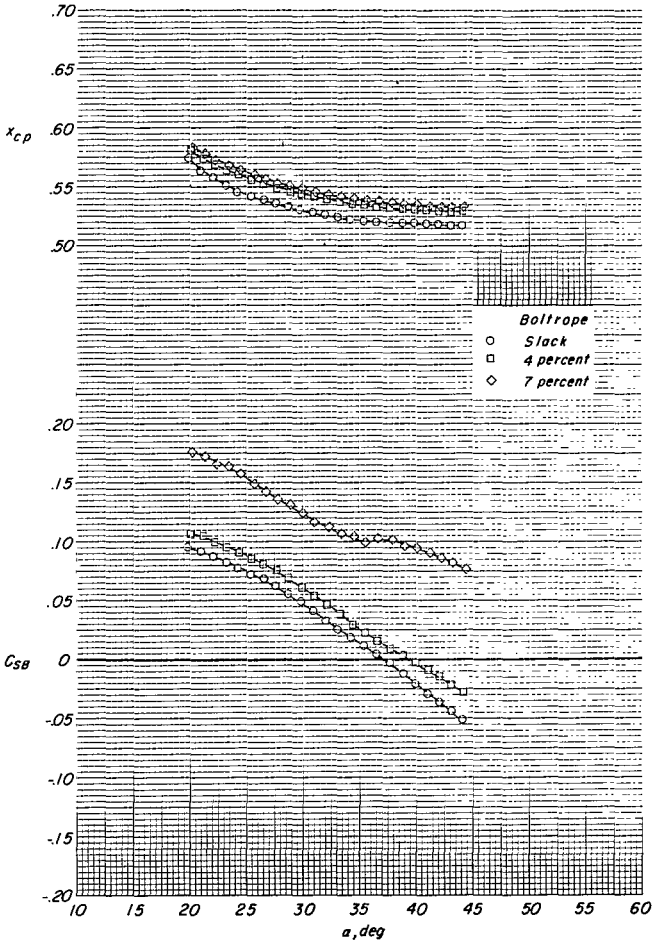

Figure 22.- Concluded.

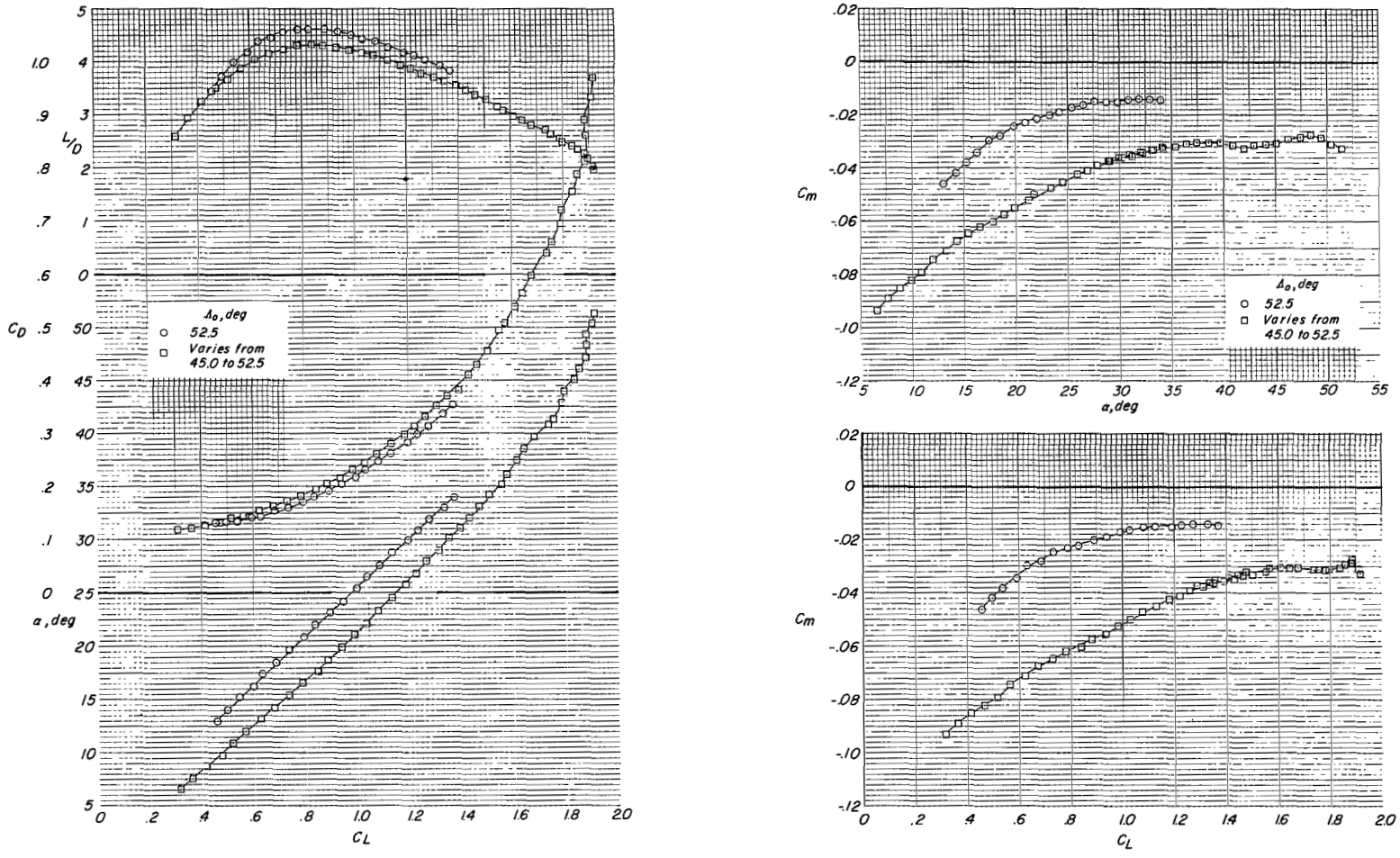

Figure 23.- Comparison of aerodynamic characteristics and spreader-bar load for the $\Lambda = 55^{\circ}$ wing having a basic $\Lambda_o = 52.5^{\circ}$ flat-pattern sweep (0-percent boltrope) and a modified canopy having a single compound gore removed from each canopy lobe.

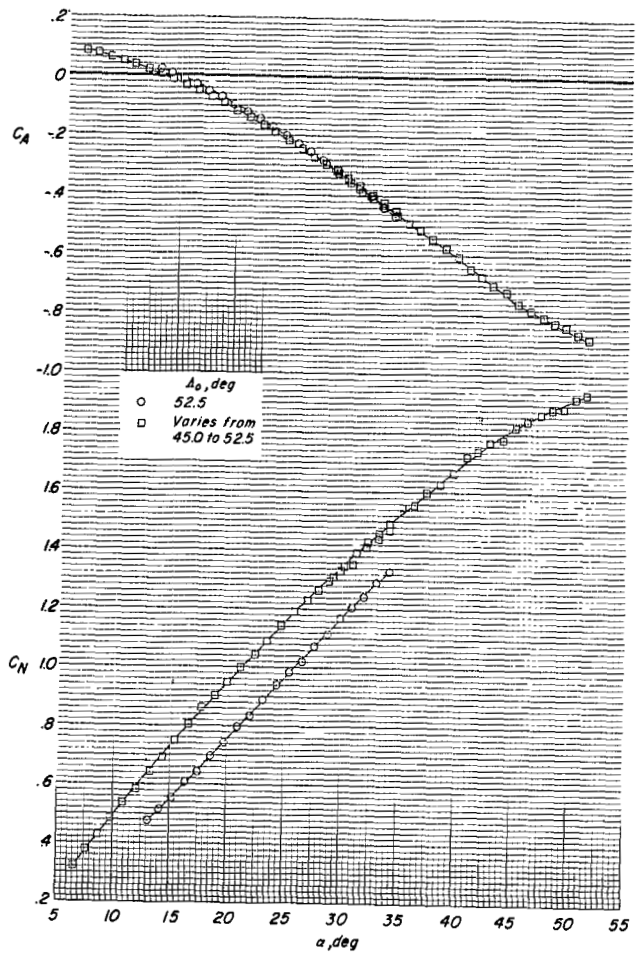

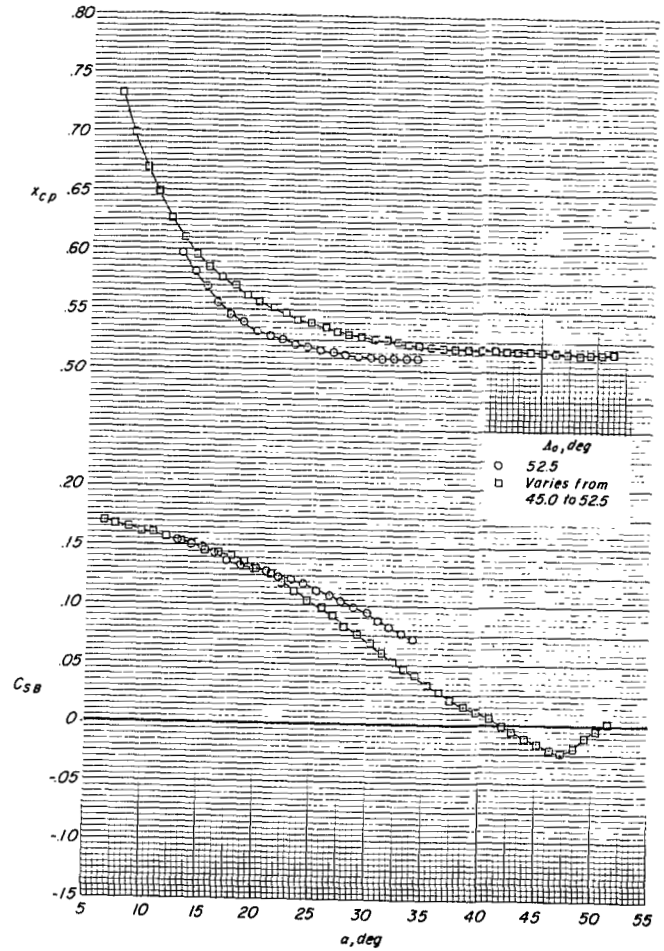

Figure 23.- Concluded.

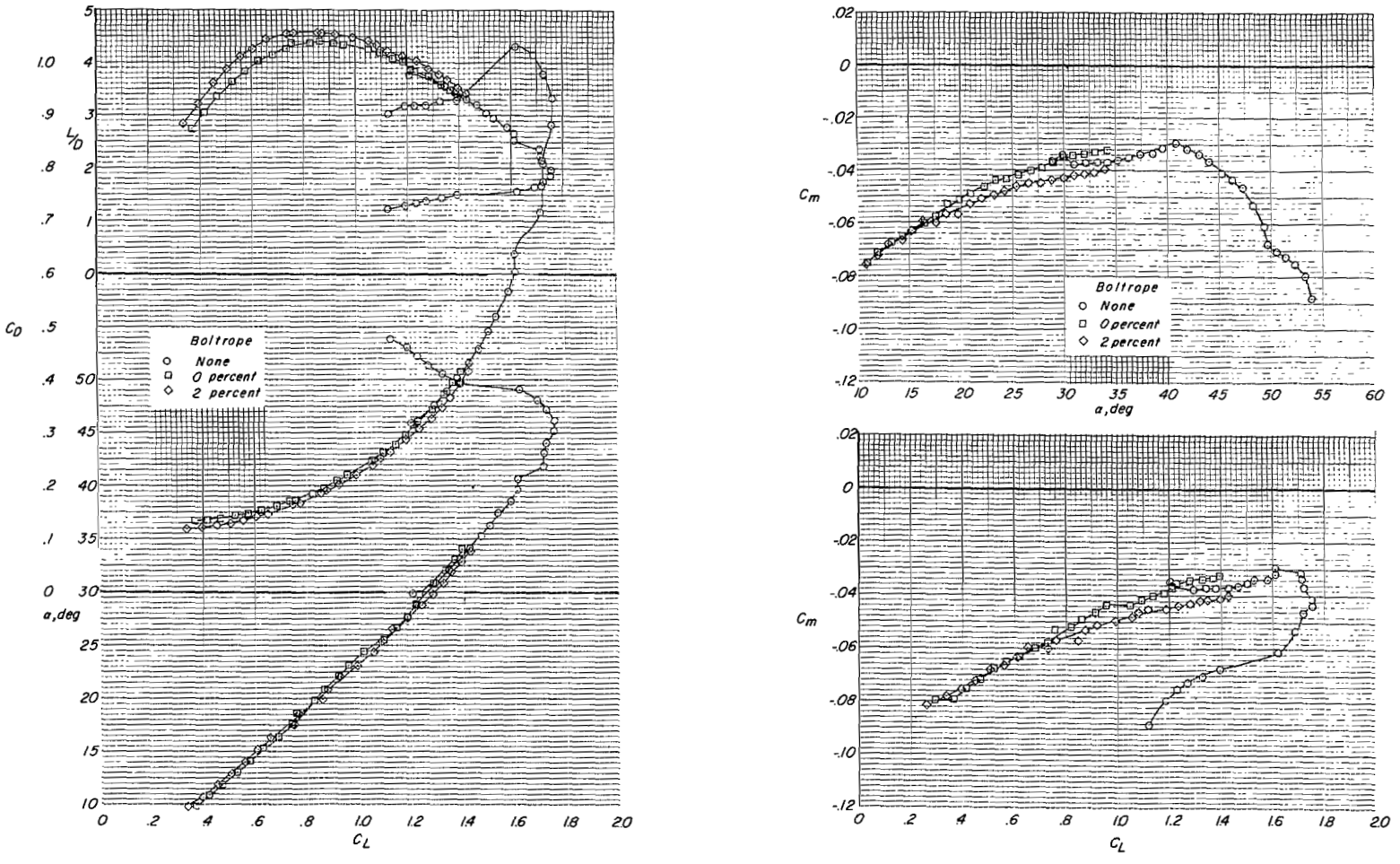

Figure 24.- Effect of boltrope length on the aerodynamic characteristics and spreader-bar load of the $\Lambda = 55^{\circ}$ wing having a cambered canopy which was constructed on a three-dimensional template.

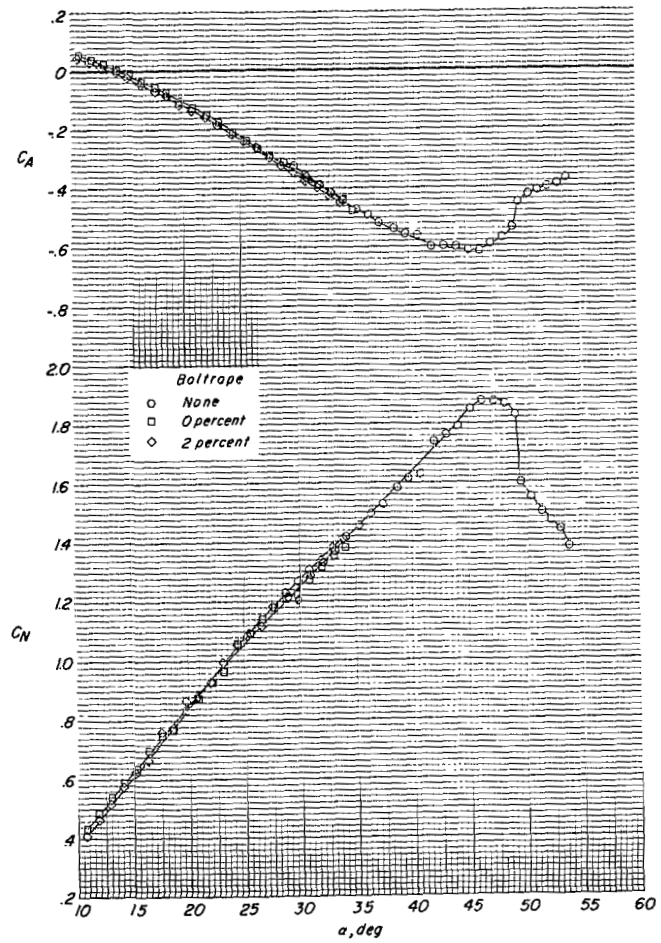

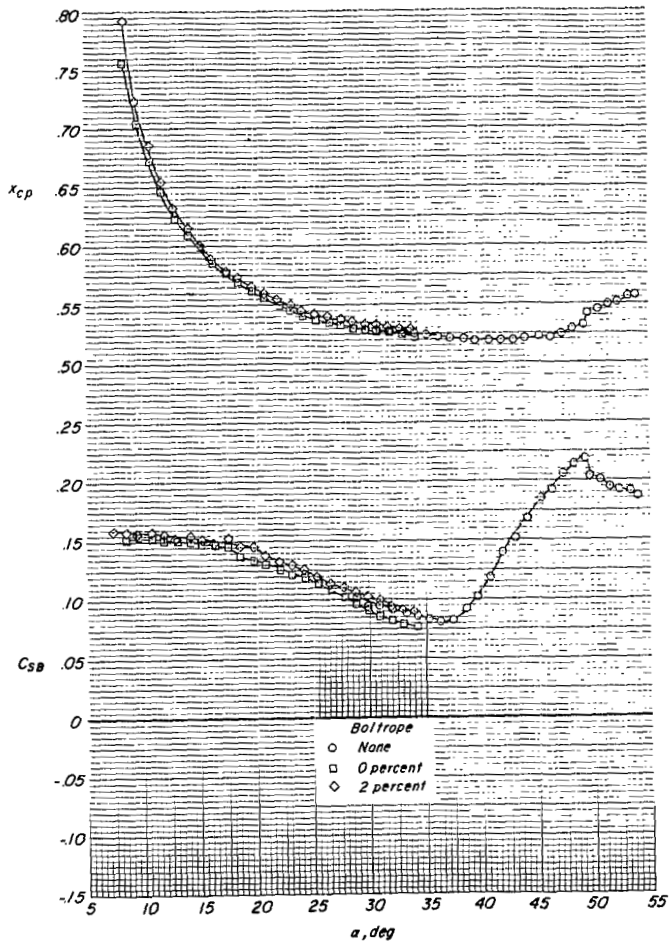

Figure 24.- Concluded.

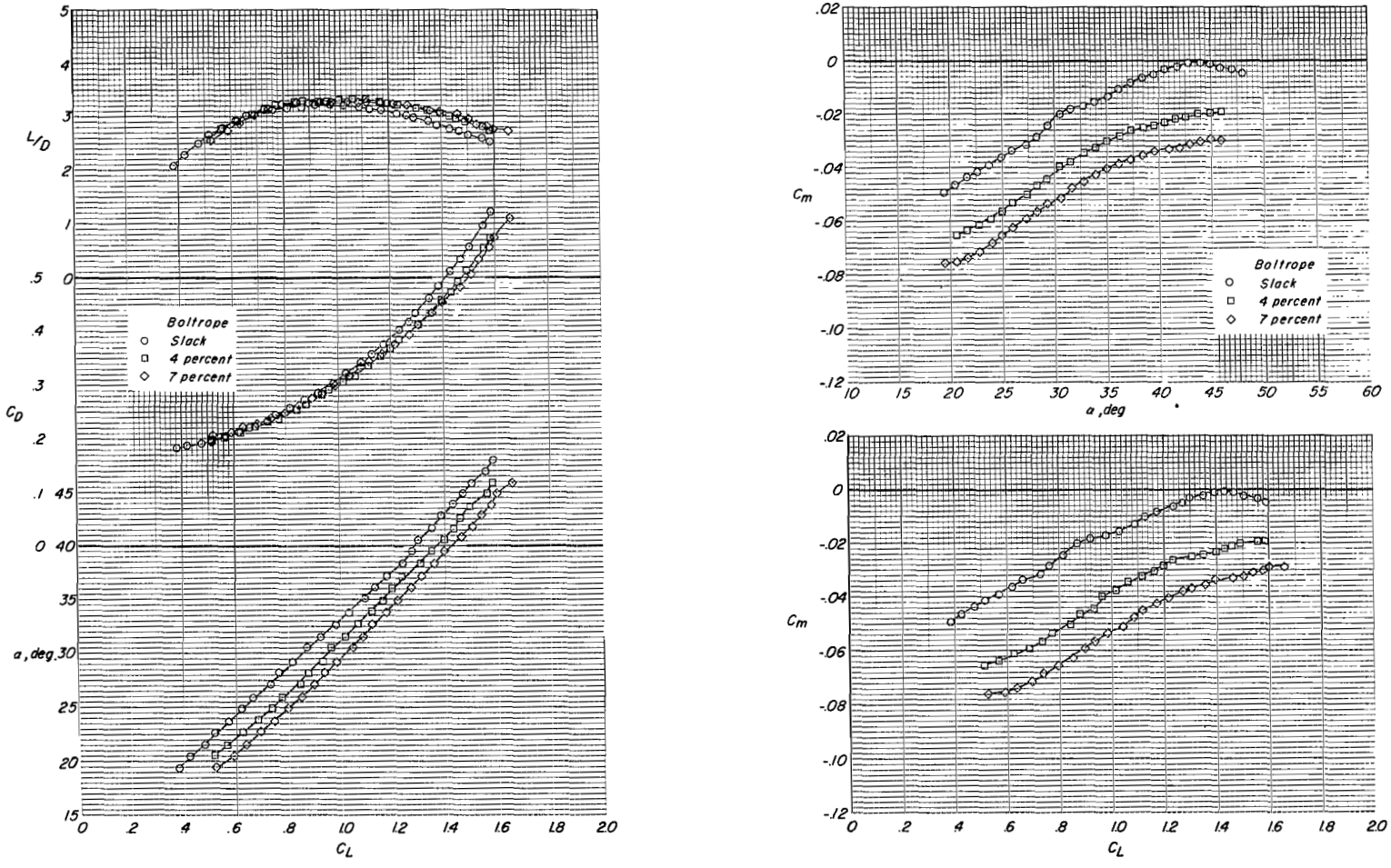

Figure 25.- Effect of boltrope length on the aerodynamic characteristics and spreader-bar load of the $\Lambda_o = 45^o$, $\Lambda = 55^o$ wing with the fabric fairing from the underside of the leading edge to the bottom surface of the canopy.

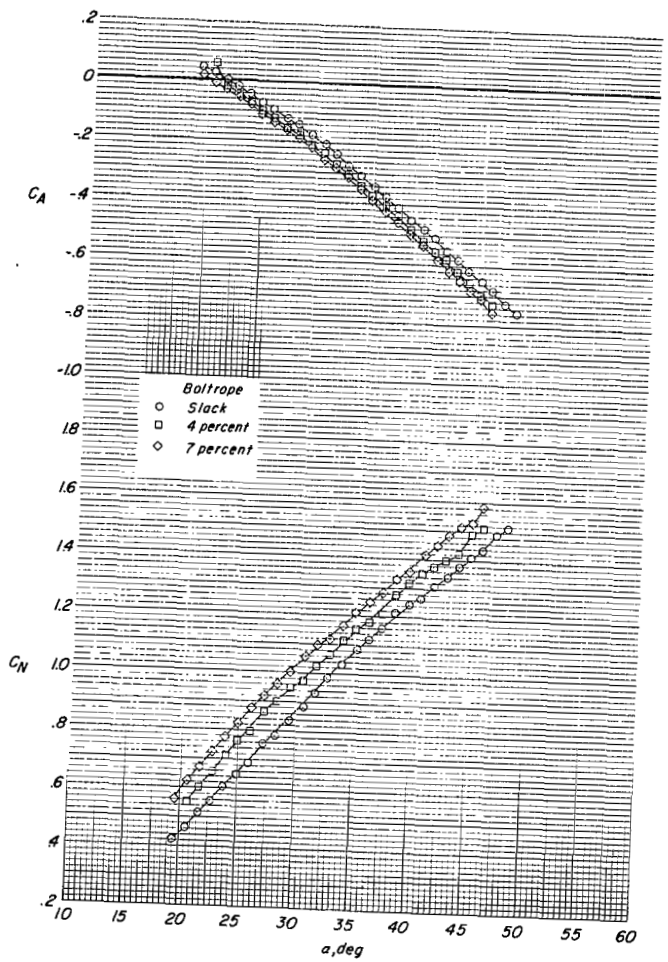

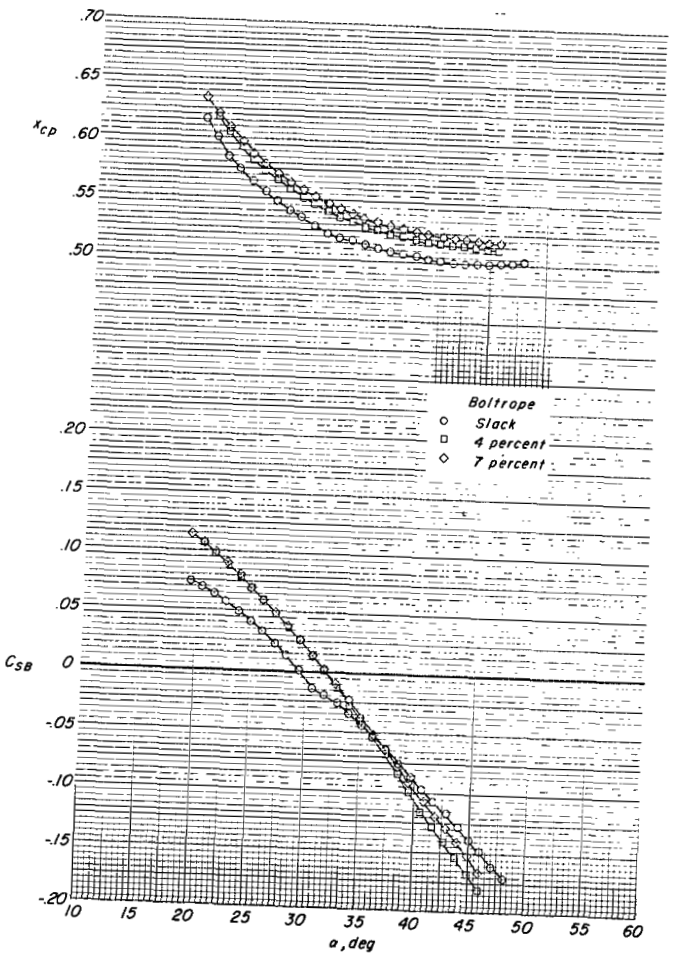

Figure 25.- Concluded.

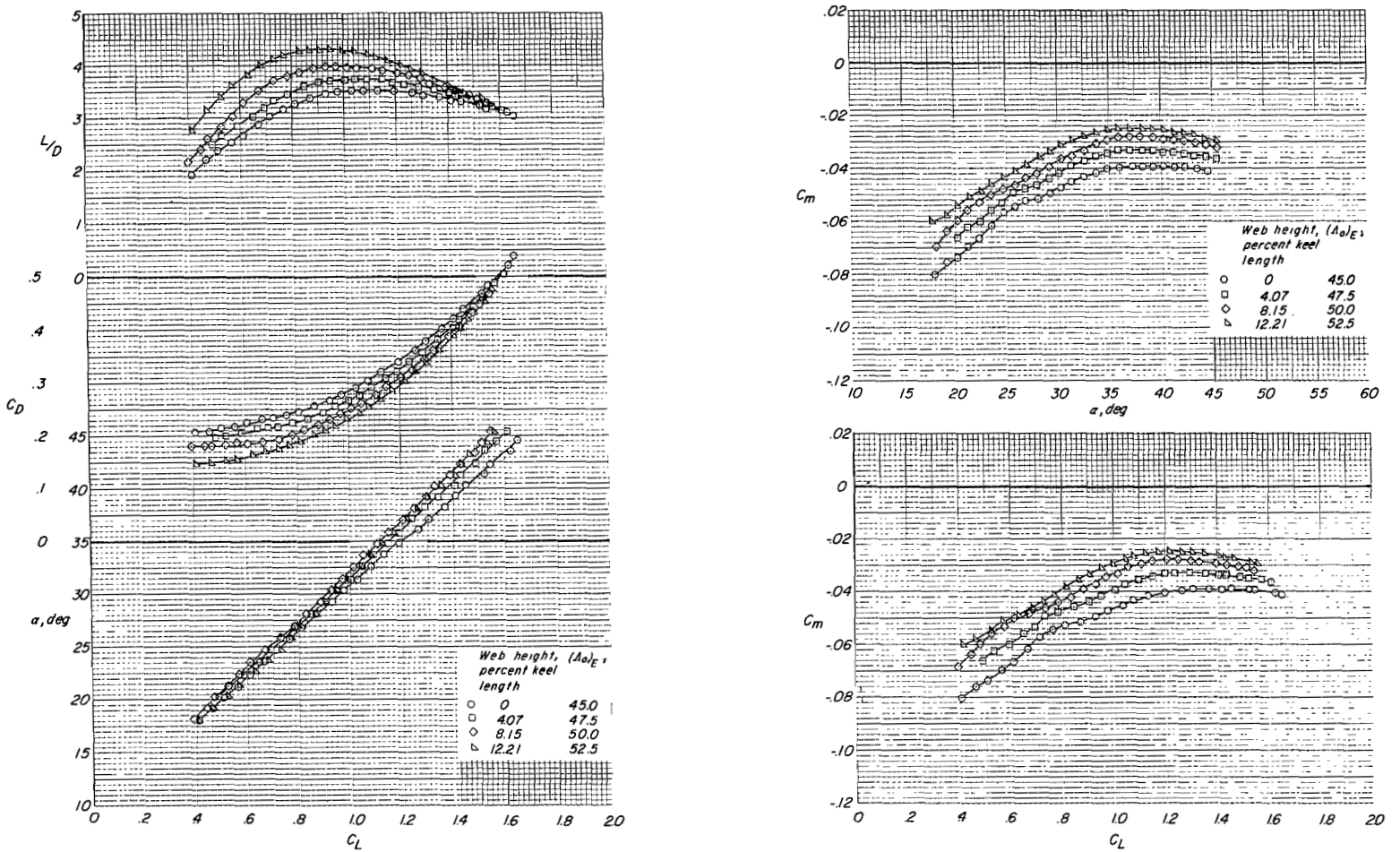

Figure 26.- Effect of keel web height on the aerodynamic characteristics and spreader-bar load of the $\Lambda = 55^\circ$ wing. The basic flat-pattern sweep of $\Lambda_o = 45^\circ$ was used for the condition of no web and the trailing-edge length varied as the web height increased. 2-percent boltrope.

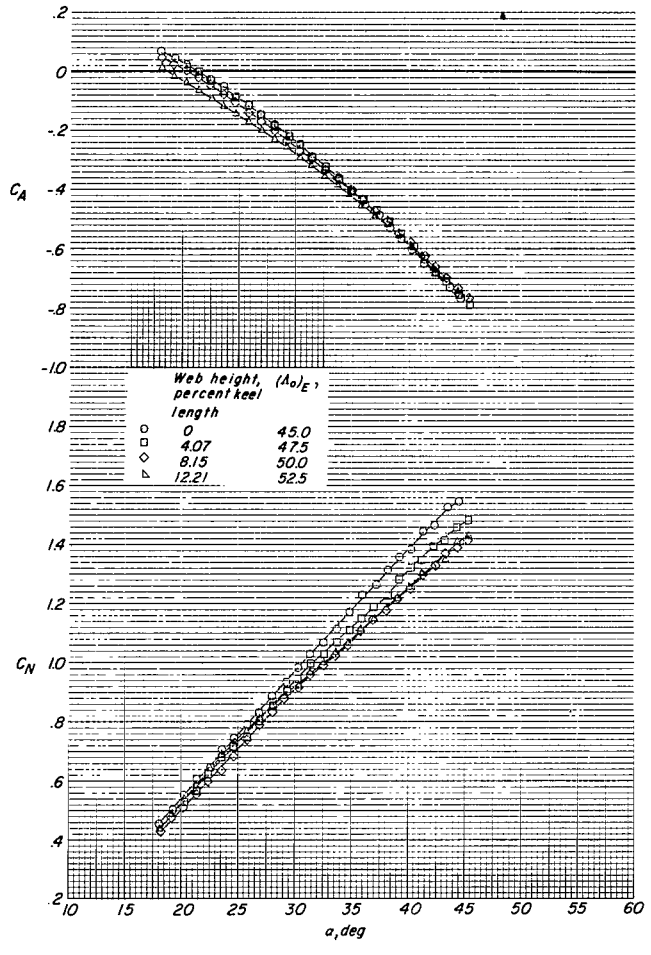

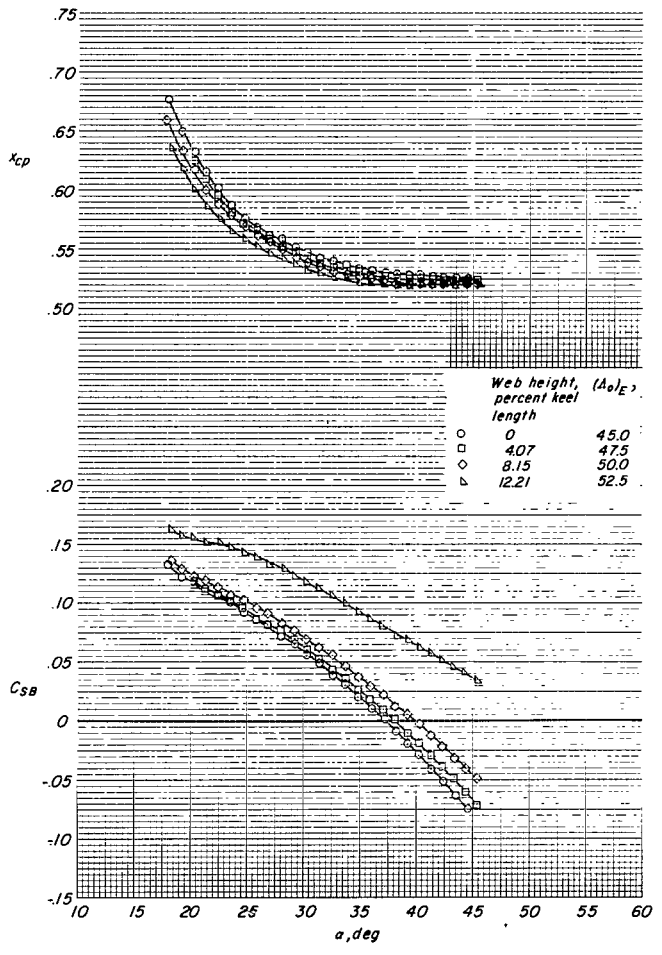

Figure 26.- Concluded.

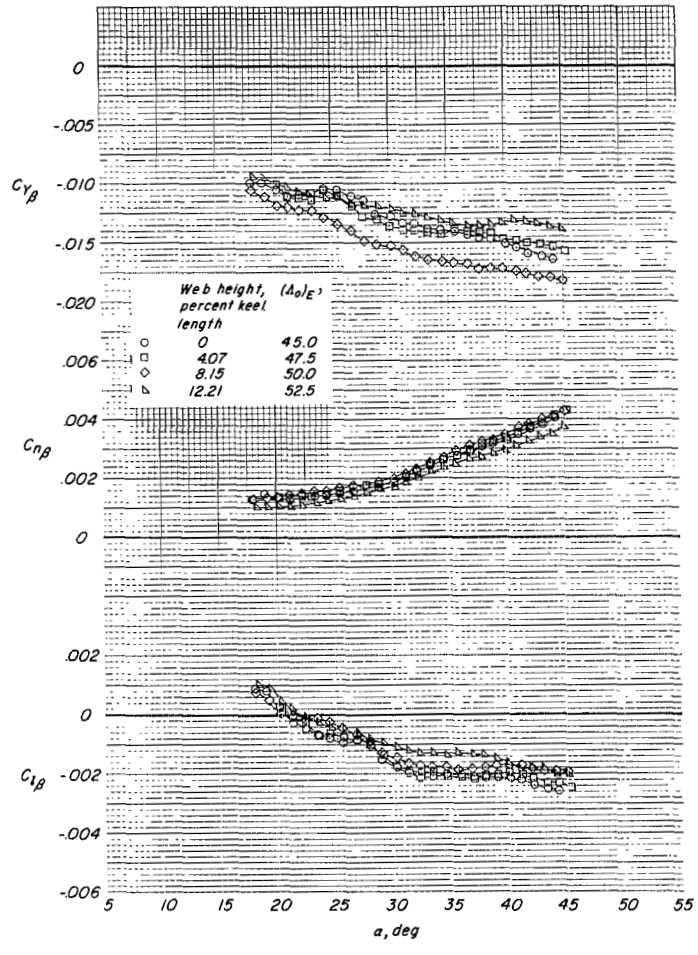

Figure 27.- Effect of keel web height on lateral stability derivatives of the $\Lambda = 55^\circ$ wing. Trailing-edge length varied with web height. 2-percent boltrope.

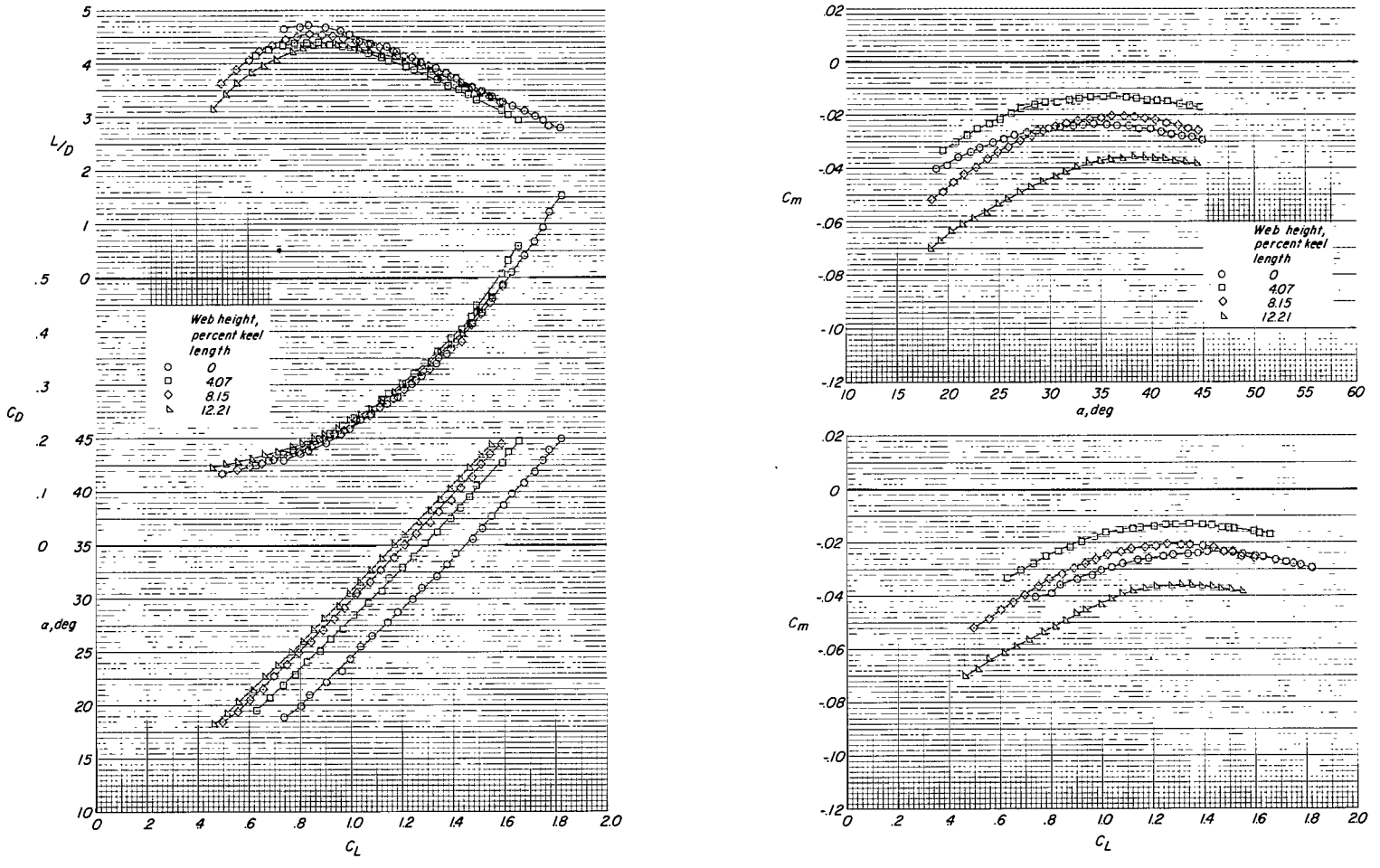

Figure 28.- Effect of keel web height on the aerodynamic characteristics and spreader-bar loads of the $\Lambda = 55^{\circ}$ wing. The basic flat-pattern sweep of $\Lambda_o = 45^{\circ}$ was used but the trailing-edge length was held constant $\left((\Lambda_o)_E = 52.5^{\circ}\right)$ as the web height varied. 2-percent boltrope.

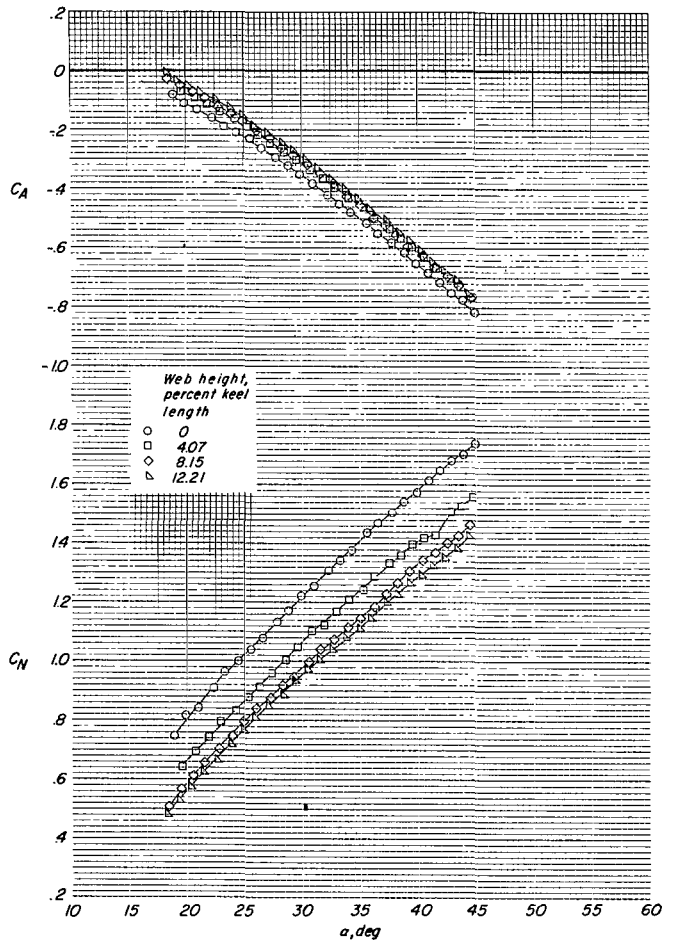

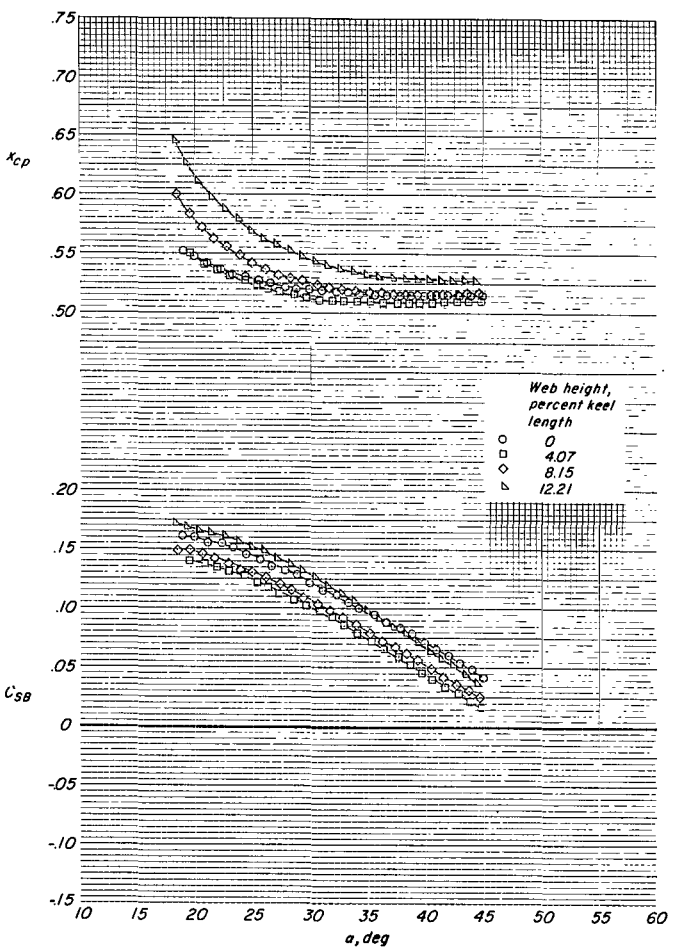

Figure 28.- Concluded.

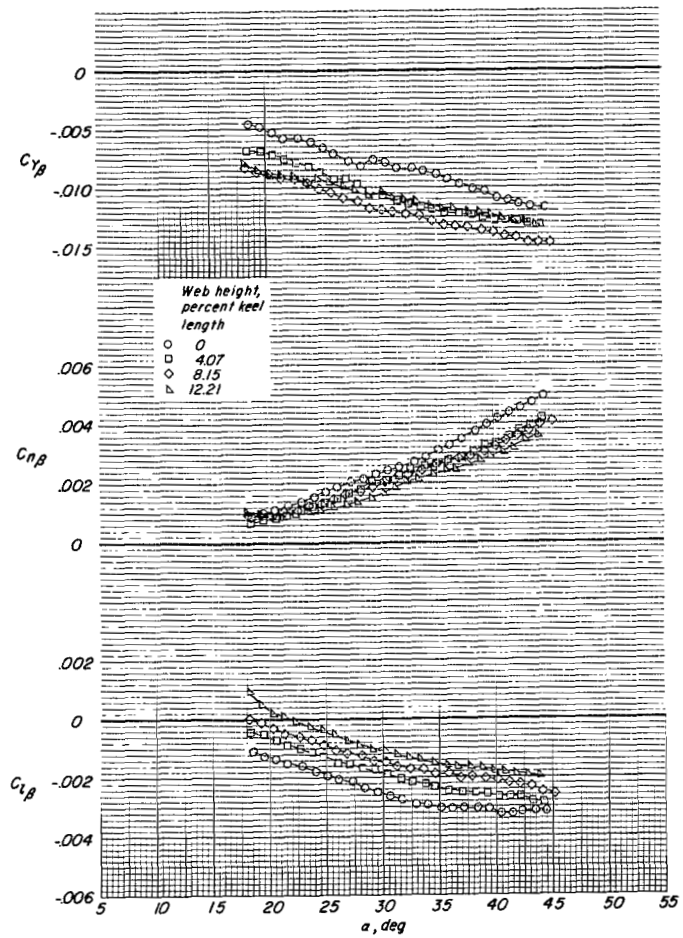

Figure 29.- Effect of keel web height on lateral stability derivatives of the $\Lambda = 55^{\circ}$ wing. Trailing-edge length was held constant. 2-percent boltrope.

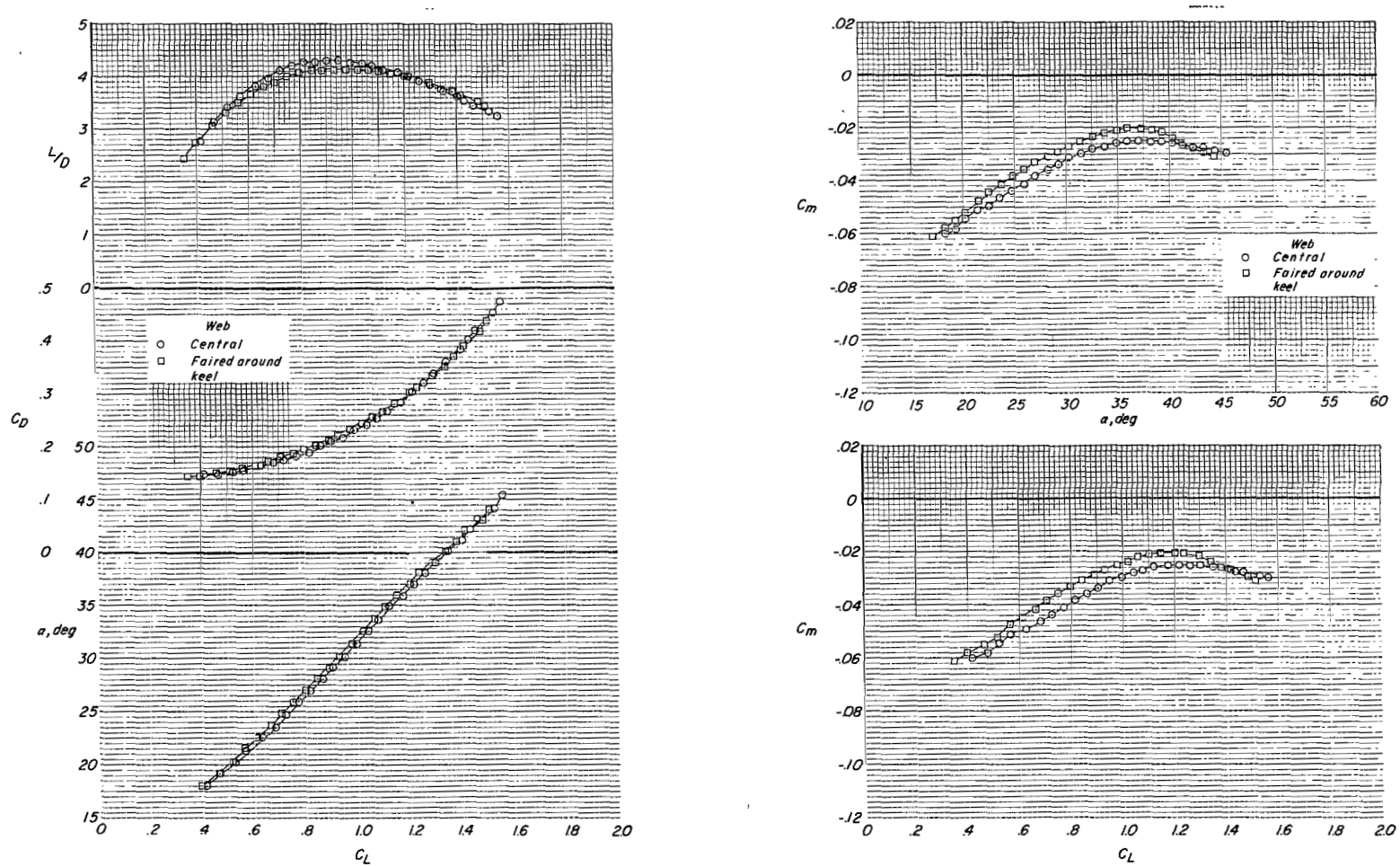

Figure 30.- Effect of the keel web fairing on the aerodynamic characteristics and spreader-bar load of the $\Lambda = 55^{\circ}$ wing. Keel web height, 12.21-percent keel length; $(\Lambda_o)_E = 52.5^{\circ}$; 2-percent boltrope.

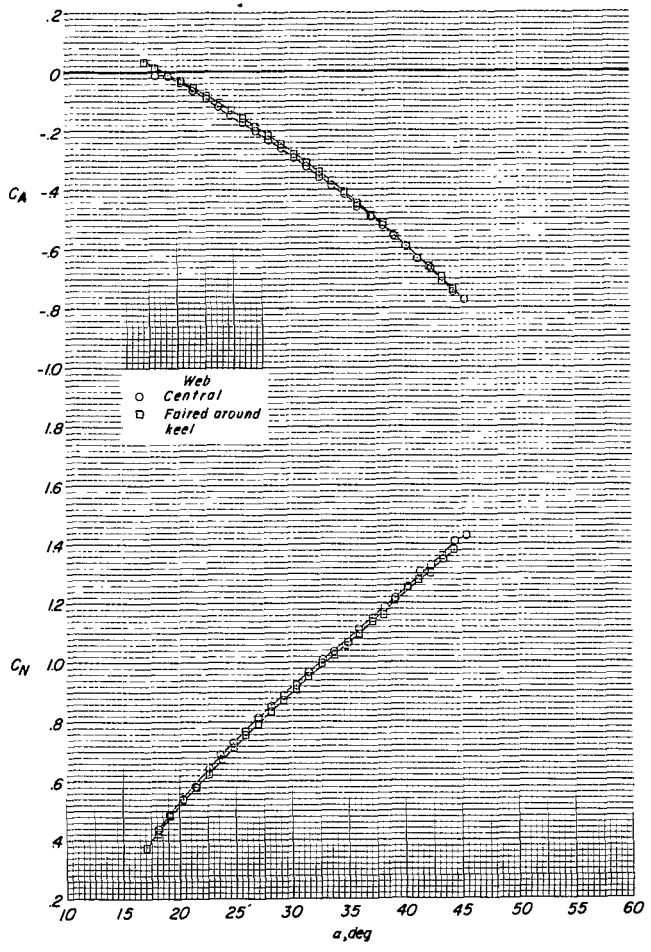

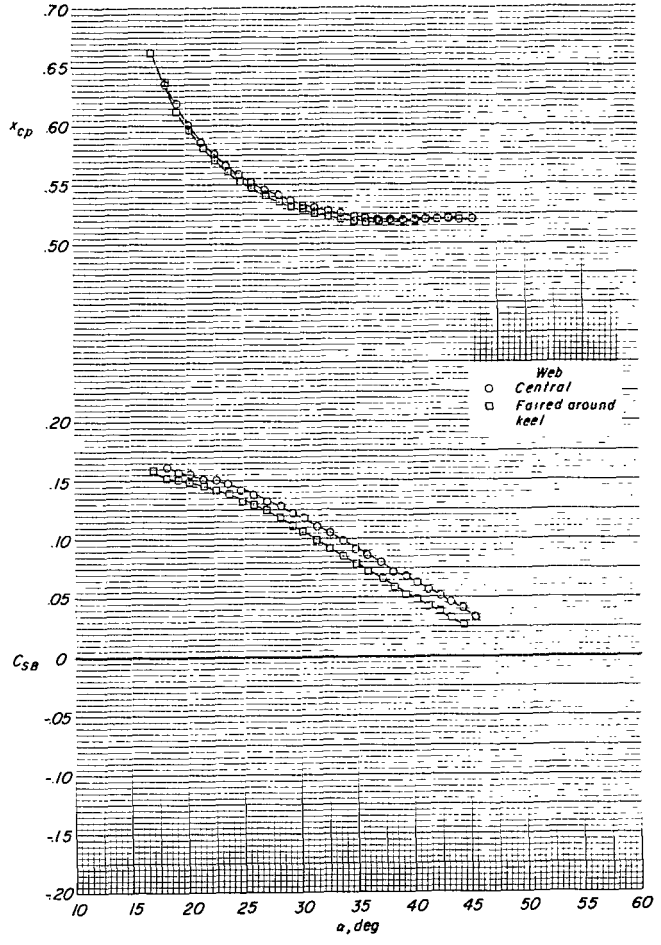

Figure 30.- Concluded.

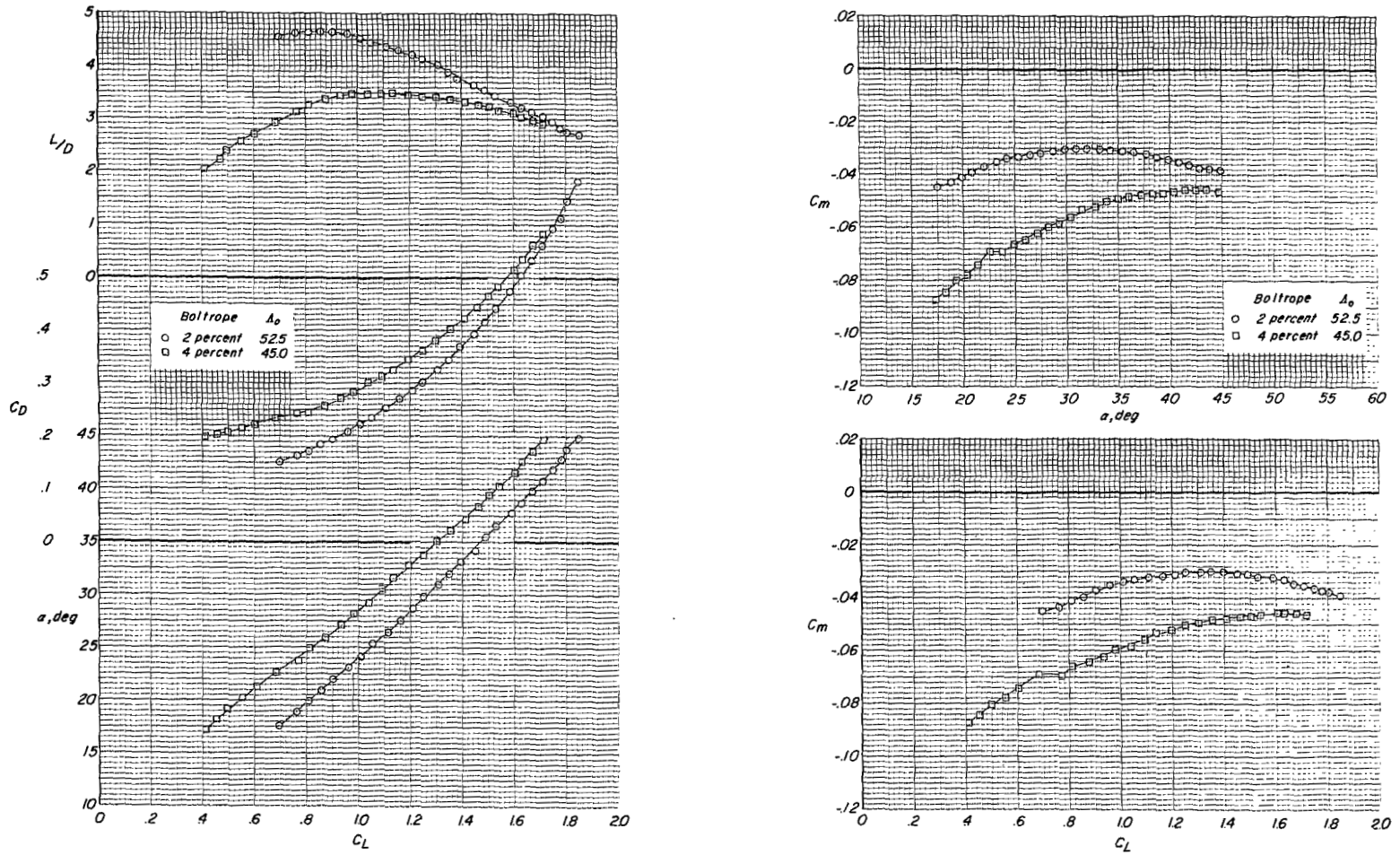

Figure 31.- Aerodynamic characteristics and spreader-bar load of the $\Lambda = 55^\circ$ wing with a simulated catenary curtain attached to the keel.

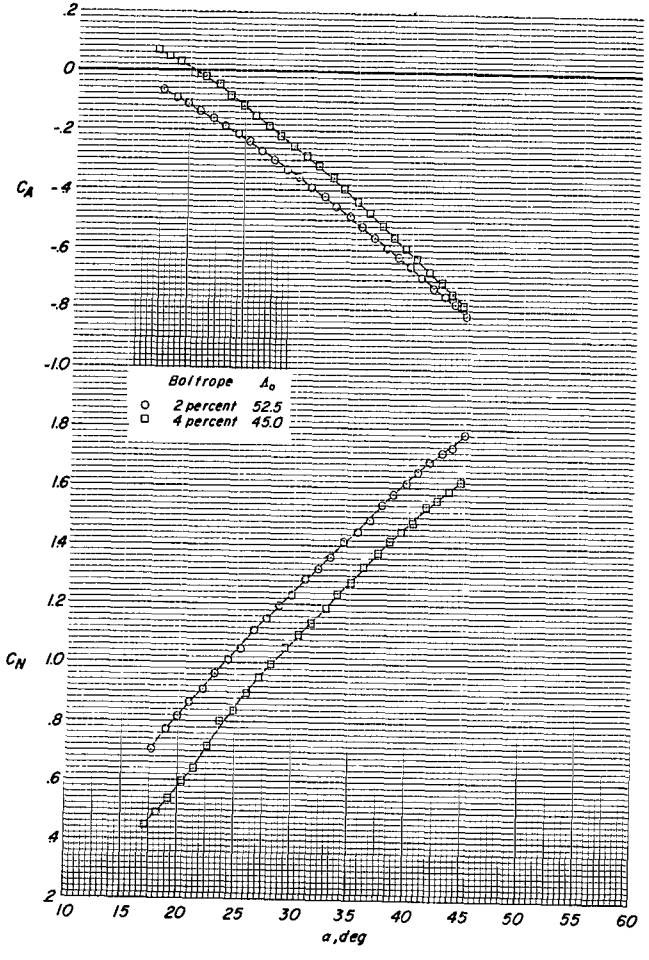

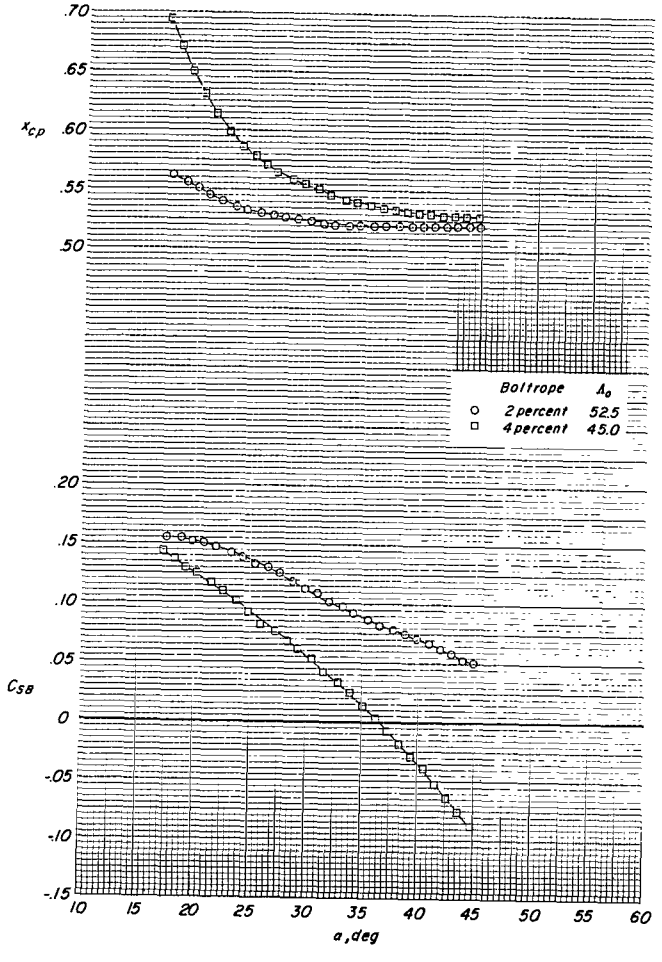

Figure 31.- Concluded.

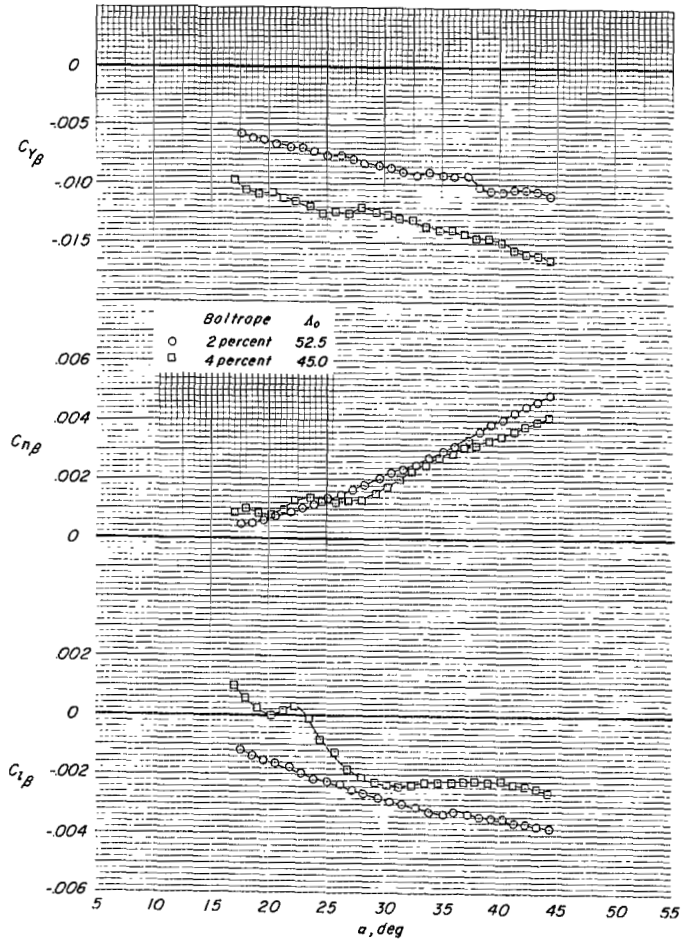

Figure 32.- Lateral stability derivatives of $\Lambda = 55^\circ$ model with keel catenary curtain.

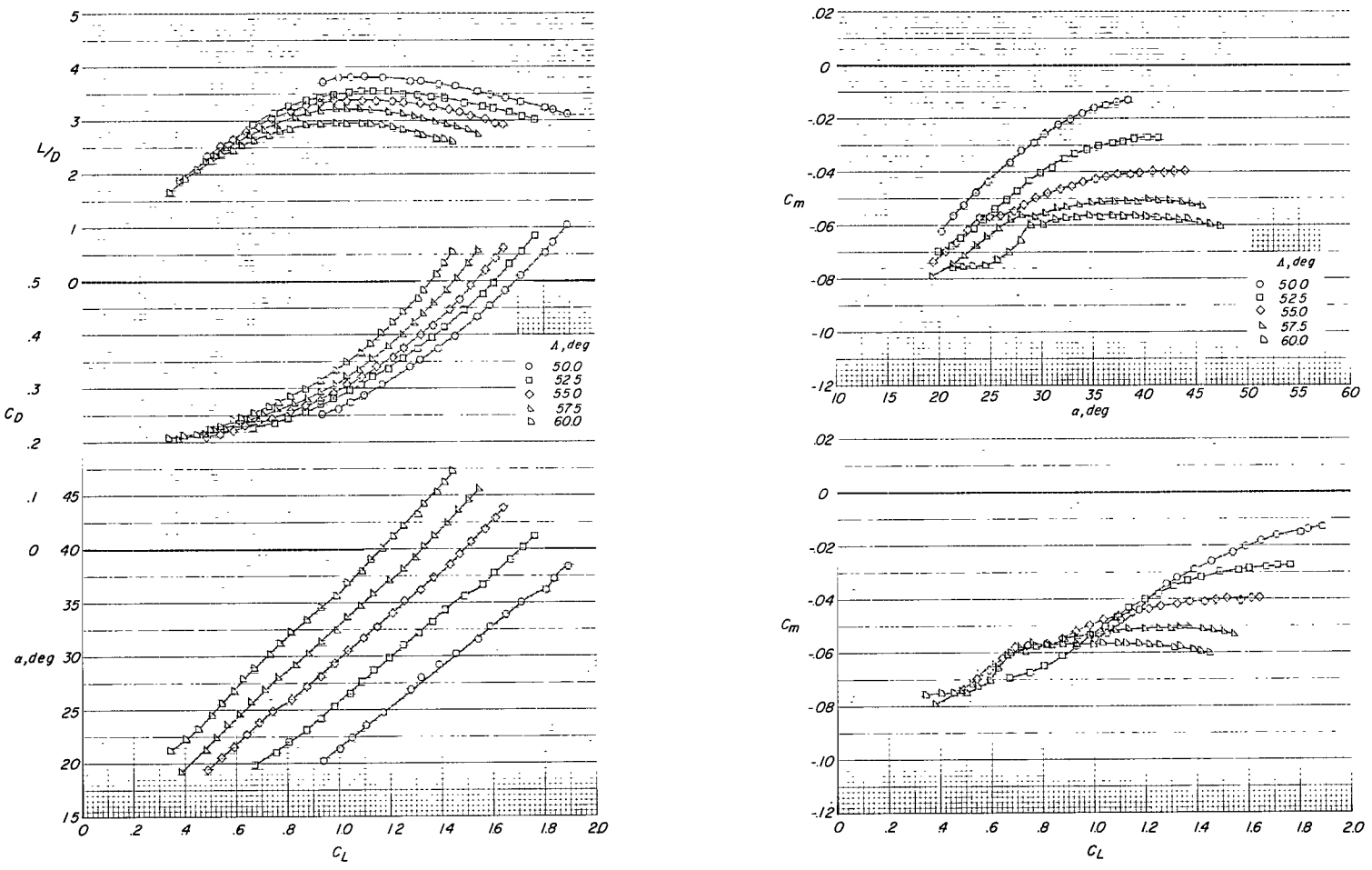

Figure 33.- Effect of leading-edge sweep angle on the aerodynamic characteristics and spreader-bar load on wings having a flat-pattern sweep $\Lambda = 45^{\circ}$. 4-percent boltrope. (Note all coefficients are based on the projected area of the $\Lambda = 55^{\circ}$ wing.)

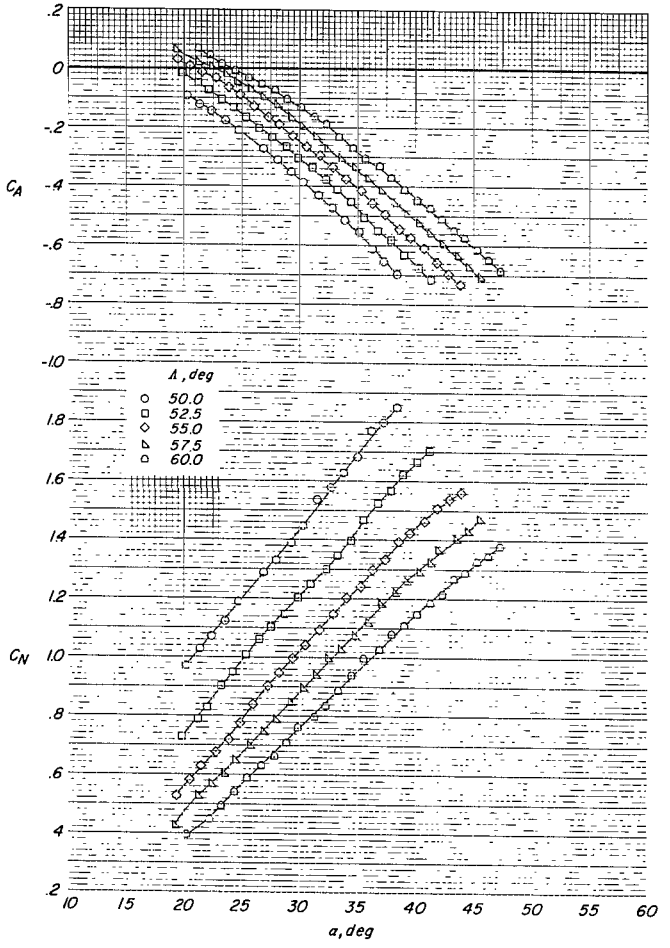

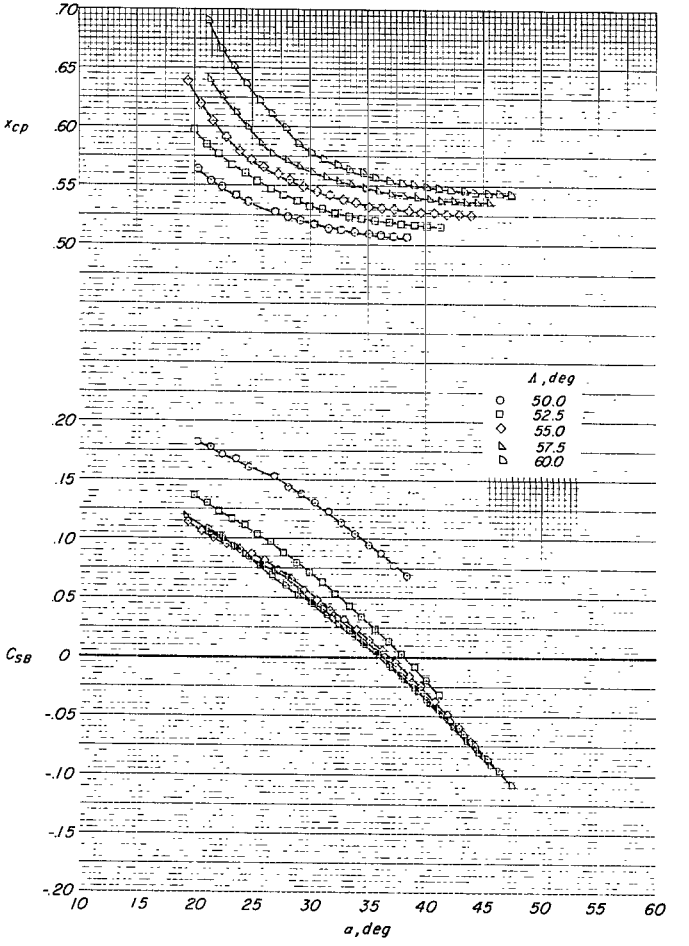

Figure 33.- Concluded.

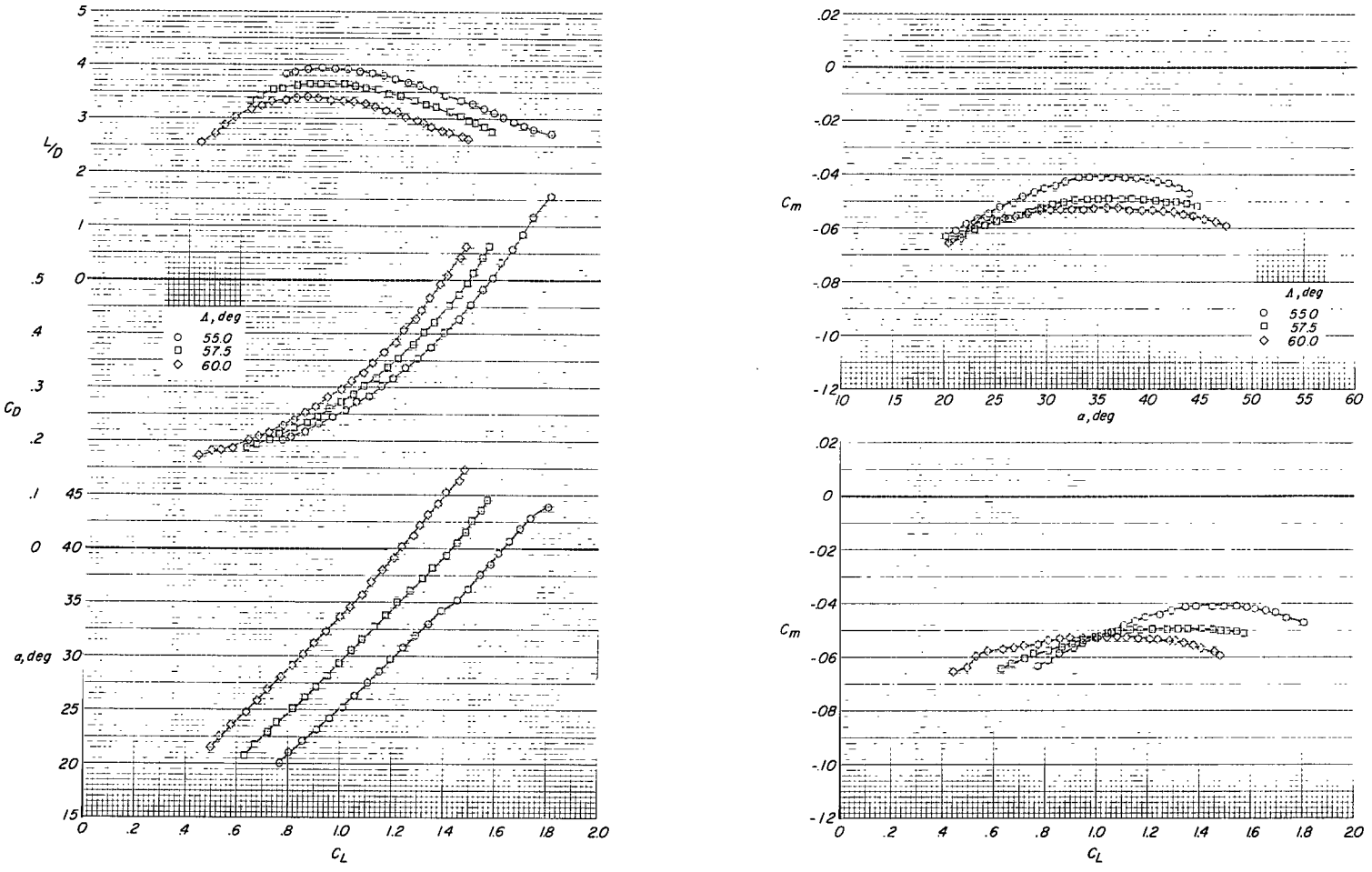

Figure 34.- Effect of leading-edge sweep angle on the aerodynamic characteristics and spreader-bar load on wings having a flat-pattern sweep $\Lambda = 50^{\circ}$. 4-percent boltrope. (Note all coefficients are based on the projected area of the $\Lambda = 55^{\circ}$ wing.)

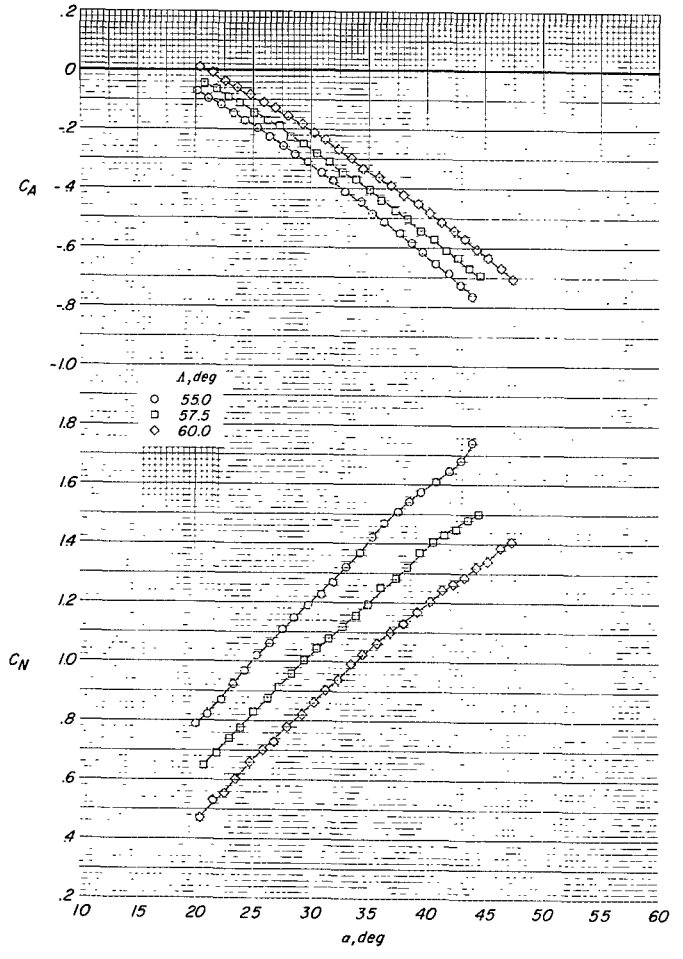

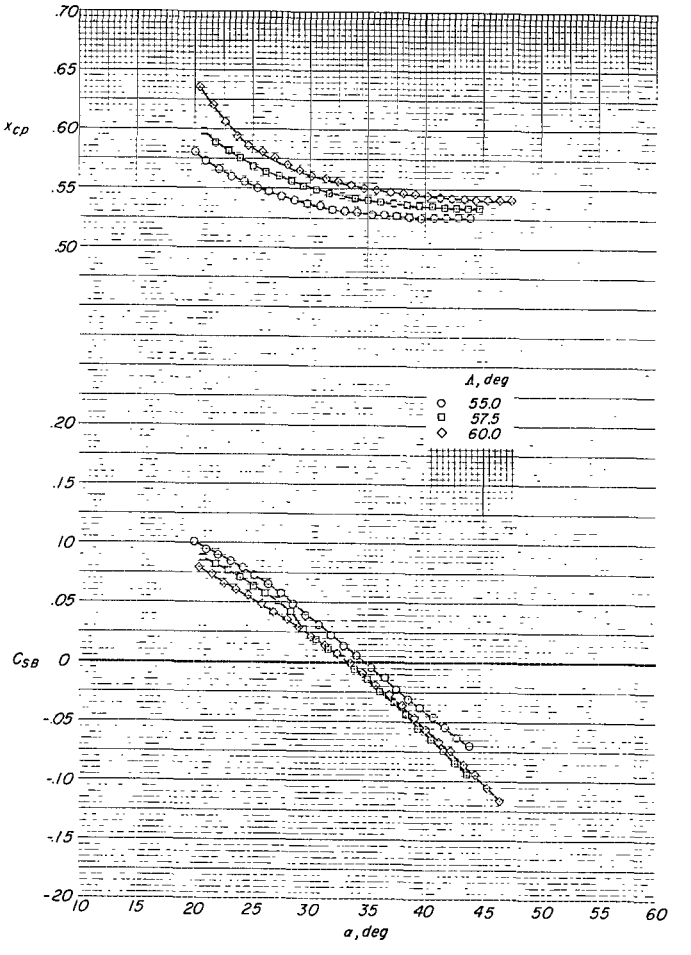

Figure 34.- Concluded.

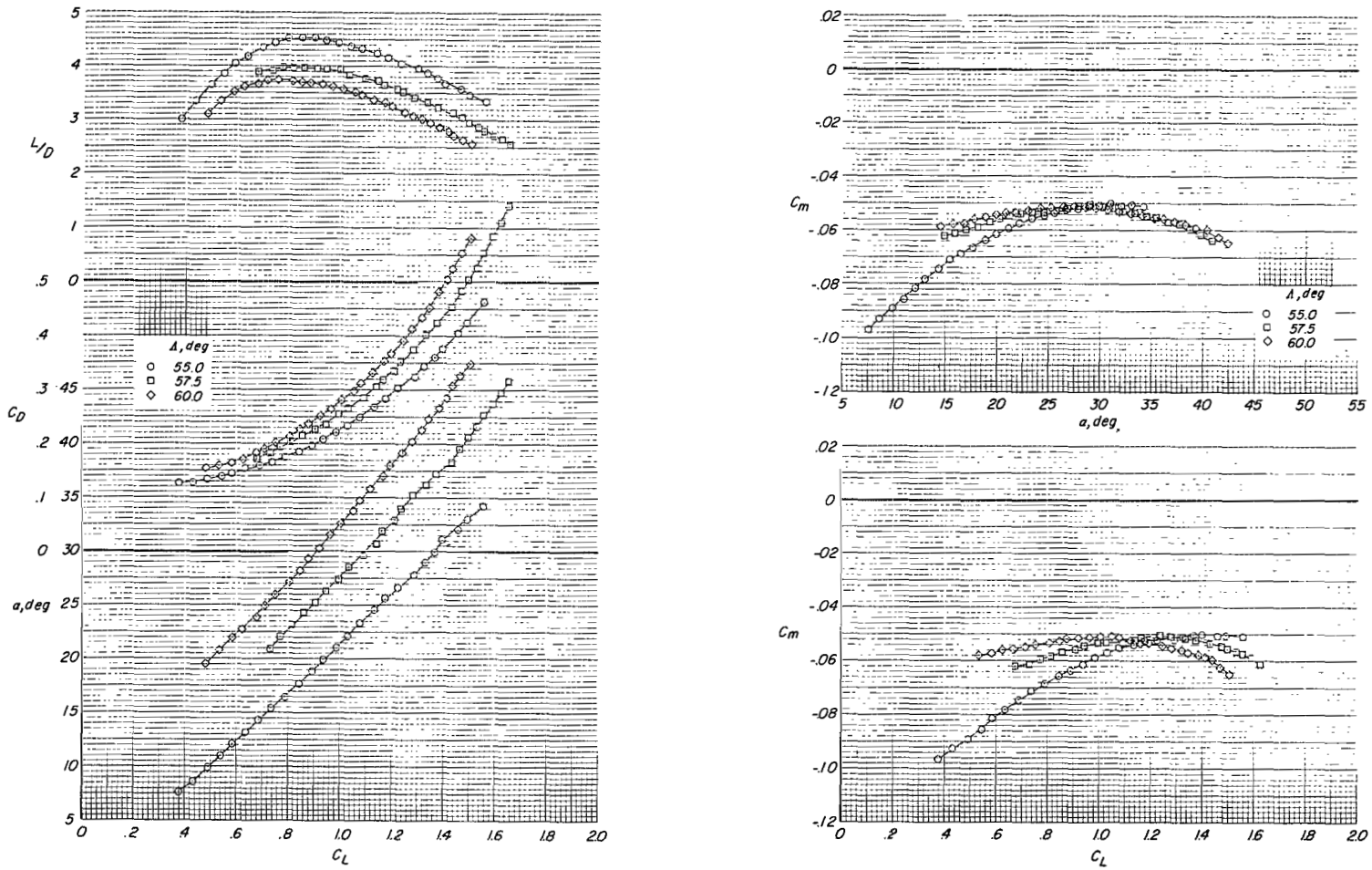

Figure 35.- Effect of leading-edge sweep angle on the aerodynamic characteristics and spreader-bar load on wings having a flat-pattern sweep $\Lambda_o = 52.5^o$. 4-percent boltrope. (Note all coefficients are based on the projected area of the $\Lambda = 55^o$ wing.)

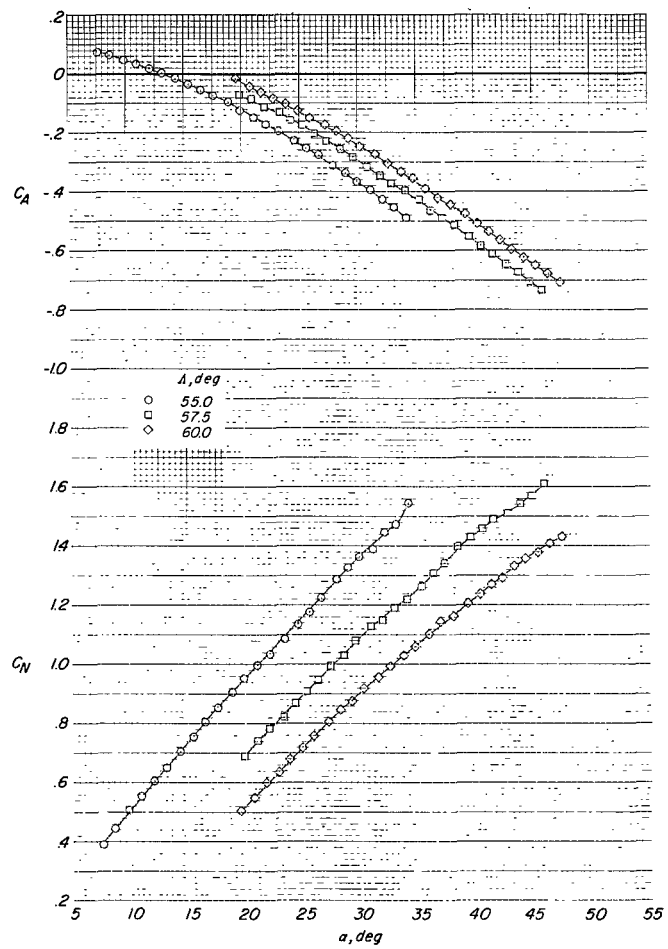

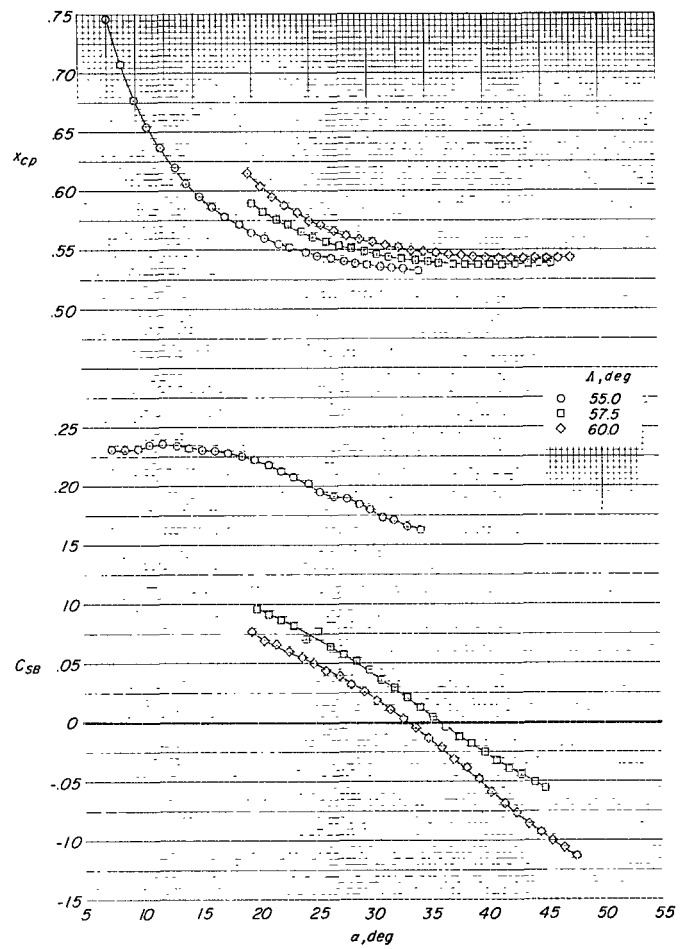

Figure 35.- Concluded.

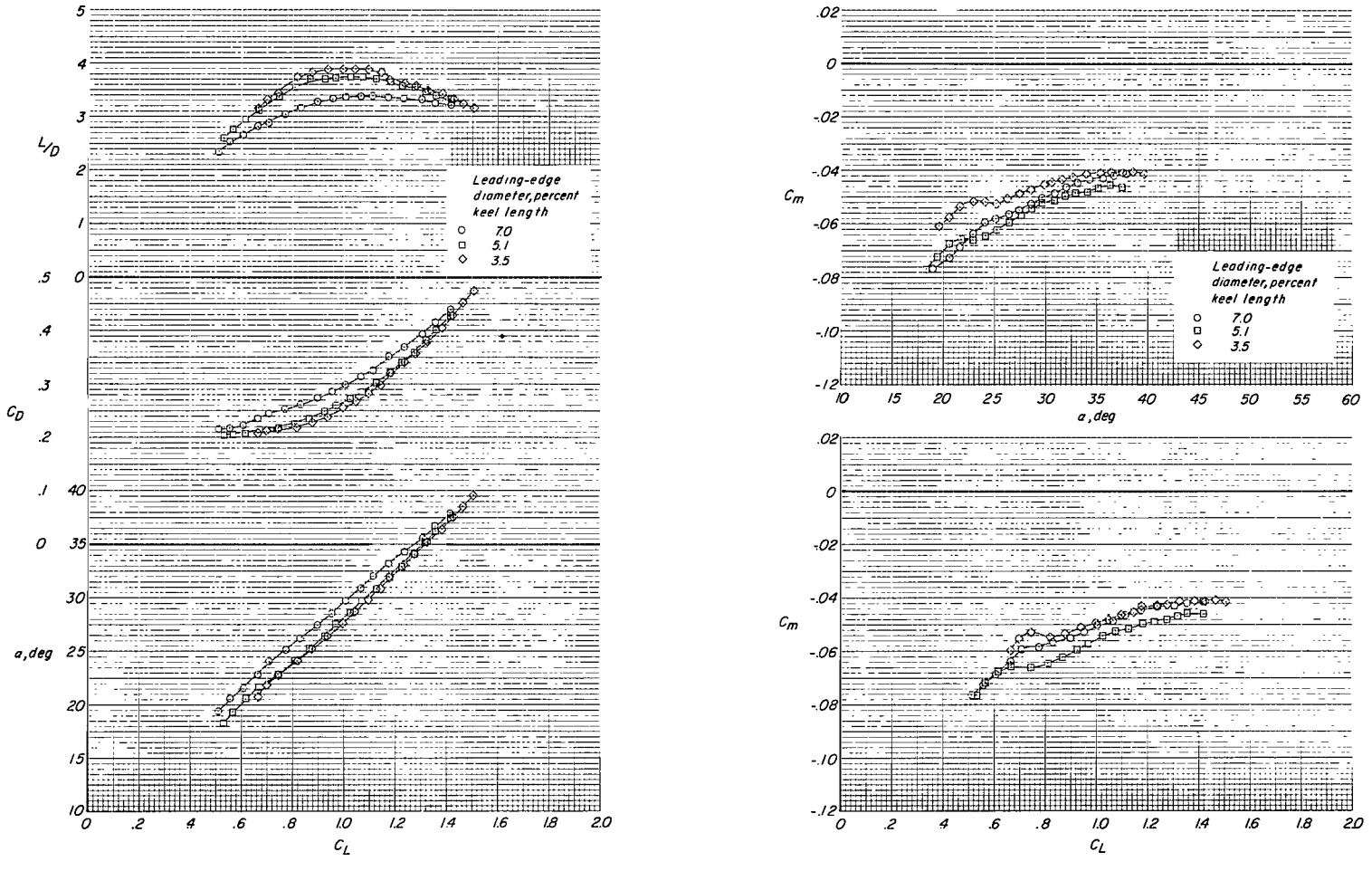

Figure 36.- Effect of leading-edge diameter on the aerodynamic characteristics and spreader-bar load on the $\Lambda_o = 45°$, $\Lambda = 55°$ wing with 4-percent boltrope. Keel diameter remained constant at 7-percent l_k; q = 20.

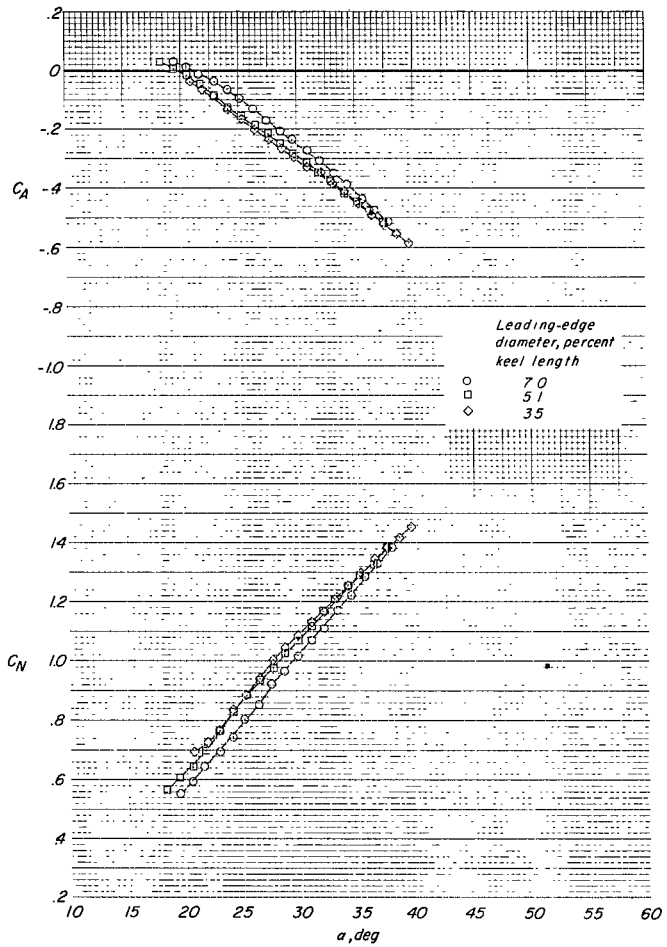

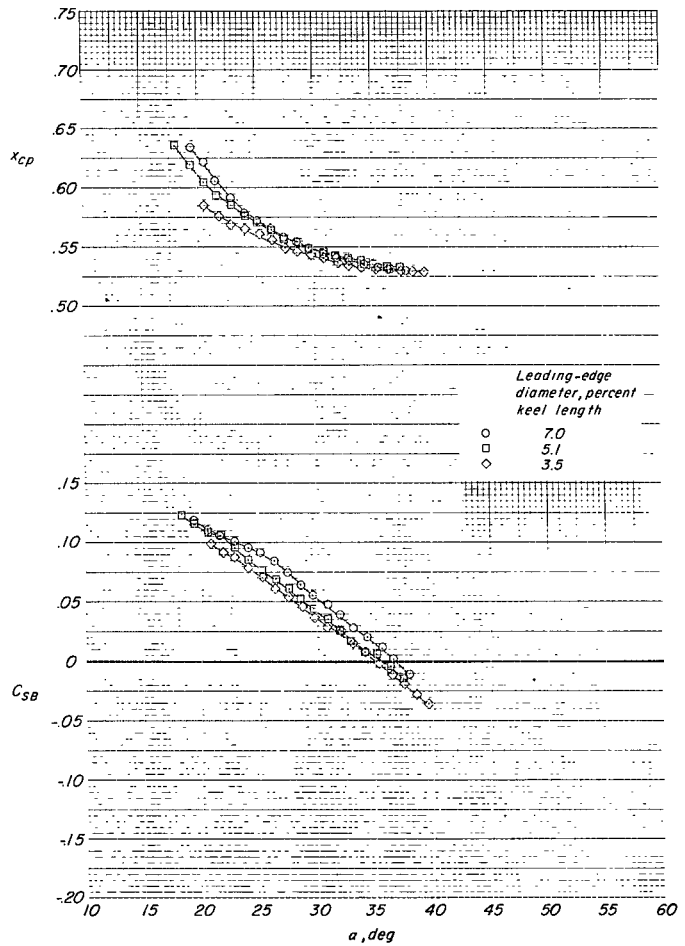

Figure 36.- Concluded.

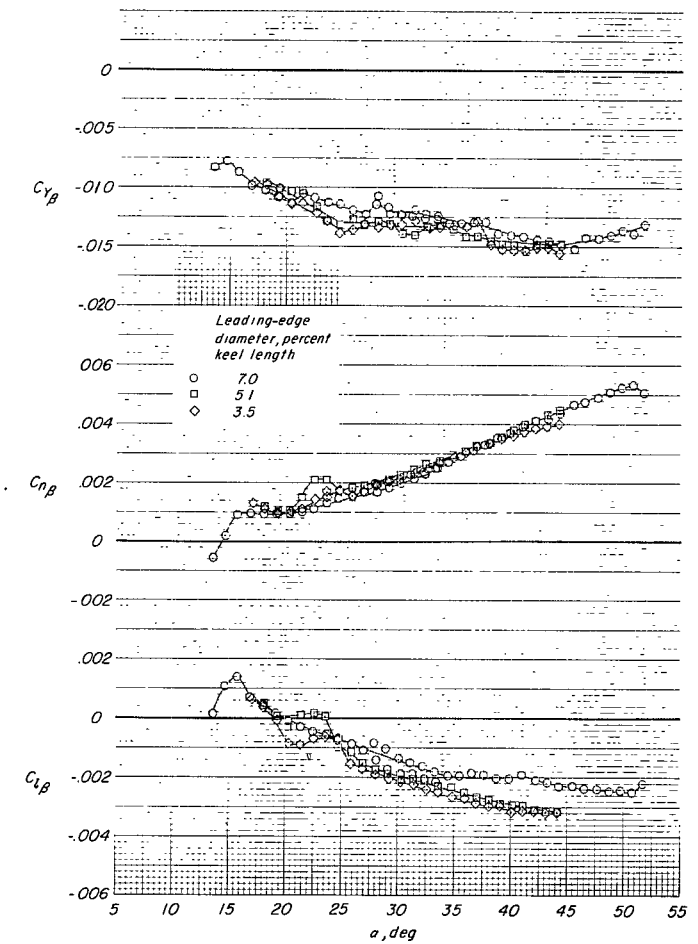

Figure 37.- Effect of leading-edge diameter on lateral stability derivatives of the $\Lambda_o = 45^o$, $\Lambda = 55^o$ wing. 4-percent boltrope; q = 10.

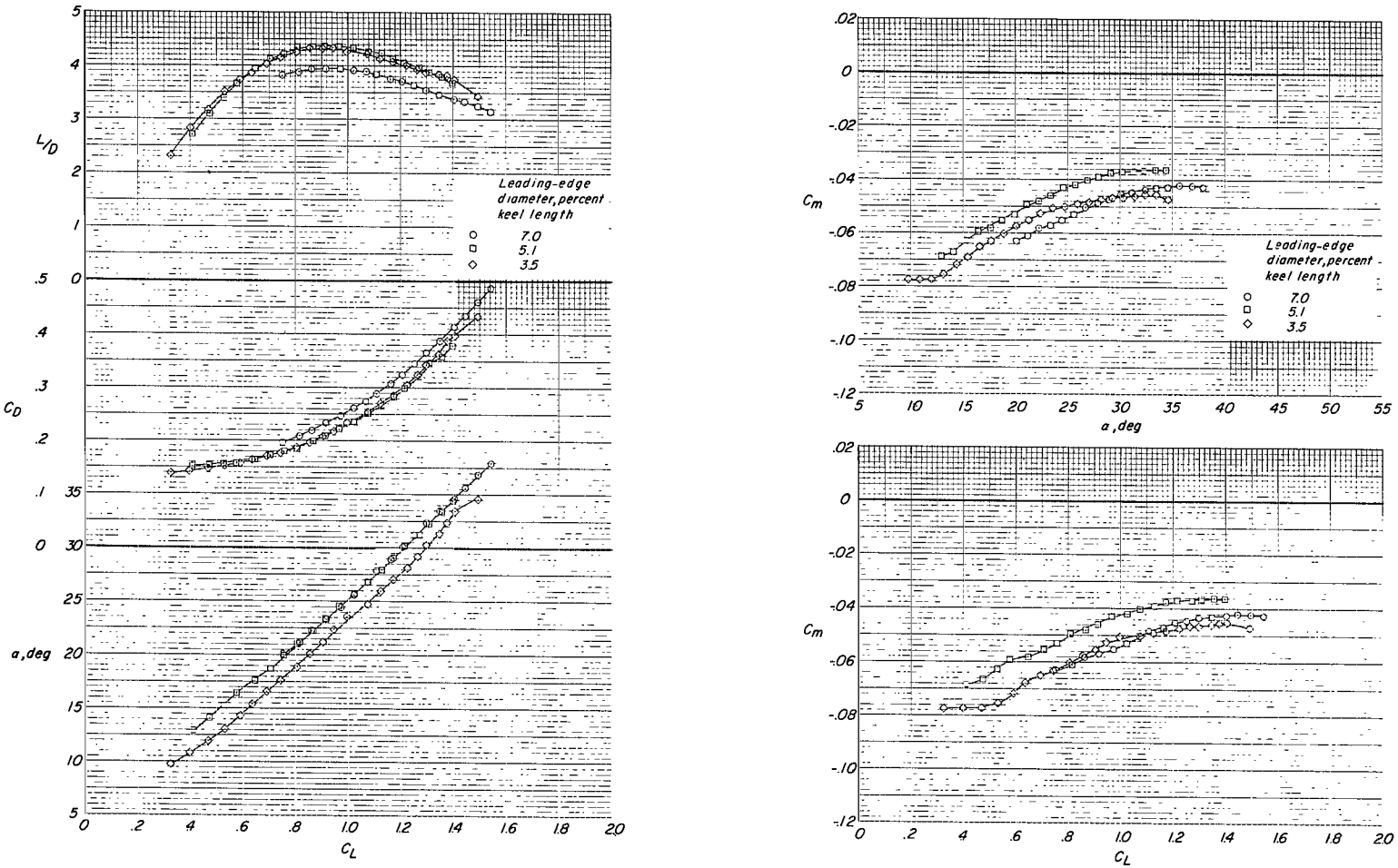

Figure 38.- Effect of leading-edge diameter on the aerodynamic characteristics and spreader-bar load on the $\Lambda_o = 50^o$, $\Lambda = 55^o$ wing with 4-percent boltrope. Keel diameter remained constant at 7-percent l_k; q = 20.

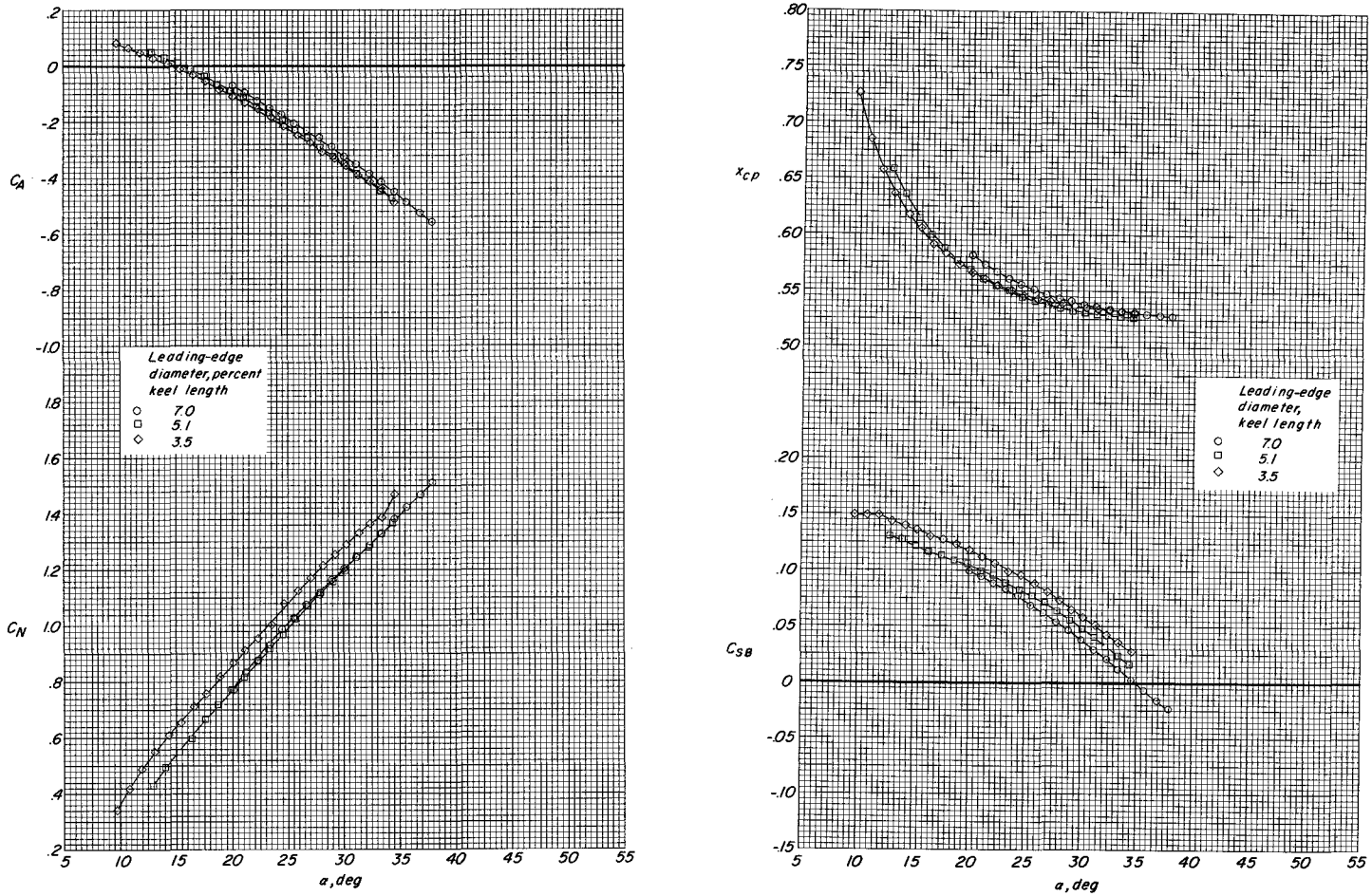

Figure 38.- Concluded.

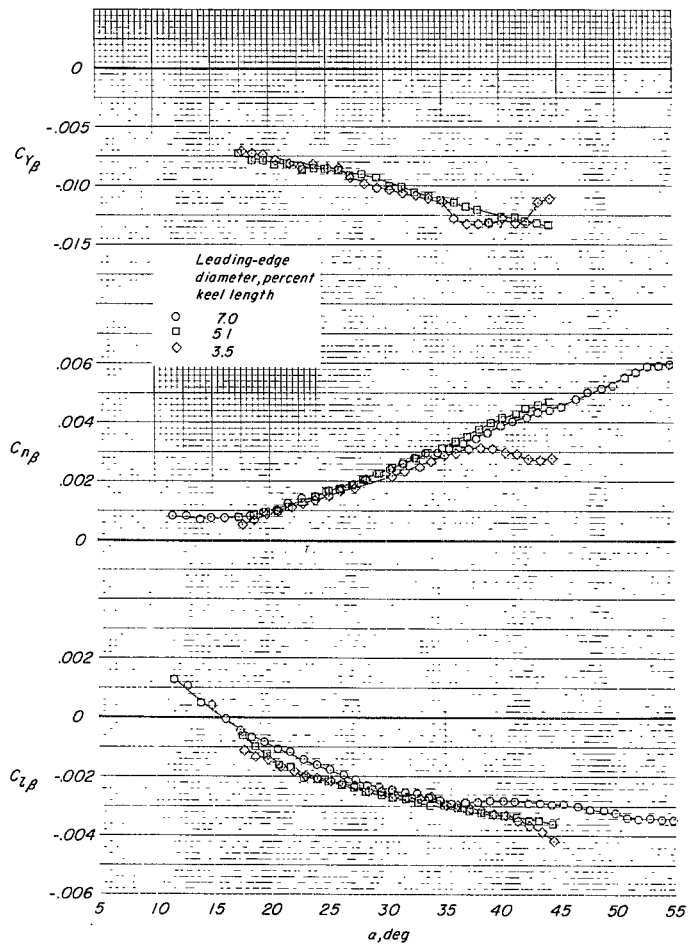

Figure 39.- Effect of leading-edge diameter on lateral stability derivatives of the $\Lambda_o = 50^\circ$, $\Lambda = 55^\circ$ wing. 4-percent boltrope; q = 10. (Note C_{Y_β} data for leading-edge diameter of 7-percent keel length omitted.)

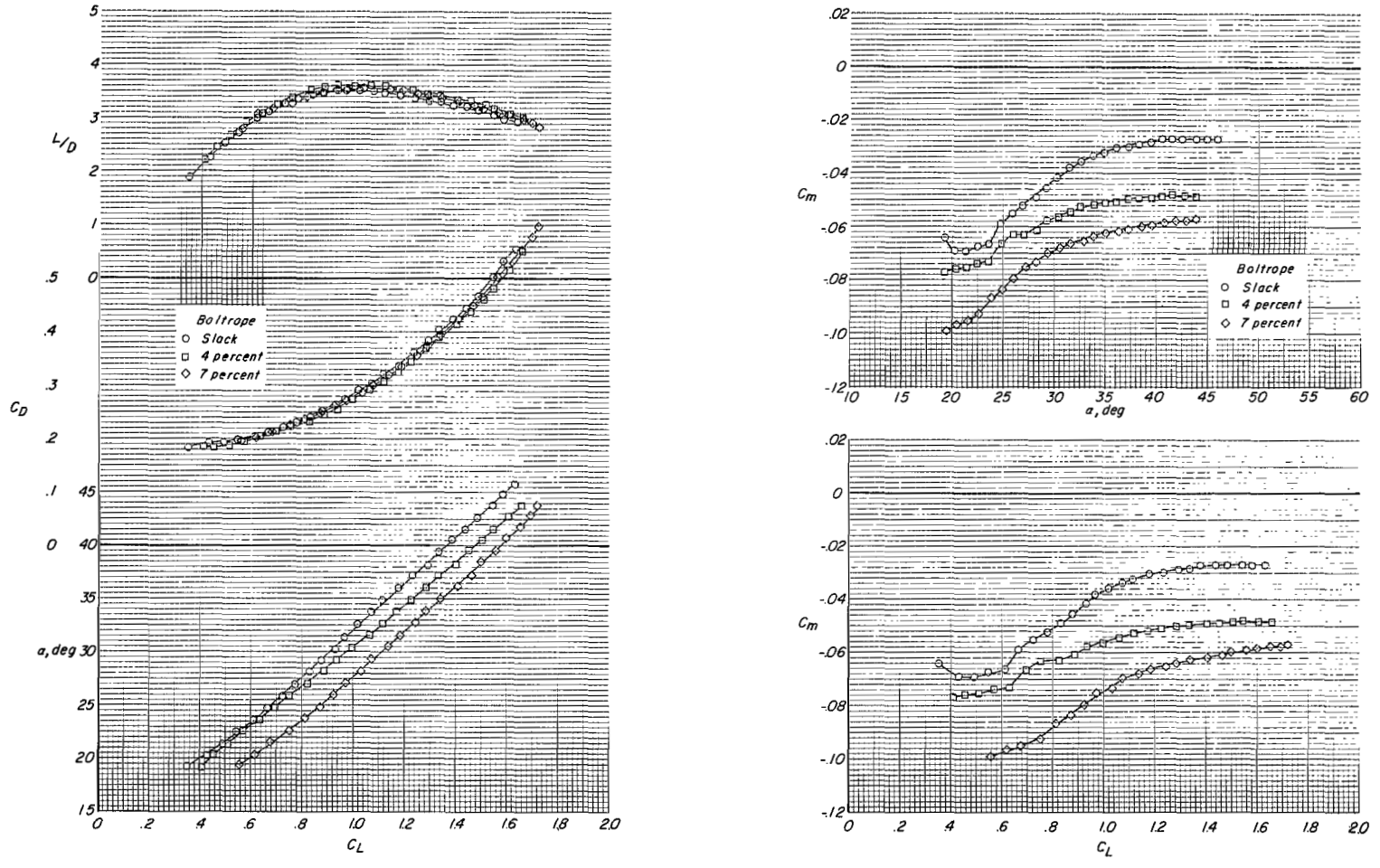

Figure 40.- Effect of boltrope length on the aerodynamic characteristics of the $\Lambda_o = 45^\circ$, $\Lambda = 55^\circ$ wing with the spreader bar removed.

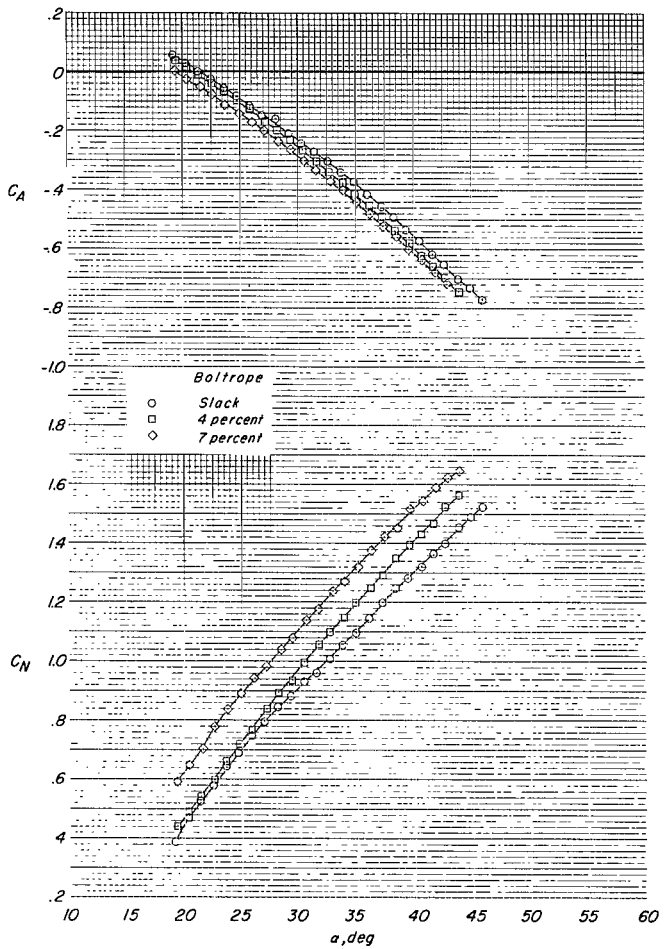

Figure 40.- Concluded.

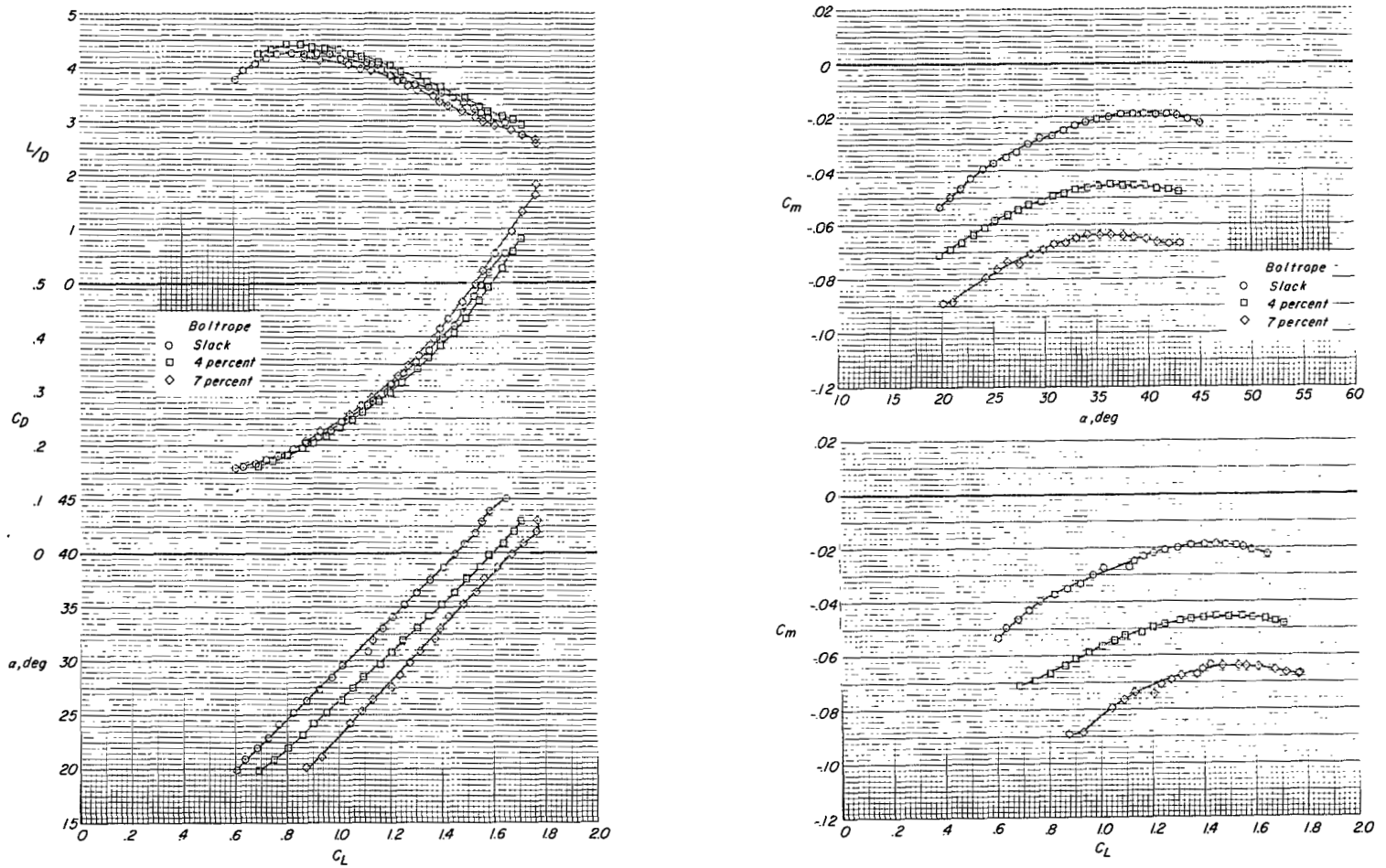

Figure 41.- Effect of boltrope length on the aerodynamic characteristics of the $\Lambda_o = 50^o$, $\Lambda = 55^o$ wing with the spreader bar removed.

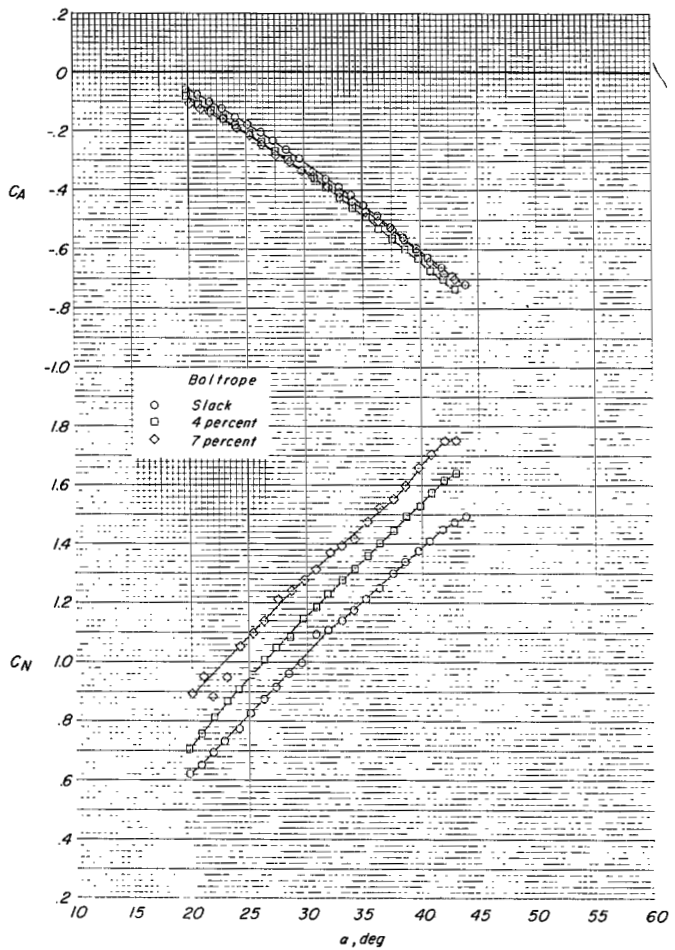

Figure 41.- Concluded.

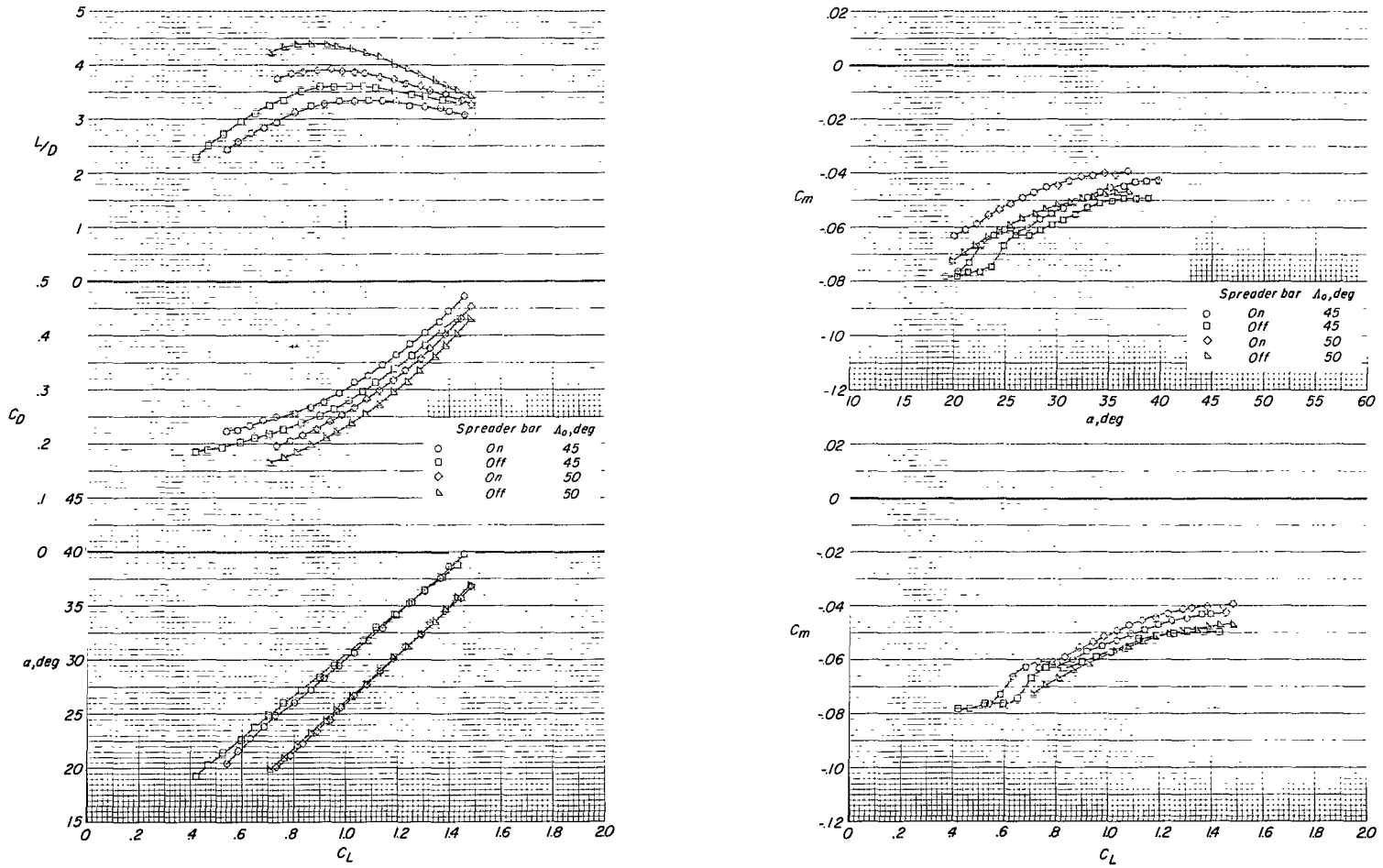

Figure 42.- Effect of the spreader bar on the aerodynamic characteristics of the $\Lambda = 55^\circ$ wing with 4-percent boltrope. q = 20.

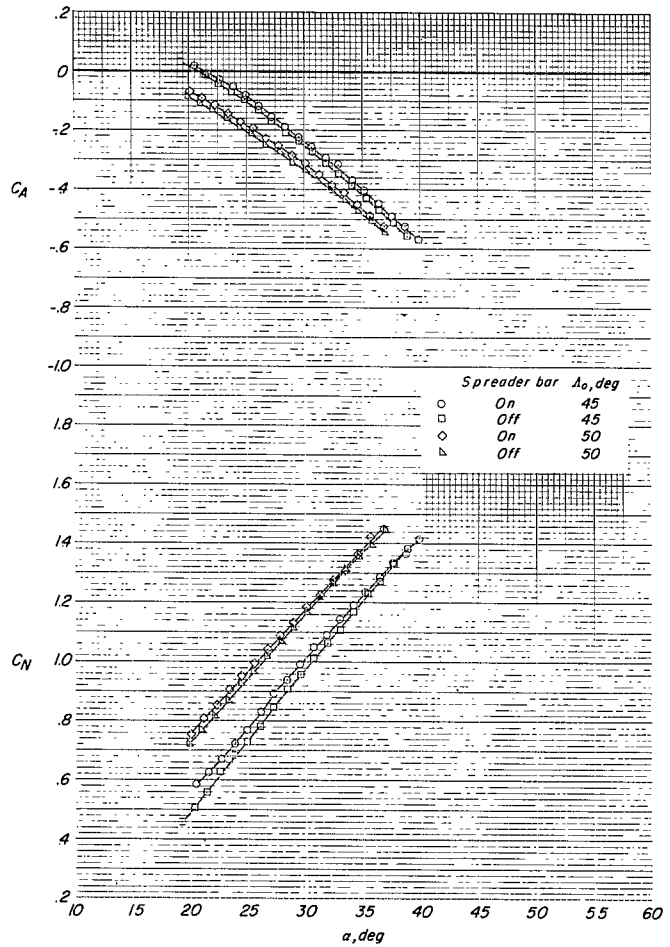

Figure 42.- Concluded.

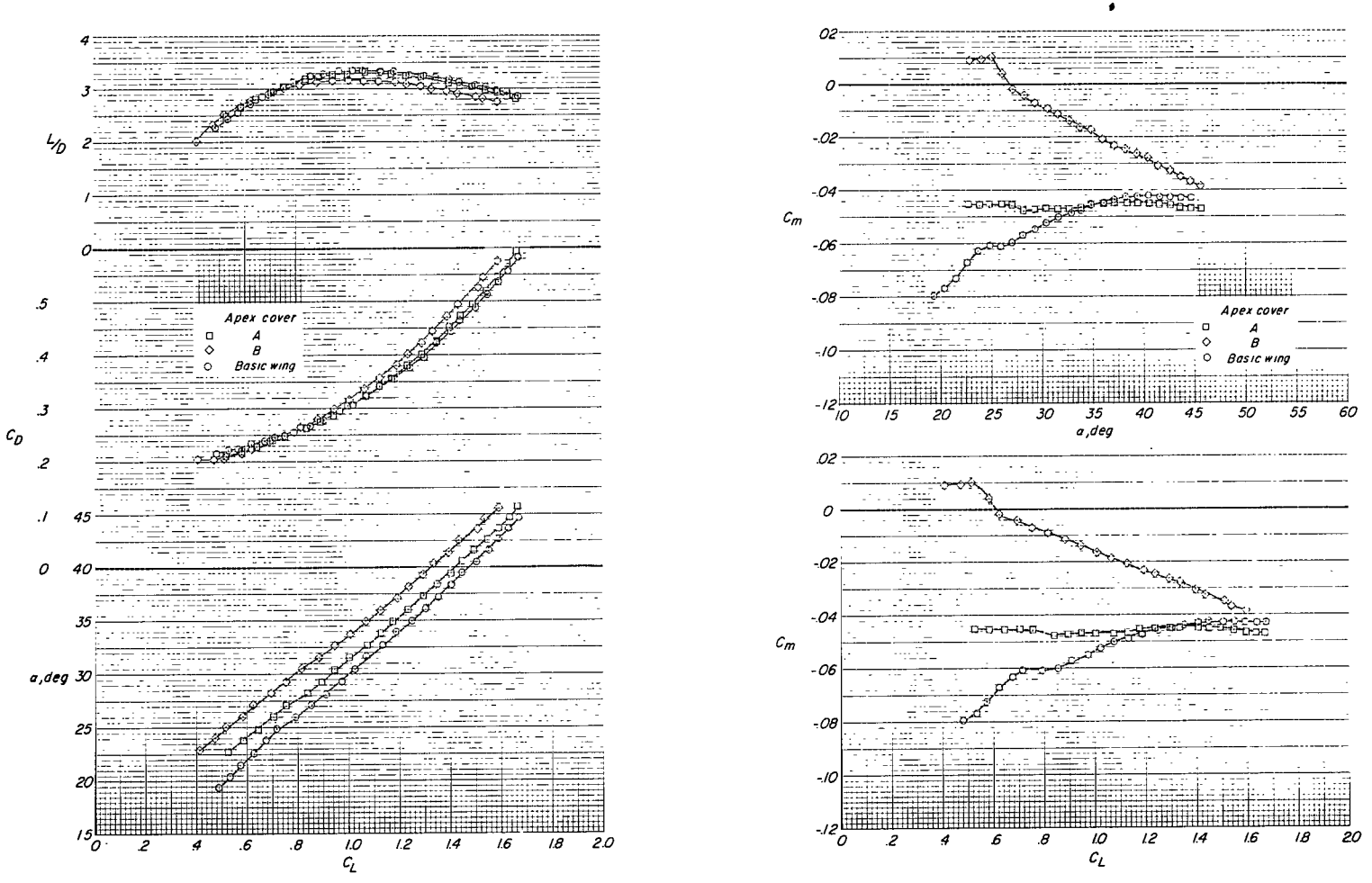

Figure 43.- Effect of two sealed apex covers on the aerodynamic characteristics of the $\Lambda_o = 45^\circ$, $\Lambda = 55^\circ$ wing. 4-percent boltrope.

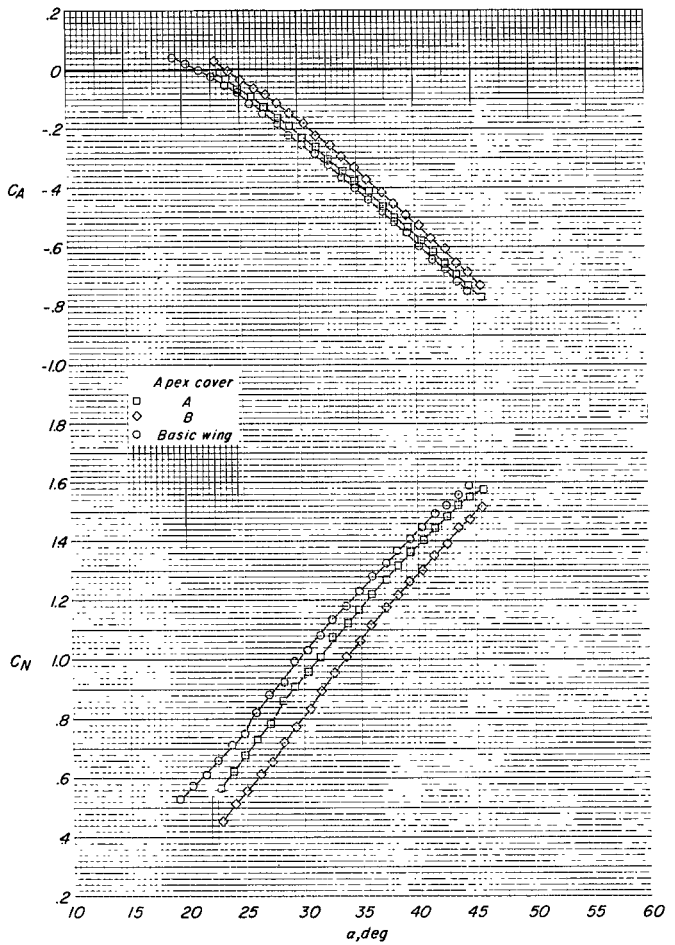

Figure 43.- Concluded.

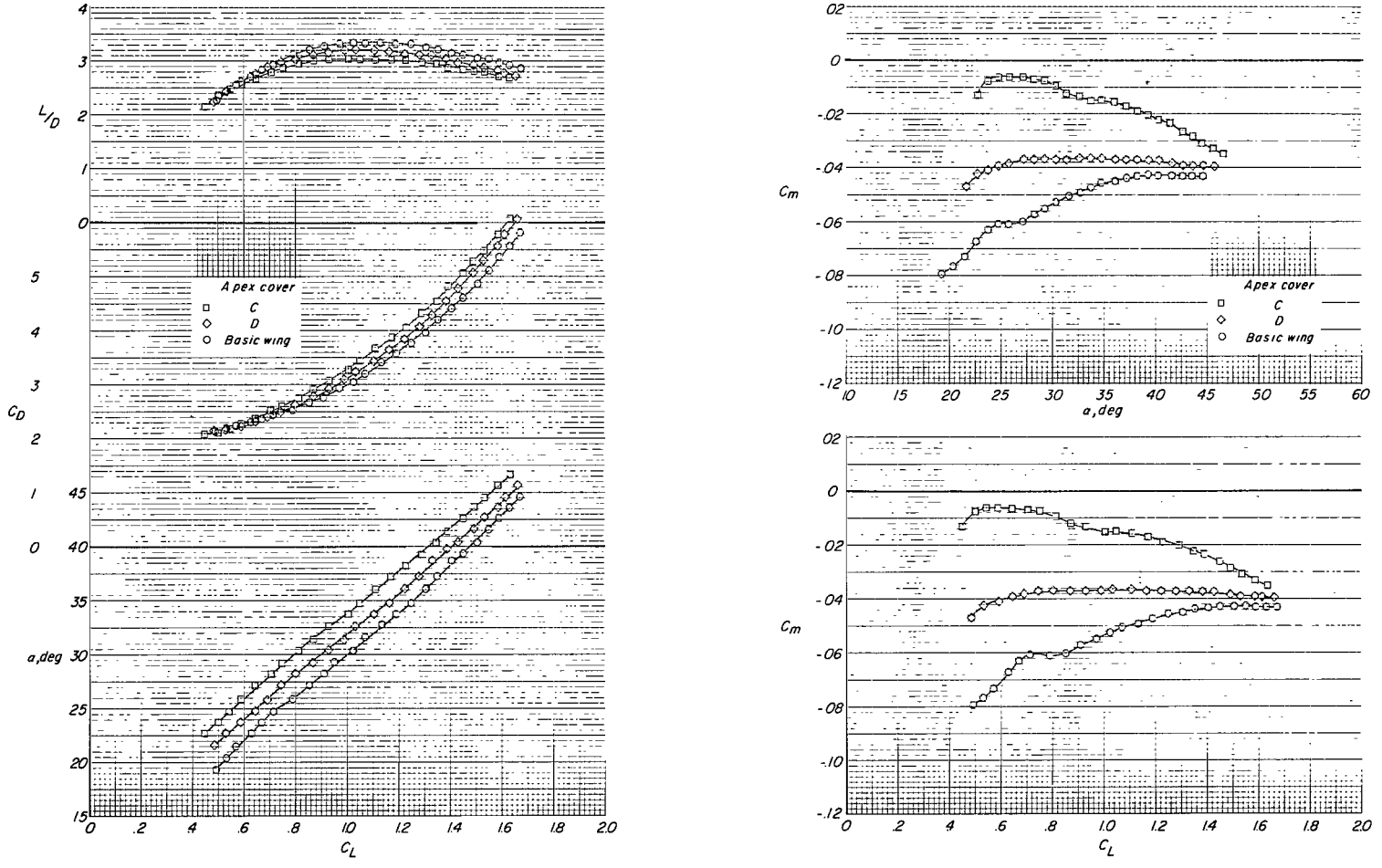

Figure 44.- Effect of two vented apex covers on the aerodynamic characteristics of the $\Lambda_o = 45^\circ$, $\Lambda = 55^\circ$ wing. 4-percent boltrope.

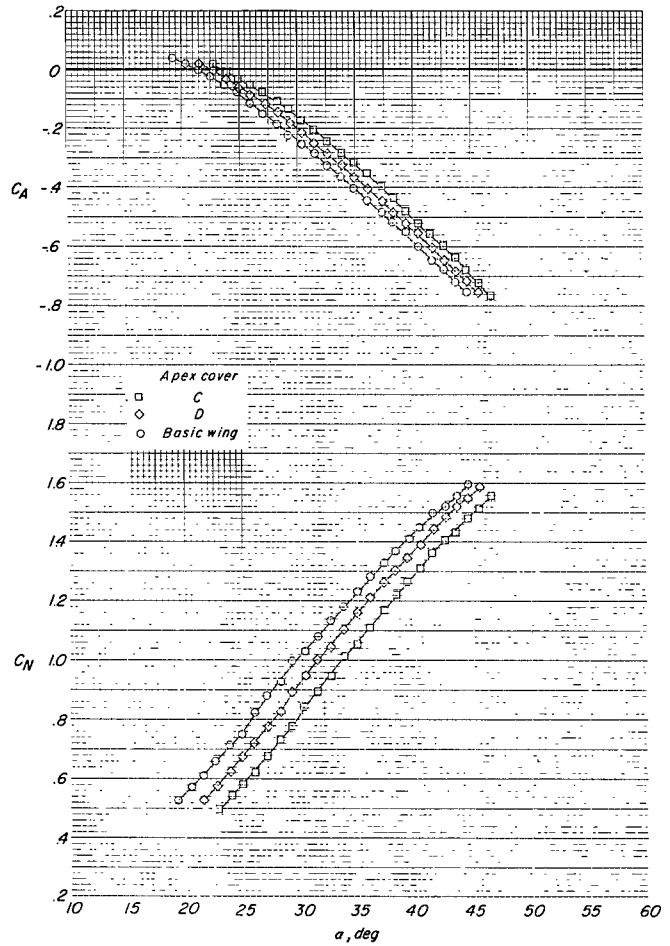

Figure 44.- Concluded.

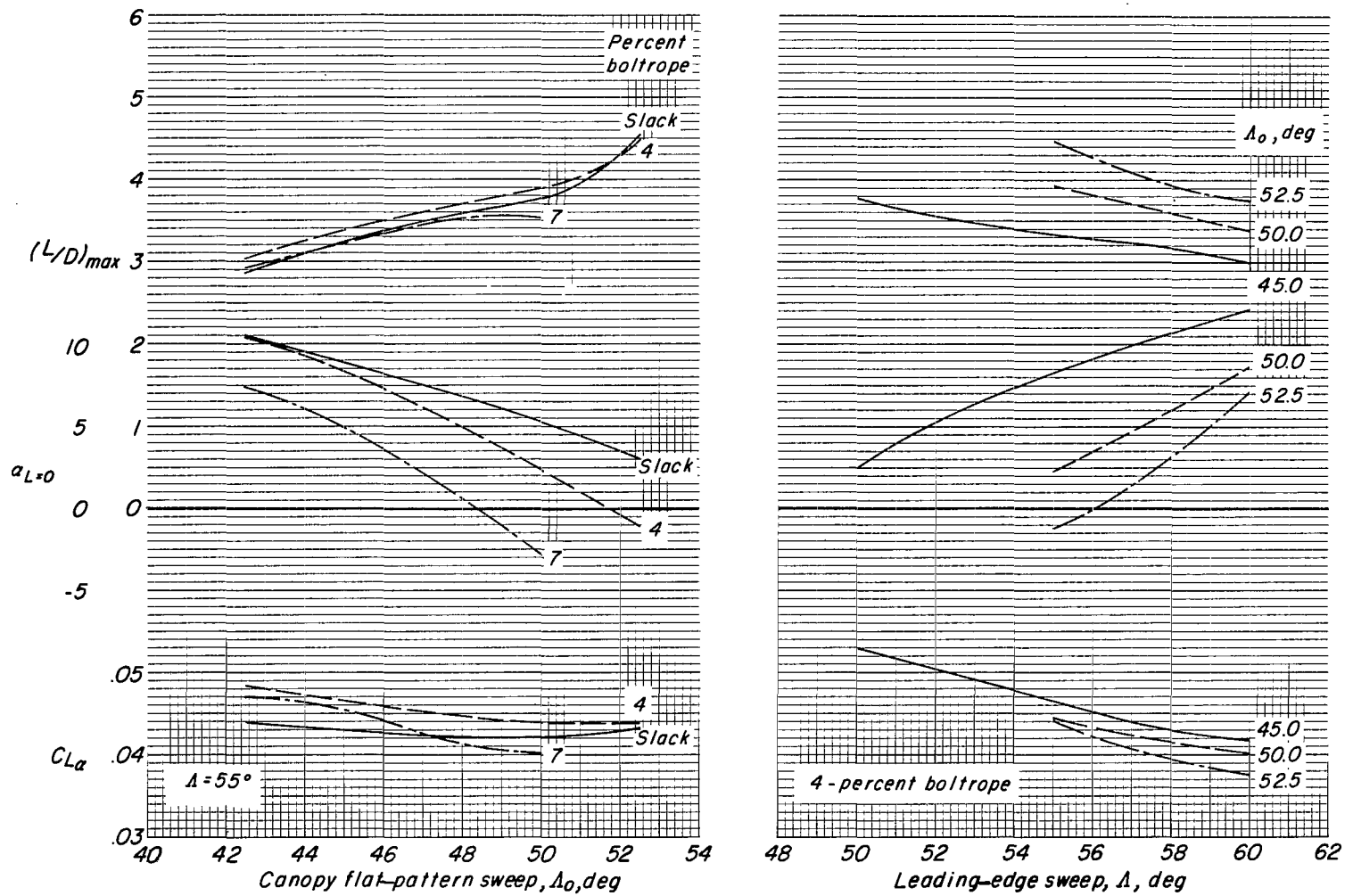

Figure 45.- Effects of canopy flat-pattern sweep and leading-edge sweep on lift-curve slopes, angles of attack for zero lift, and maximum lift-drag ratio. q = 20.

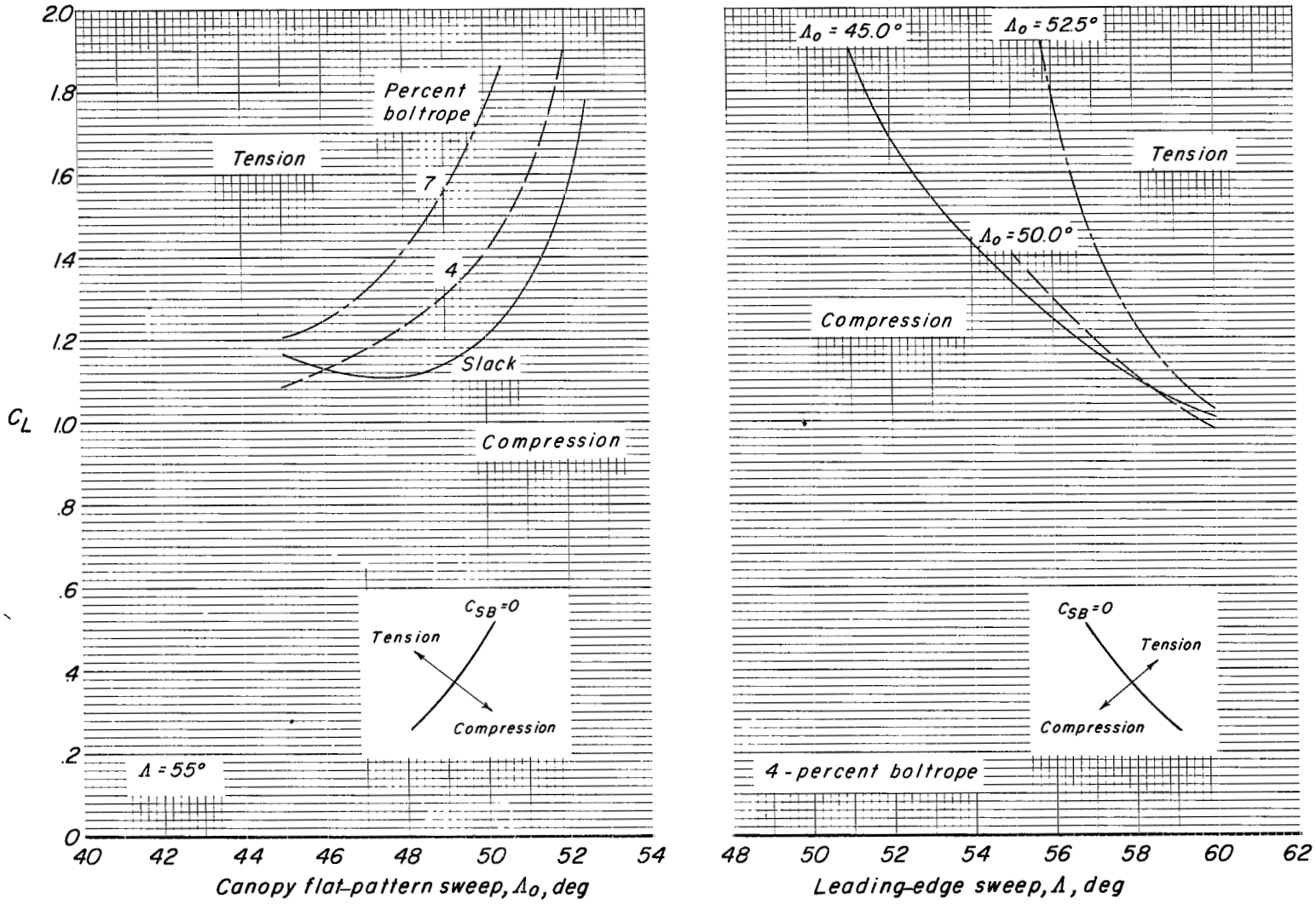

Figure 46.- Effect of canopy flat-pattern sweep and leading-edge sweep on the lift coefficient for zero spreader-bar load. q = 15.

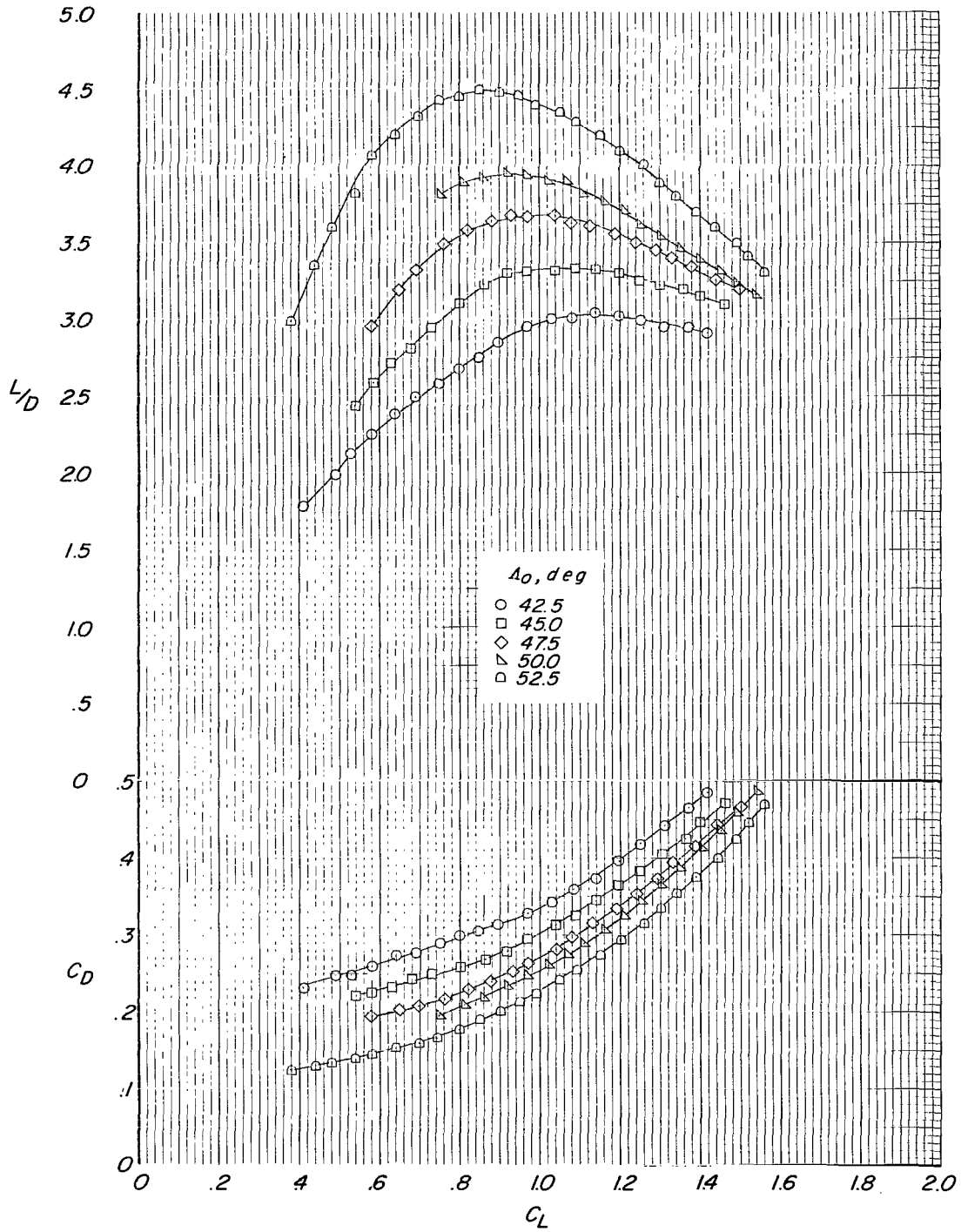

Figure 47.- Effect of canopy flat-pattern sweep on the variation with lift coefficients of drag coefficients and lift-drag ratios of the $\Lambda = 55^{\circ}$ wing. 4-percent boltrope; q = 20.

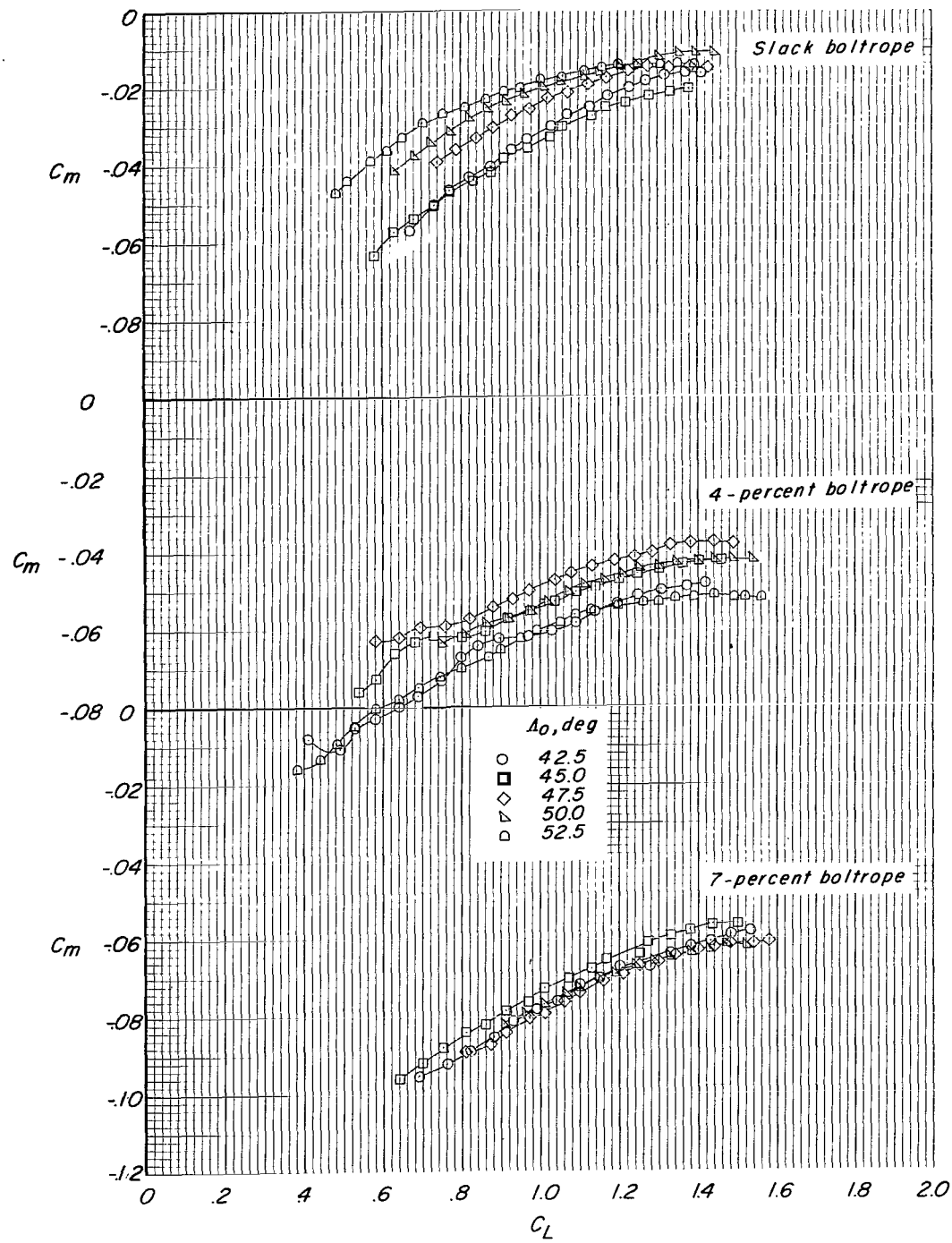

Figure 48.- Effect of canopy flat-pattern sweep on pitching-moment characteristics of the $\Lambda = 55^\circ$ wing. $q = 20$.

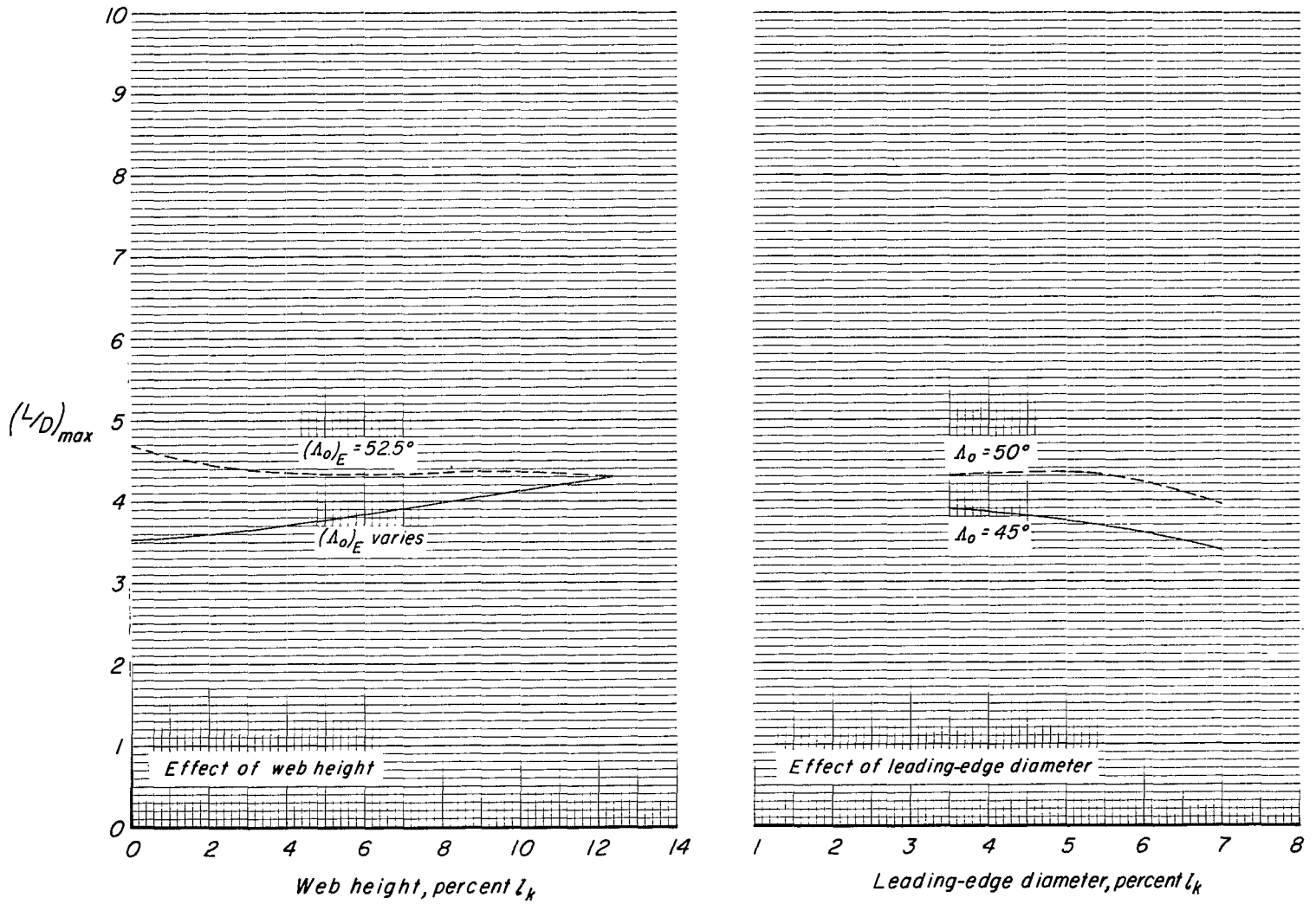

Figure 49.- Effect of keel web height and leading-edge diameter on maximum lift-drag ratios of the $\Lambda = 55^{\circ}$ wing. 2-percent boltrope; q = 20.

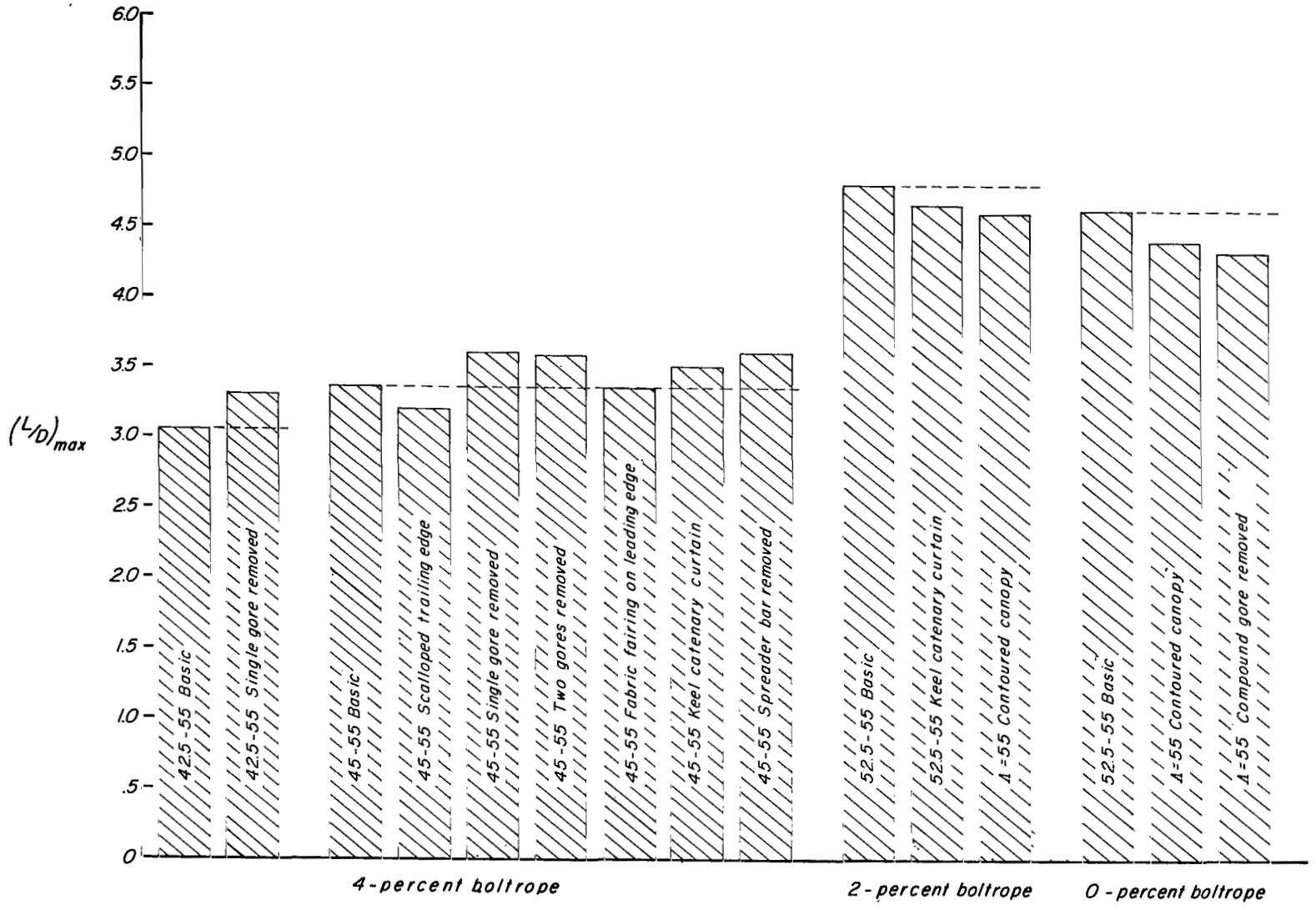

Figure 50.- Summary of maximum lift-drag ratios for various canopy modifications tested on the $\Lambda = 55^{\circ}$ wing.

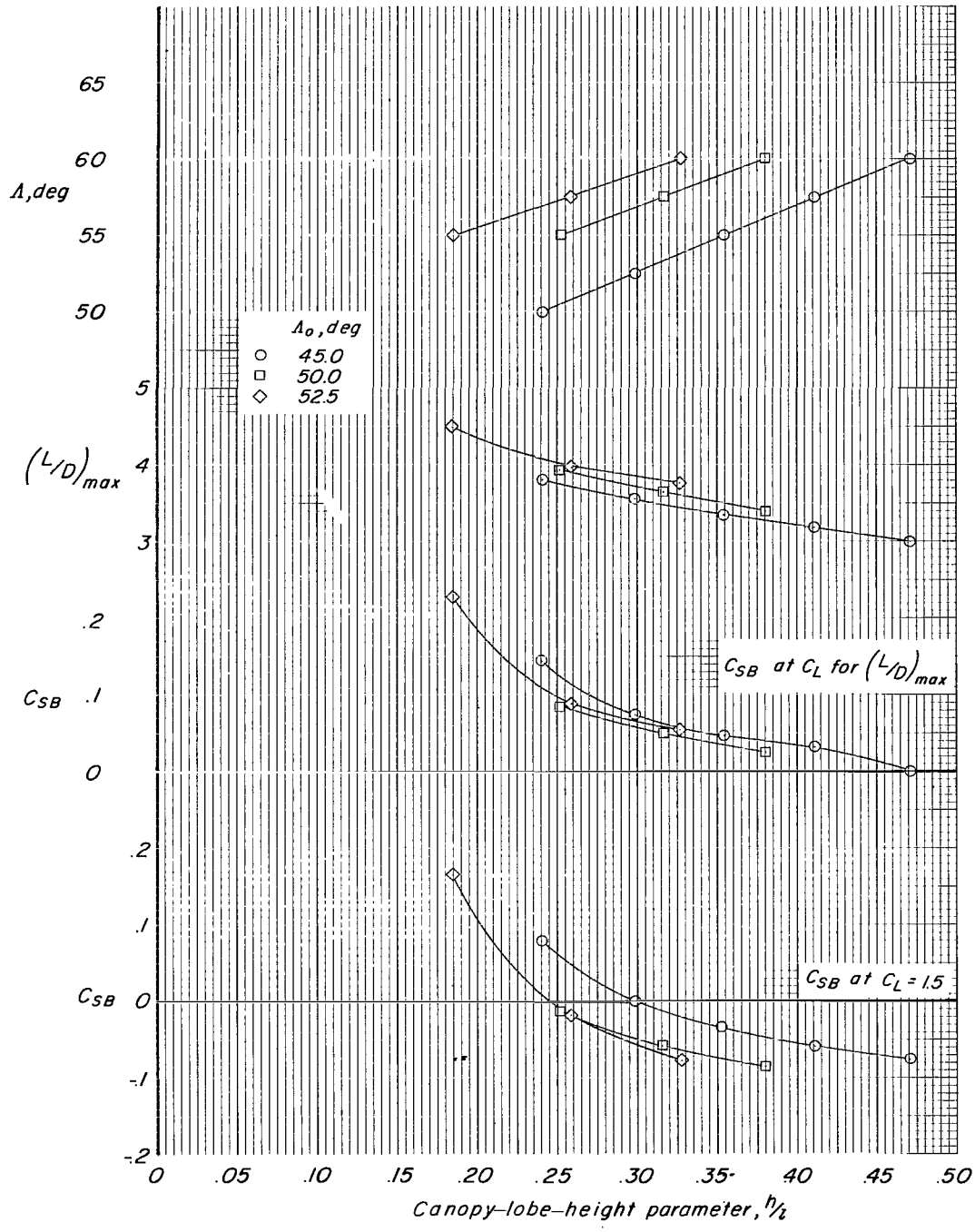

Figure 51.- Variation with canopy-lobe-height parameter of maximum lift-drag ratios and spreader-bar load coefficients. Coefficients are based on projected area between leading-edge center lines for each sweep angle. 4-percent boltrope; q = 15.

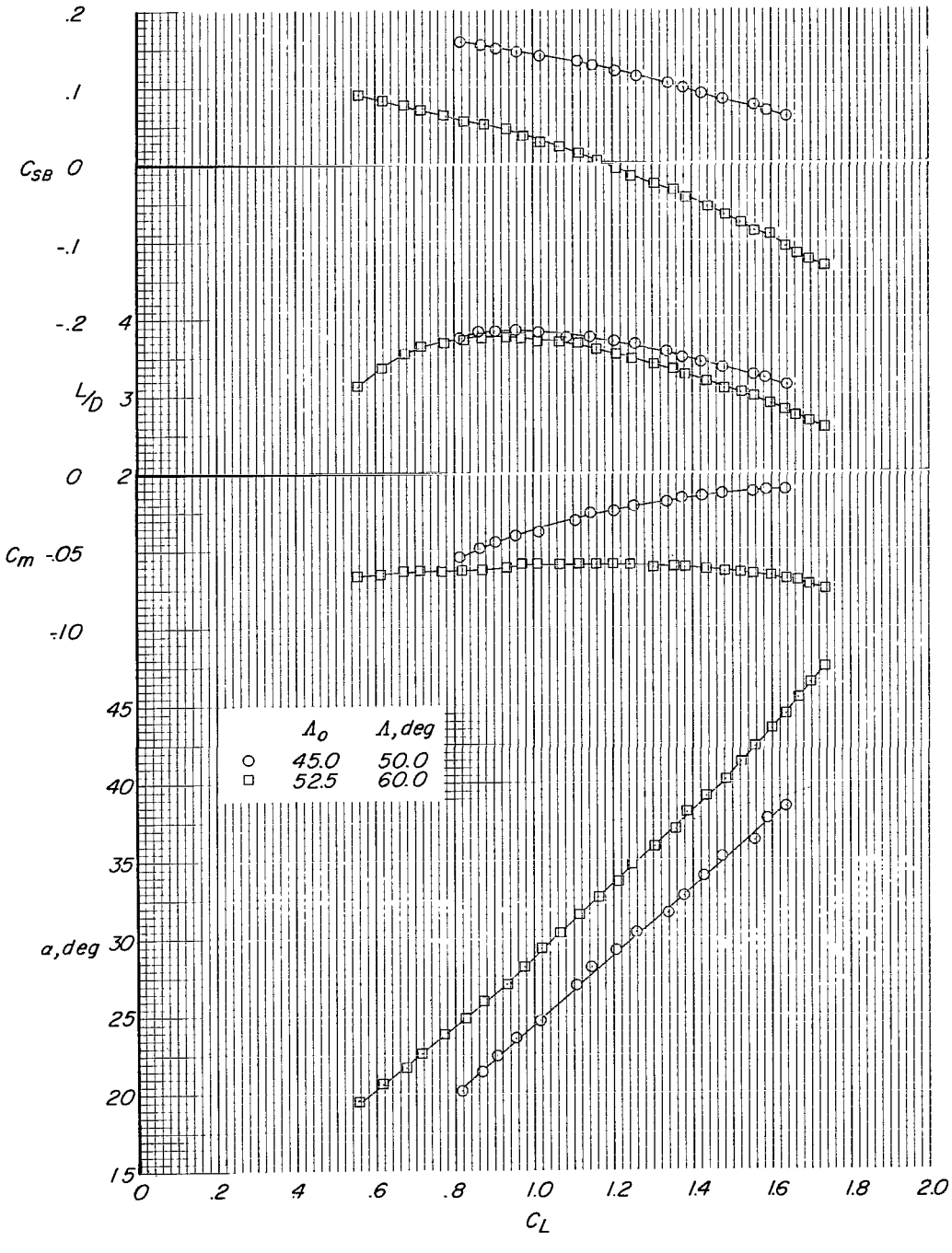

Figure 52.- Aerodynamic characteristics and spreader-bar loads for two different combinations of canopy flat-pattern sweep and leading-edge sweep that provide approximately the same maximum lift-drag ratio. Coefficients are based on projected area between leading-edge center lines for each sweep angle. 4-percent boltrope; q = 15.

2/11/25

"The aeronautical and space activities of the United States shall be conducted so as to contribute . . . to the expansion of human knowledge of phenomena in the atmosphere and space. The Administration shall provide for the widest practicable and appropriate dissemination of information concerning its activities and the results thereof."

—NATIONAL AERONAUTICS AND SPACE ACT OF 1958

NASA SCIENTIFIC AND TECHNICAL PUBLICATIONS

TECHNICAL REPORTS: Scientific and technical information considered important, complete, and a lasting contribution to existing knowledge.

TECHNICAL NOTES: Information less broad in scope but nevertheless of importance as a contribution to existing knowledge.

TECHNICAL MEMORANDUMS: Information receiving limited distribution because of preliminary data, security classification, or other reasons.

CONTRACTOR REPORTS: Technical information generated in connection with a NASA contract or grant and released under NASA auspices.

TECHNICAL TRANSLATIONS: Information published in a foreign language considered to merit NASA distribution in English.

TECHNICAL REPRINTS: Information derived from NASA activities and initially published in the form of journal articles.

SPECIAL PUBLICATIONS: Information derived from or of value to NASA activities but not necessarily reporting the results of individual NASA-programmed scientific efforts. Publications include conference proceedings, monographs, data compilations, handbooks, sourcebooks, and special bibliographies.

Details on the availability of these publications may be obtained from:

SCIENTIFIC AND TECHNICAL INFORMATION DIVISION

NATIONAL AERONAUTICS AND SPACE ADMINISTRATION

Washington, D.C. 20546